行政院原子能委員會
放射性物料管理局
委託研究計畫研究報告

蒙地卡羅方法應用於
用過核子燃料乾式貯存設施
輻射屏蔽特性之研究

受委託機關（構）：財團法人國家同步輻射研究中心
計畫主持人：許榮鈞
計畫編號：942005FCMA007
報告日期：中華民國 94 年 12 月 9 日

目錄

1. 中文摘要

本計畫之目的為提升用過核燃料乾式貯存設施安全分析報告中有關輻射屏蔽計算部分的審查與驗證能力。台電公司預定於 95 年 5 月提送核一廠用過核燃料乾式貯存設施建造執照之申請，物管局將規劃邀請會外專家和其同仁合組專案審查小組，執行該設施安全分析報告與試運轉之審查。在用過核燃料乾式貯存設施安全分析報告中有關輻射安全與屏蔽設計的部分預計將以蒙地卡羅計算方法為主來進行，蒙地卡羅計算方法具有非常多的優點，一般被視為是最準確的計算方法，常常被用來驗證與評估其他計算方法所得結果的準確度。但是蒙地卡羅模擬計算最大的缺點在於計算時間太長，特別是當該問題所牽涉到的輻射強度衰減比例非常巨大之時，如果沒有正確且有效地使用變異數降低技巧往往無法求得可靠的結果。變異數降低技巧在蒙地卡羅模擬計算上是一道兩面刃，正確使用將大幅縮短計算所需時間，使用的不好可能無法達到預期加速的目的，甚至造成錯誤結果而使用者不自知，因此如何針對蒙地卡羅計算的結果進行檢驗與建立平行驗證等關鍵能力對於輻射屏蔽的審查至為重要。本計畫將在個人電腦與叢集平行電腦上建立 MCNP5 蒙地卡羅與其他程式計算環境，規劃參考案例作為測試與驗證比較之用，特別著重在蒙地卡羅變異數降低技巧使用於用過核燃料乾式貯存設施輻射屏蔽計算相關特性研究與先期假想案例分析，為未來正式審查做好準備工作。

2. 英文摘要

The purpose of this project is to enhance the abilities to review and verify the radiation shielding calculation in the design of the spent fuel interim storage facility (SFISF). According to the schedule of Taiwan Power Company (TPC), the construction license application for the SFISF at Chin-Shan site will be submitted to Atomic Energy Council around May 2006. The shielding design of the SFISF consists of two parts, namely, the shielding design of the spent fuel cask and the shielding design or dose analysis of the storage site. The Monte Carlo code MCNP was expected to be used mostly in the shielding calculation in TPC's proposal. Monte Carlo method is considered to be the most accurate method presently available for solving radiation transport problems and has many applications in the field of nuclear engineering. However, it is extremely expensive computationally especially when large scale attenuation process from source to detector was involved. To make a difficult Monte Carlo shielding calculation computationally practical or possible, variance reduction techniques are indispensable in most cases. The variance reduction techniques in Monte Carlo simulation are usually very powerful and effective, but they must be used with great care because it may lead to a wrong answer if not used properly. The main tasks of this project are to build the MCNP5 computing platform on personal computer and Linux cluster, to establish a reference case similar to the shielding design of SFISF for benchmarks, to perform detailed Monte Carlo calculations on radiation shielding of SFISF including the test of many variance reduction schemes and related sensitivity study.

3. 計畫目的

本計畫之目的為提升用過核燃料乾式貯存設施安全分析報告中有關輻射屏蔽計算部分的審查與驗證能力。在用過核燃料乾式貯存設施屏蔽設計主要包含兩大部分：用過核燃料貯存桶的屏蔽設計與貯存場址的輻射劑量分析。台電公司預定於 95 年 5 月提送核一廠用過核燃料乾式貯存設施建造執照之申請，物管局將規劃邀請會外專家和其同仁合組專案審查小組，執行該設施安全分析報告與試運轉之審查。在用過核燃料乾式貯存設施安全分析報告中有關輻射安全與屏蔽設計的部分預計將以蒙地卡羅計算方法為主來進行，主要使用的工具應該是美國 Los Alamos 國家實驗室所發展的 MCNP 蒙地卡羅程式。蒙地卡羅計算最主要的特色是可靠準確，在模擬物理過程與幾何形狀上皆不需妥協，唯一的缺點是計算速度慢，但是近年來在電腦科技快速進步下，此一缺點也正在逐漸減輕當中。雖然蒙地卡羅計算方法具有非常多的優點，配合電腦科技的快速發展，現在幾乎被使用到所有有關輻射遷移的計算上，但是當該問題所牽涉到的輻射強度衰減比例非常巨大之時，如果沒有正確且有效地使用變異數降低技巧往往無法求得可靠的結果。例如以本案例來說，由用過核燃料貯存桶內的輻射源要利用蒙地卡羅計算方法追蹤至場界，可以想像這中間輻射強度變化的程度，此時電腦再快也算不出來，非得引進所謂變異數降低技不可，如何正確的使用完全看使用者的經驗與能力了。使用的不恰當，可能只有影響計算效率，更嚴重一點，連最後答案也會被影響到，這部分的問題不太像是使用者輸入方面的錯誤,事實上是非常難發現的，因此對於這部分結果的驗證或是 OA/OC 就相當重要了。因此如何針對蒙地卡羅計算的結果進行檢驗與建立確認分析等關鍵能力對於輻射屏蔽的審查至為重要。本計畫將在個人電腦與叢集平行電腦上建立 MCNP5 蒙地卡羅與其他程式計算環境，規劃參考案例作為測試與驗證比較之用，特別著重在蒙地卡羅變異數降低技巧使用於用過核燃料乾式貯存設施輻射屏蔽計算相關特性研究與先期假想案例分析，為未來正式審查做好準備工作。

4. 計畫緣起

台電公司核一廠正式商業運轉至今已有 26 年，更換下來用過之乏燃料均暫存於用過燃料池，該池之貯存容量設計不足存放 40 年運轉之用過燃料，而台電公司規劃最終處置廠希望能於 2030 年完成，因此必須採用中期貯存的方式過渡式貯存在廠區內。在未採用核燃料再處理的核能發電使用國家中均普遍採用濕式或乾式貯存的方式，經過評估後，台電公司決定採用乾式貯存設施，並在核一廠廠區內選定場址，預定於民國 100 年底之前完成 1366 束用過核燃料之裝載與貯存。依預定時程，考慮建造、試運轉，以及執照申請審查之時間，台電公司已預先向原子能委員會表示預定於 95 年 5 月提送設施建造執照申請。

根據了解，未來台電公司用過核燃料乾式貯存設施安全分析報告中有關輻射屏蔽計算部分將以蒙地卡羅計算機程式 MCNP（Monte Carlo N-particle transport code）為主來進行，該程式亦為用過核燃料乾式貯存護箱/設施審查標準(NUREG-1536/NUREG-1567)所建議的常用屏蔽分析程式之一。蒙地卡羅計算方法在傳統核工領域的應用非常廣泛，因為它具有非常多的優點，特別是在幾何形狀的模擬與反應截面的精確度上，一般被視為是最準確的計算方法，常常被用來驗證與評估其他計算方法所得結果的準確度。但是蒙地卡羅模擬計算最大的缺點在於計算時間太長，特別是當該問題所牽涉到的輻射強度衰減比例非常巨大之時，如果沒有正確且有效地使用變異數降低技巧往往無法求得可靠的結果。沒有運用變異數降低技巧的蒙地卡羅模擬計算基本上是非常單純的，只要使用者在射源、屏蔽與偵檢器的描述上沒有問題，一般而言計算結果是非常可靠的，而且不易出錯。但是對於像過核燃料乾式貯存設施輻射屏蔽計算這樣的問題，我們可以想像輻射強度由射源位置到最後偵檢器之間的衰減幅度一定非常巨大，這樣的計算過程純粹運用類比式的蒙地卡羅模擬幾乎是不可能的，一定需要用到很多不同種類的變異數降低技巧以加速計算過程。

變異數降低技巧在蒙地卡羅模擬計算上是一道兩面刃，正確使用將大幅縮短計算所需時間，使用的不好可能無法達到預期加速的目的，甚至造成錯誤結果而使用者不自知。以非常有名的蒙地卡羅模擬計算程式 MCNP 為例，它內建了非常多種的變異數降低技巧供使用者搭配運用，每一種變異數降低技巧又有很多參數必須由使用者自行挑選決定，所以最後結果的好壞端視使用者是否做了正確的判斷。但是誠如 MCNP 程式其中兩位作者所述：The selection of parameters is more art than science (Booth and Hendricks, 1984)，因此如何針對蒙地卡羅計算的結果進行檢驗與建立平行驗證等關鍵能力對於輻射屏蔽的審查至為重要，本計畫將著重在蒙地卡羅變異數降低技巧使用於用過核燃料乾式貯存設施輻射屏蔽計算進行特性研究與先期假想案例分析，為未來正式審查做好準備工作。

5. 執行方法與及進行步驟

用過核燃料乾式貯存設施安全分析報告(SAR)的內容主要關鍵性的安全評估項目可歸納如：結構評估、密封性能評估、熱傳評估、屏蔽評估、臨界評估等章節。物管局相對應的負責參與同仁有劉志添(結構)、陳文泉(密封性)、陳志行(熱傳)、劉文忠(屏蔽)、和徐源鴻、鄭武昆(臨界)等幾位先生，另外還有多位同仁負責其他章節的審查。本計畫主要著重在輻射屏蔽的部分, 因此將偕同會內同仁共同研究如何提升對輻射屏蔽計算結果的審查與驗證能力。如上節所述, 怎麼樣來對蒙地卡羅計算的結果進行檢驗與建立平行驗證能力對於輻射屏蔽的審查非常重要, 因此本計畫將著重在蒙地卡羅變異數降低技巧使用於用過核燃料乾式貯存設施輻射屏蔽計算進行一般特性研究與先期假想案例分析，為未來正式審查做好準備工作。

本計畫進行步驟大致安排如下：

(1) 物管局規劃有定期的技術研習會，邀請國外專家介紹相關資訊，我們亦將選擇切題項目參與研習討論，吸收新知，加強互動以利於未來審查工作的配合。
(2) 收集與研讀用過核燃料乾式貯存設施輻射屏蔽計算相關資訊，據此建立一個簡化的先期假想案例模型以利後續進行分析測試。
(3) 根據假想案例模型，在個人電腦與叢集平行電腦上建立 MCNP5 蒙地卡羅與其他程式計算環境，整理蒙地卡羅模擬計算相關注意要點與熟悉該程式中關於變異數降低技巧的內容與正確使用方法。
(4) 驗證與比較蒙地卡羅與其他程式不同計算方法所得結果的差異，特別針對蒙地卡羅變異數降低技巧使用於用過核燃料乾式貯存設施輻射屏蔽計算進行特性研究、靈敏度分析與假想案例分析測試。

預計可能遭遇之困難及解決途徑：若台電公司未依規劃時程決標和提供相關廠商之設計資料, 則無法針特定之設施型式與設計進行審查準備, 但參與計畫之物管局同仁技術養成訓練部份仍可如期執行，本計畫的預期結果依然具有參考價值。

6 完成之工作項目及具體成果

本計畫完成之工作項目及具體成果：

(1) 完成用過核燃料乾式貯存設施參考案例輻射屏蔽 MCNP 蒙地卡羅計算分析，並利用此簡化案例與其他輻射遷移計算程式（ANISN、DORT、TORT）所得結果作比較分析與互相驗證。

(2) 研究發展適用於用過核燃料乾式貯存設施輻射屏蔽計算的變異數降低技巧, 以達到有效加速蒙地卡羅模擬計算並確保結果的正確性。

(3) 建立蒙地卡羅程式（MCNP, version 5, parch 1.30）使用手冊，詳細說明參考案例中相關的程式輸入、輸出與執行步驟, 強化研究人員乾式貯存設施輻射屏蔽平行驗證計算之能力，有效提升輻射屏蔽審查品質。

(4) 建立用過核燃料乾式貯存設施安全分析報告(SAR)輻射屏蔽相關審查注意要點，以利未來審查工作的進行。

(5) 本計畫預期成果除做好核一廠設施的輻射屏蔽安全審查作準備外, 亦可為未來相關設施安全審查建立基礎，有效落實用過核燃料中期貯存技術之本土化。

以下我們將針對上述項目一一詳細說明：

6.1 參考案例分析

6.1.1 參考案例模型（用過核燃料乾式貯存桶）

由於本研究著重在方法上的探討，為了方便各種不同程式描述起見，我們參考文獻中實際案例建立一個相對簡化的用過核燃料乾式貯存桶模型。事實上要建立非常詳細真實的計算模型並不算很難，但是對於研究目標所要呈現的分析比較會造成困擾，因此在此我們利用下列描述的計算模型來討論相關問題。用過核燃料乾式貯存桶計算幾何模型的幾何形狀與尺寸如圖 6.1.1a 所示，其中物質材料組成如表 6.1.1 所列。我們假設射源均勻分布於中間有效燃料區內，強度為每秒每單位體積發射一個射源粒子，其中子與加馬射線射源能譜取至 NAC-UMS 系統的 SAR，分別如圖 6.1.1b 與圖 6.1.1c 所示，圖中我們也可以看到重整為 BUGLE 能群結構的射源能譜。針對計算結果的比較部分，我們擺設兩個主要的偵檢器 Top Detector 與 Side detector 當作比較基準點，位置如圖 6.1.1a 所示，它們都是具有一定體積的體偵檢器（Volume Detector），先計算求得偵檢器內平均的中子或加馬射線通率，再分別乘上對應的通率劑量轉換因子可得到劑量率，我們採用最新的 ICRP-74 報告中所建議的數值（圖 6.1.1d）。除了 Top Detector 與 Side detector 之外，我們也打算把整個空間每一點的劑量求出來並繪圖以增加對於劑量分佈的了解。

表 6.1.1：用過核燃料乾式貯存桶計算幾何模型的物質組成。

Region	Isotope	Atomic density
Fuel	^{10}B	1.204E-4[a]
	^{11}B	3.832E-4
	^{nat}C	1.004E-4
	^{16}O	8.092E-3
	^{27}Al	5.576E-4
	^{56}Fe	7.463E-3
	^{nat}Zr	2.155E-3
	^{238}U	4.038E-3
Iron	^{56}Fe	8.487E-2
Concrete	^{1}H	7.860E-3
	^{16}O	4.380E-2
	^{23}Na	1.050E-3
	^{nat}Mg	1.400E-4
	^{27}Al	2.390E-3
	^{nat}Si	1.580E-2
	^{nat}K	6.900E-4
	^{nat}Ca	2.920E-3
	^{56}Fe	3.100E-4
Air	^{14}N	4.020E-5
	^{16}O	1.070E-5

[a]Read as 1.204×10^{-4}. (Unit: ×10^{24} cm^{-3})

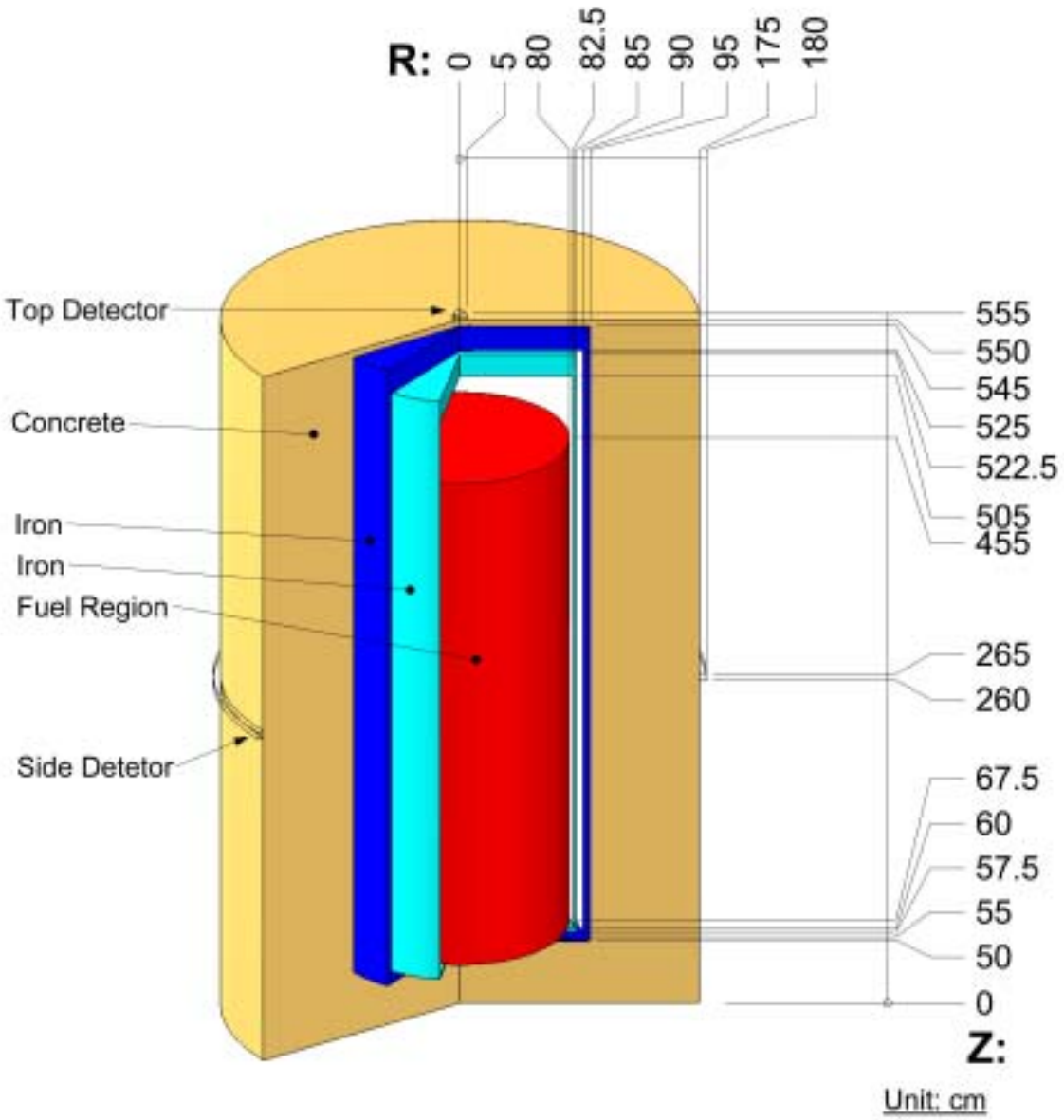

圖 6.1.1a：用過核燃料乾式貯存桶計算幾何模型。

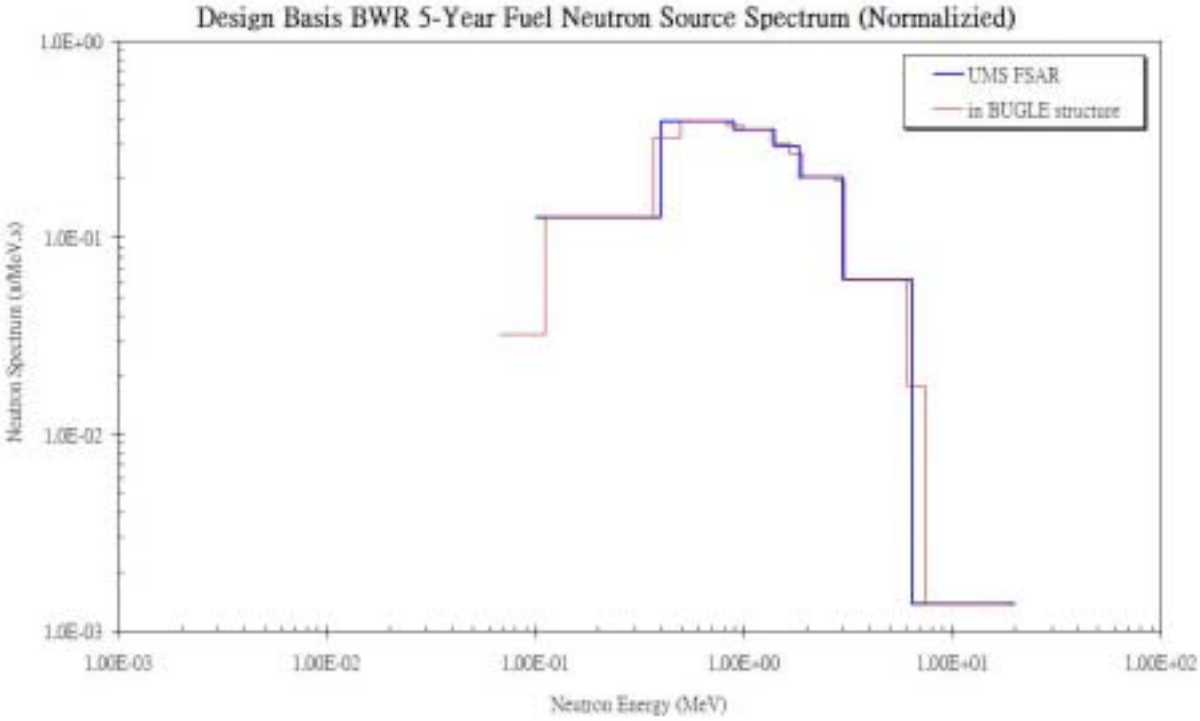

圖 6.1.1b：用過核燃料乾式貯存桶幾何模型的中子射源能譜。

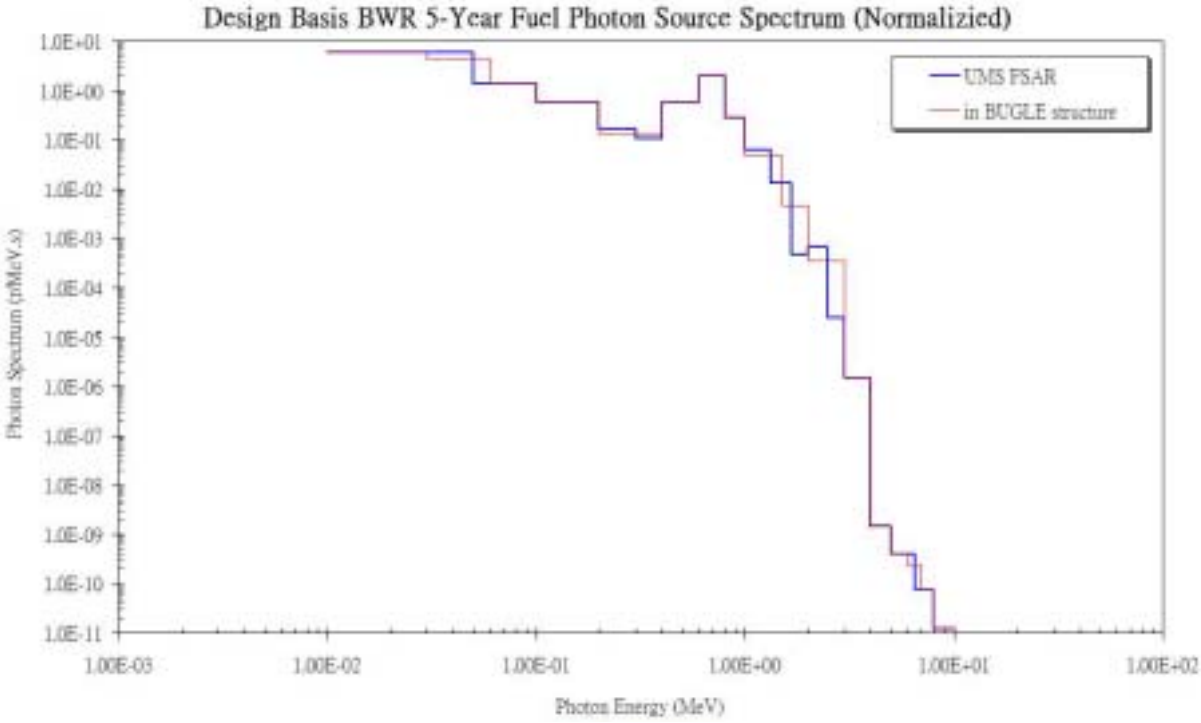

圖 6.1.1c：用過核燃料乾式貯存桶幾何模型的加馬射線射源能譜。

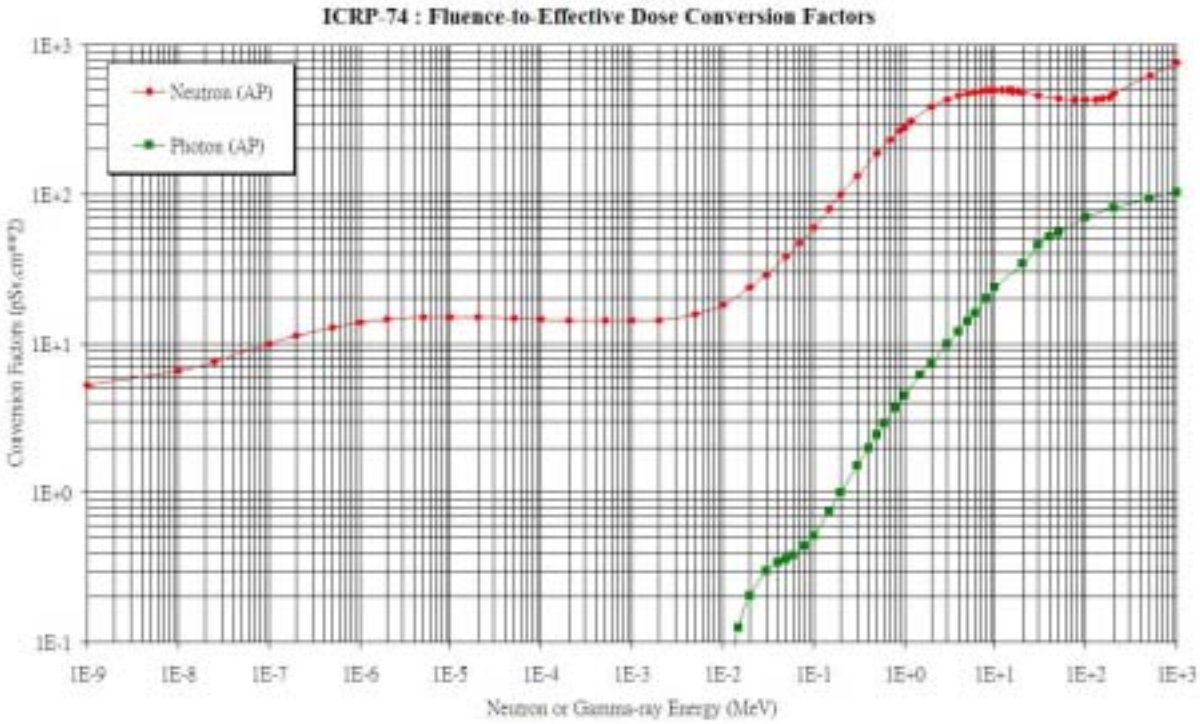

圖 6.1.1d：ICRP-74 通率劑量轉換因子。

6.1.2 計算方法與工具

關於處理輻射遷移計算主要有兩大類不同的方法：Deterministic Method 和 Monte Carlo Method。其中 Deterministic Method 最常使用的方法是所謂的 Discrete Ordinates（S_N） Method，它把整個相空間（包括位置、角度與能量）切割成許多離散的格點，利用數值方法直接求解輻射遷移方程式。它的優點是計算速度快，一次計算可得整個相空間所有的答案，缺點就是利用離散的格點來近似真正的相空間，產生許多可能造成誤差的來源，例如：Angular Mesh Distribution、Spatial Mesh Distribution、Multigroup Cross-Section Library、Multidimensionality Effect、Material Homogenization 等等。相反的，Monte Carlo Method 直接利用亂數取樣模擬粒子在物質中遷移的情況，原則上只要對於描述物理作用的知識足夠清楚，它可以產生最準確的結果，不需要在物理與幾何模型模擬上最太多妥協，使用上也相對簡單，他最大的問題在於費時，必須引進 Variance Reduction Techniques 來幫忙增加計算效率。這兩類方法有本質上的差異，各有優缺點，視問題不同與使用者本身的經驗，已經各自獨立發展了幾十年，近年來發現它們也可以搭配使用而得到非常好的效果。

在本研究中，我們利用三種計算方法求解同一個問題：分別是 Deterministic Method、Monte Carlo Method 和 Hybrid Deterministic/ Monte Carlo Method。使用的計算工具（反應作用截面庫）如下列所示：

Deterministic Method：ANSIN、DORT、TORT codes（BUGLE-96）。

Monte Carlo Method：MCNP code（ENDF/B-VI）。

Hybrid Deterministic/ Monte Carlo Method：TORT/MCNP Coupling Approach。

在 Deterministic Method 方面，因為計算幾何模型相對簡單且具有一定對稱性，我們可以分別利用一維的 ANISN、二維的 DORT 與三維的 TORT 程式來計算，除了計算工具不同之外，Discrete Ordinates Code 中還有很多的參數可以調整，我們也順便測試一下改變它們對結果的影響，增加對計算結果的信心。為什麼要如此大費周章使用不同的工具與選項來處理同樣的問題，最大的好處就是互相驗證，分析它們之間的差異並找出可能原因，這是一個可靠的安全分析報告所必經的步驟（Uncertainty Study and Sensitivity Study）。我們還可進一步互相利用不同方法彼此的優點，大幅改善 Monte Carlo Method 的計算效率，除了將原來非常困難的問題變為可行之外，對於最後答案的品質也將非常有信心。

6.1.3 計算結果與比較討論

針對用過核燃料乾式貯存桶假想案例，我們先將利用 Discrete Ordinates Method 與 Monte Carlo Method 計算的結果表列如下：

表 6.1.3 針對用過核燃料乾式貯存桶假想案例，利用不同程式與選項解輻射遷移計算所得結果之比較。

Detectors(μSv/h)	Side (neutron)	Side (photon)	Top (neutron)	Top (photon)
MCNP (relative error)	4.35E-3 (6.24%)	5.57E-3 (1.45%)	1.46E+0 (2.59%)	6.61E-3 (12.54%)
TORT (Δs=2.5, P3S8)	2.32E-3	3.90E-3	6.43E-1	7.06E-3
TORT/MCNP	0.53	0.70	0.44	1.07
TORT (adjoint) (Δs=2.5, P3S8)	2.46E-3	3.98E-3	7.00E-1	7.48E-3
TORT (θ=0.3) (Δs=2.5, P3S8)	2.35E-3	3.91E-3	6.94E-1	7.21E-3
TORT (Δs=2.5, P5S8)	2.32E-3	3.91E-3	6.44E-1	7.07E-3
DORT (Δs=2.5, P3S16)	2.35E-3	3.96E-3	6.47E-1	6.89E-3
DORT (Δs=1.25, P3S16)	2.43E-3	3.99E-3	6.45E-1	7.05E-3
ANISN (Δs=2.5, P3S16)	2.25E-3	3.84E-3	1.38E+0	2.07E-2
ANISN (Δs=0.625,P3S16)	2.39E-3	3.94E-3	1.39E+0	2.13E-2

針對本案例貯存桶表面劑量率來說，貯存桶上方劑量率明顯高於側邊，中子引發之二次加馬射線所產生的劑量不容忽視，其強度與原中子射源產生的效果差不多。但是因本案例模型並非是一真實的用過核燃料乾式貯存桶，在此我們並不在意輻射劑量率絕對值的大小，而是著重於計算方法與工具的探討。從上表明顯可見，使用 Discrete Ordinates Method（TORT with multigroup BUGLE-96）與 Monte Carlo Method（MCNP with continuous energy ENDF/B-VI）的結果有明顯的差異（~50%）。一般而言，我們相信 Monte Carlo Method 的結果應該比較接近真正的答案，因為在此我們並未使用任何明顯的假設或近似，而且也尚未刻意使用 Variance Reduction Techniques。相反的，Discrete Ordinates Method 有太多的假設隱含在內（例如 Angular Mesh Distribution、Spatial Mesh Distribution、Multigroup Cross-Section Library、Multidimensionality Effect 等等），程式也有許許多多的數值選項有待測試驗證，因此我們利用利用不同程式與選項解同樣輻射遷移問題，代表性計算所得之結果也列於上表。根據上表所做之測試與分析，絕大部分 Discrete Ordinates Method 的結果都收斂於相近的答案，因此這個結果應該就具有相當可信度。除了貯存桶表面劑量率的結果，我們也想把整個空間劑量率的分布求出來，以方便讀者了解。這個要求對 Discrete Ordinates Method 來說是先天就具備的，但是對 Monte Carlo Method 來說是相當困難的，必須利用 MCNP 最新版本才有的功能（Mesh Tally）加上非常久的計算時間才可得，最後一系列的結果繪於下圖 6.1.3。

Dose Map: TORT (Neutron)

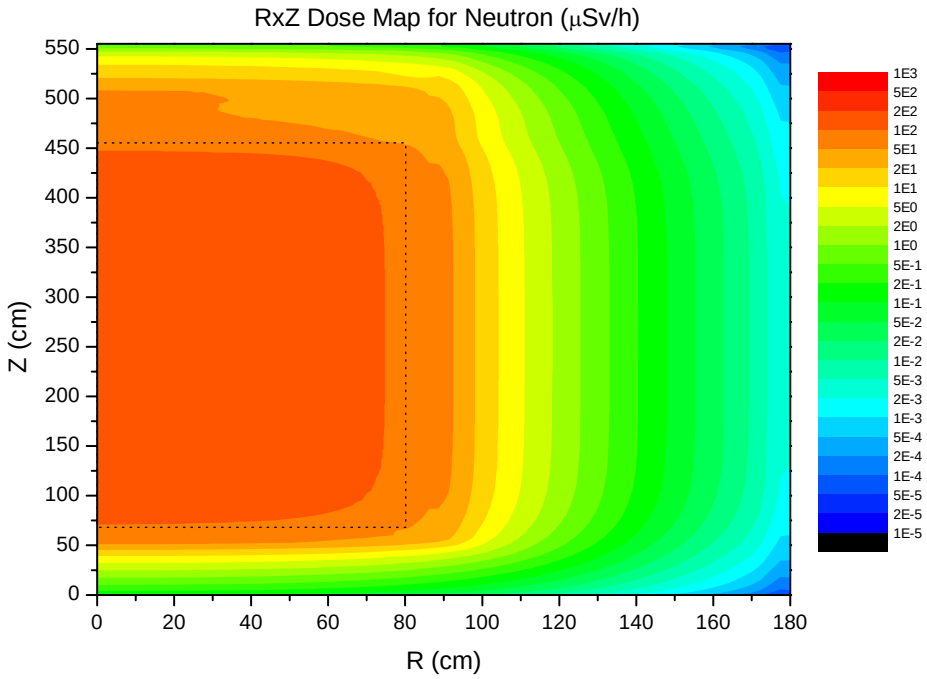

Dose Map: MCNP (Neutron)

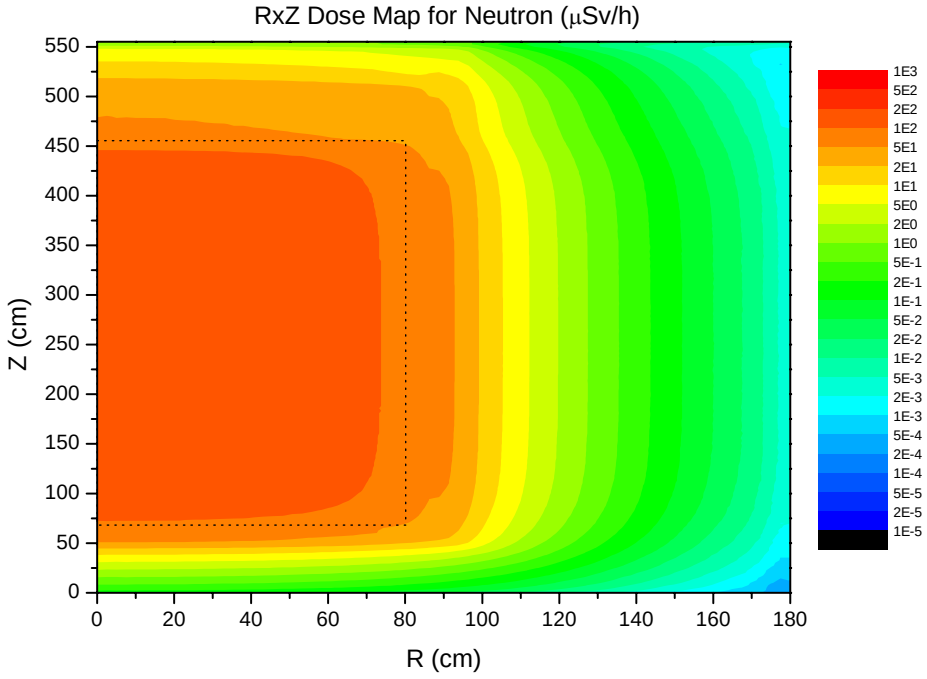

圖 6.1.3a：用過核燃料乾式貯存桶中子輻射劑量空間分布圖
（分別利用 TORT 與 MCNP 程式計算的結果）。

Dose Map: TORT (Induced gamma-ray)

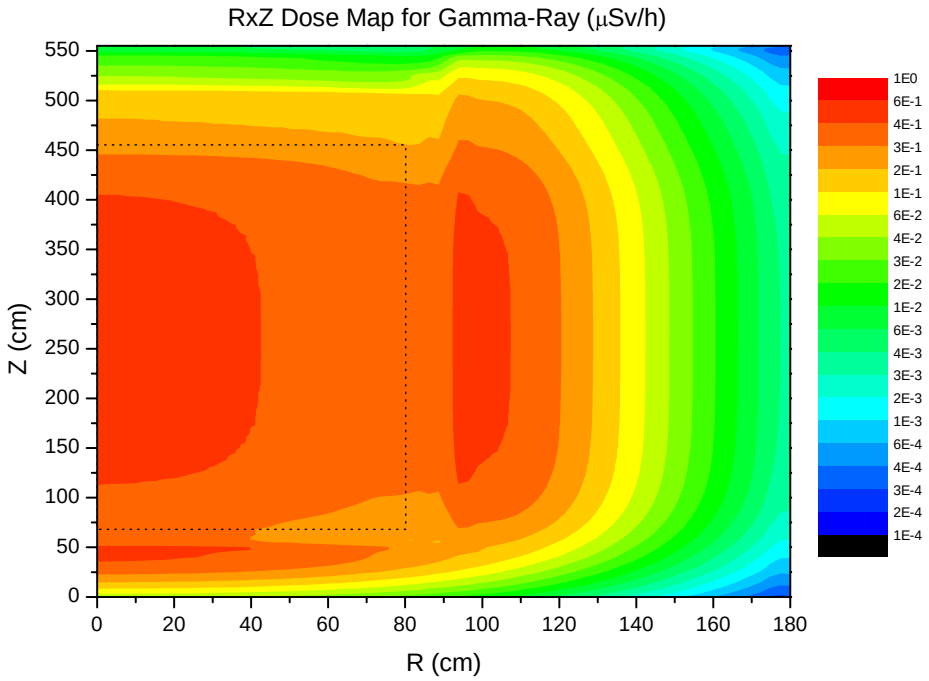

Dose Map: MCNP (Induced gamma-ray)

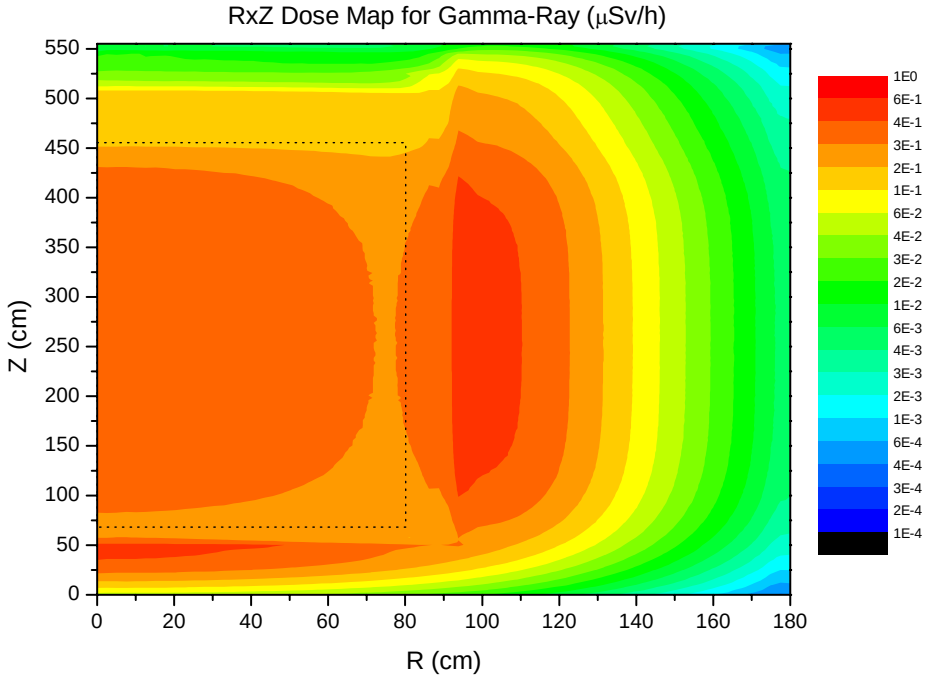

圖 6.1.3b：用過核燃料乾式貯存桶中子引發之二次加馬射線輻射劑量空間分布圖（分別利用 TORT 與 MCNP 程式計算的結果）。

Dose Map: TORT/MCNP (Neutron)

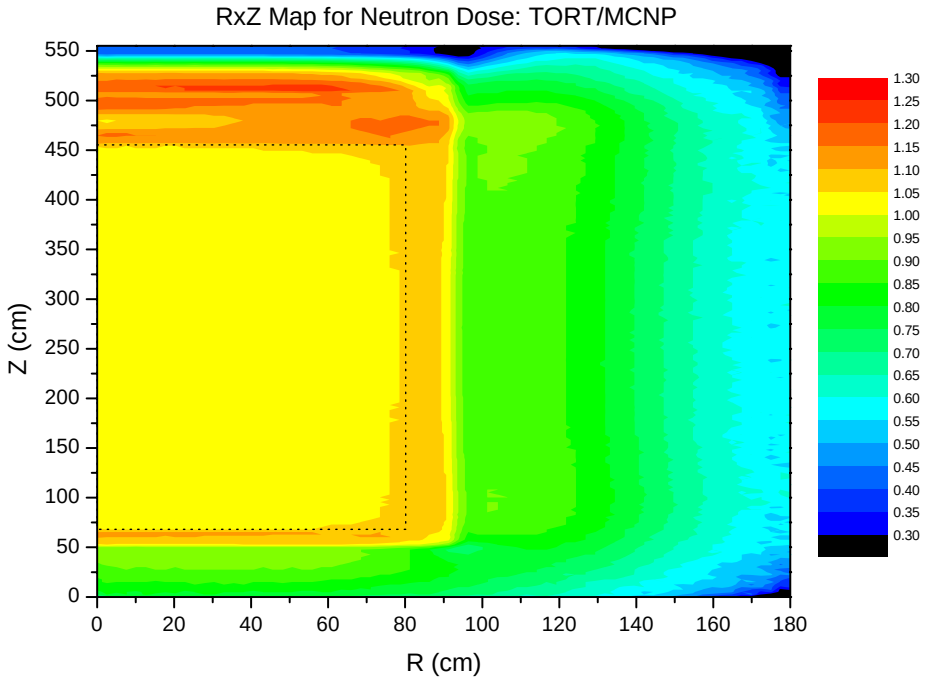

Dose Map: TORT/MCNP (Induced gamma-ray)

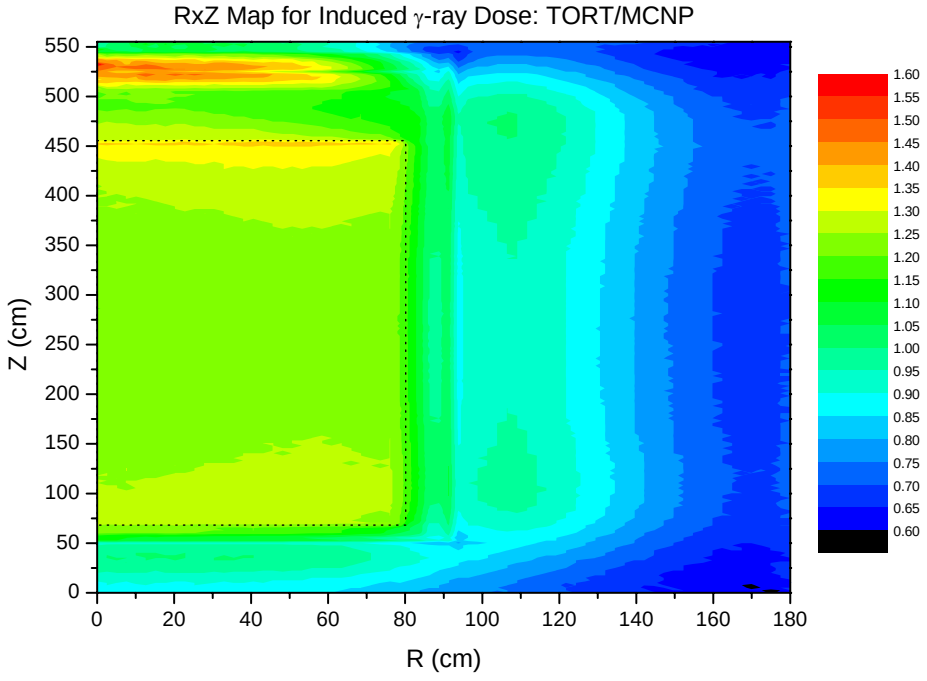

圖 6.1.3c：用過核燃料乾式貯存桶中子與引發之二次加馬射線輻射劑量空間分布圖（TORT 與 MCNP 程式計算結果的比較）。

Flux Map: TORT (Neutron: 0.82 ~ 1.00 MeV)

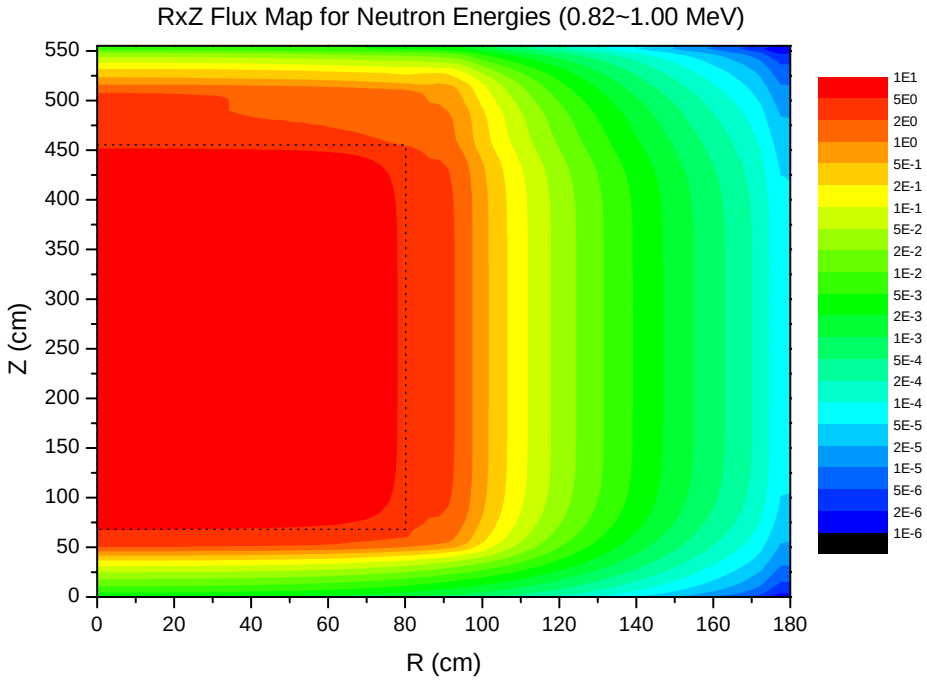

Flux Map: TORT (Induced gamma-ray: 0.8 ~ 1.0 MeV)

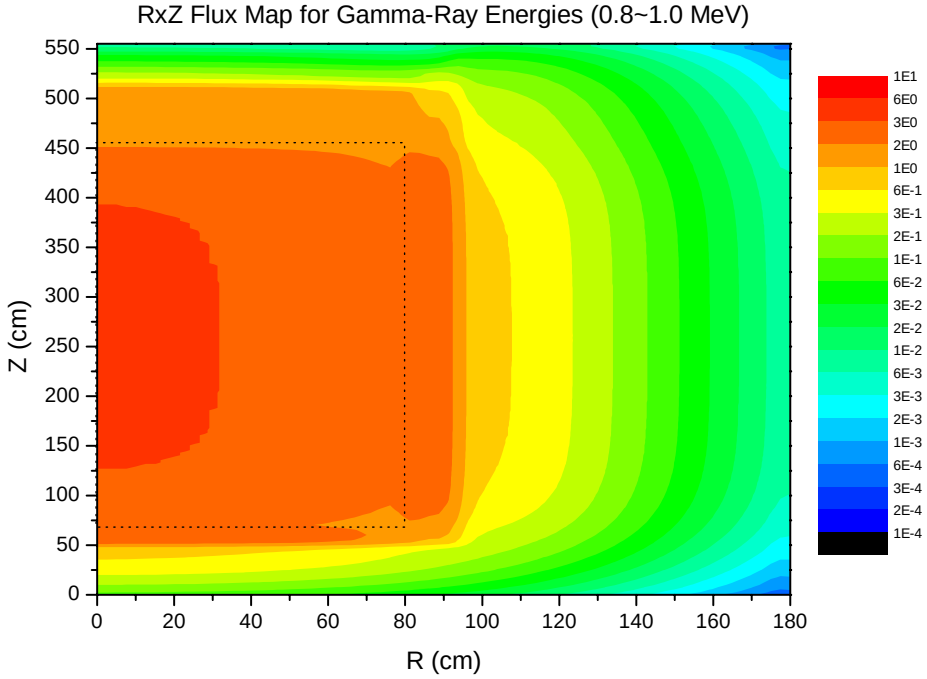

圖 6.1.3d：用過核燃料乾式貯存桶中子（0.82 ~ 1.00 MeV）與引發之二次加馬射線（0.8 ~ 1.0 MeV）通率空間分布圖。

一個很明顯的問題就是：兩種方法計算貯存桶表面劑量率有接近 50%的差異是來自什麼原因？為加深讀者的了解，我們先將上圖空間輻射劑量的結果挑選 RZ 方向各別繪圖如下：

圖 6.1.3e：TORT 與 MCNP 計算用過核燃料乾式貯存桶徑向與軸向劑量率分布圖。

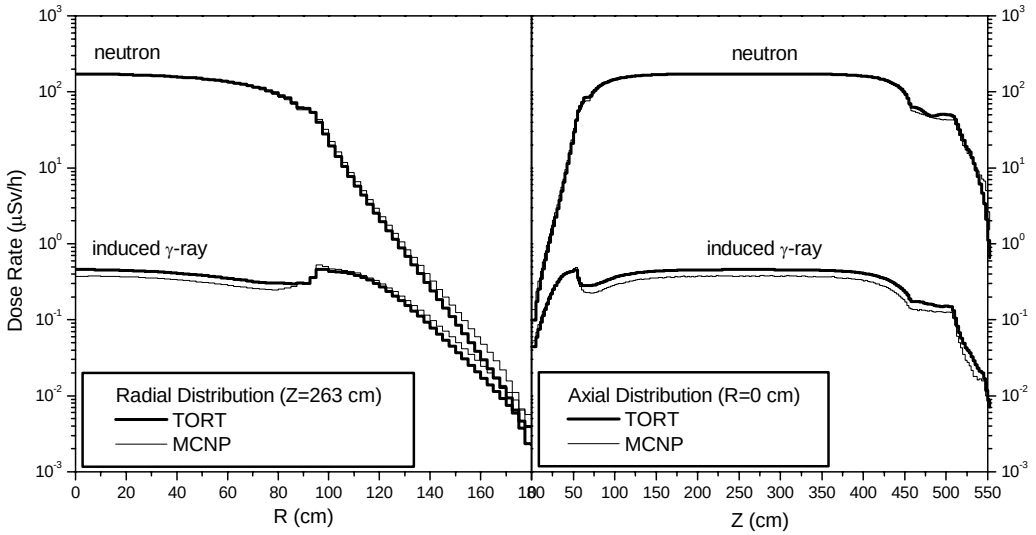

圖 6.1.3f：TORT 與 MCNP 計算用過核燃料乾式貯存桶徑向與軸向劑量率比例分布圖。

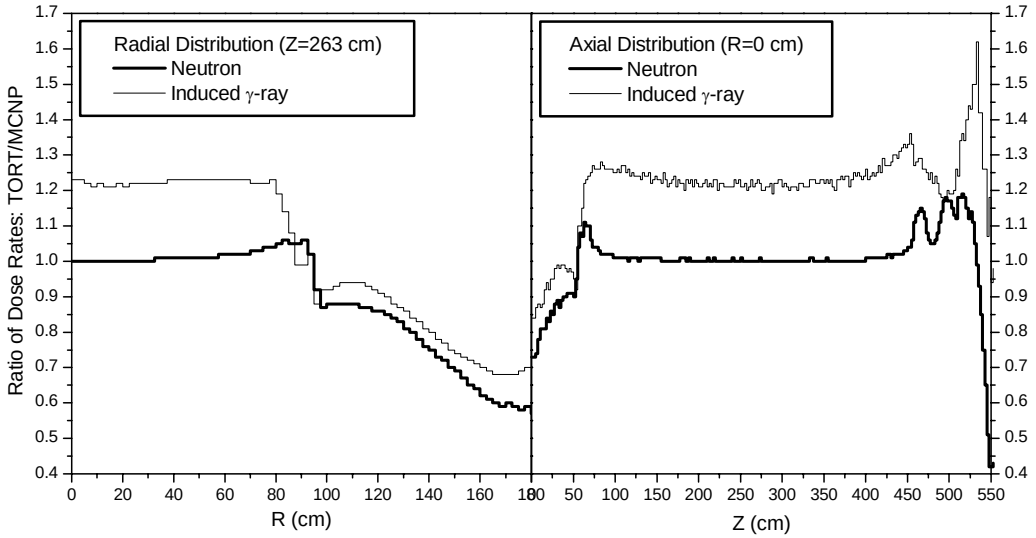

兩種方法計算的差異明顯隨屏蔽厚度增加而加大，TORT 結果傾向低估。是來自什麼原因根據文獻上的報告與我們自己針對本案例所作之研究，最大的可能原因是來自兩種方法所使用之反應截面庫的不同。MCNP 使用 continuous energy 的截面庫，無庸置疑具有最佳準確度，Discrete Ordinates Method 受限於先天限制，必須使用處理過的 Multigroup cross-section library，因此處理的過程就變得相當重要。我們撰寫一程式擷取 continuous

energy ENDF/B-VI、multigroup BUGLE-96 與 CASK-81 截面庫的中子反應總截面（本案例所使用到的核種），並將它們共同繪圖於附件二，使用者可以直接查詢看看截面的變化與不同截面庫之間的差異。在此我們並無時間與適當工具來分析截面處裡的問題，留待未來再探討。

值得注意的是，大多數分析 ISFSI 所採用的計算程式都是利用 deterministic or analytical method，例如 NAC-UMS SAR 中所採用的方式，根據文獻以及本研究的結果顯示，使用這兩種方法在 ISFSI 的分析時，比起 Monte Carlo method 的結果來說，deterministic method 通常傾向於低估最後的結果。如果使用完全相同的反應截面庫，兩種方法可能有只有 10%左右的誤差，若是使用不同的反應截面庫，則兩者之間的差距可能會超過 30%以上。通常 Monte Carlo method 搭配 continuous-energy cross sections 的結果應該是最準確可靠的，利用 deterministic method 搭配 multigroup cross sections 可能會有一定程度的低估，這對輻射安全來說是不好的傾向，必須在設計之時納入考量（可以利用額外的安全因子或是事先自行驗證）。

在這裡我們只針對中子射源及其引發加馬射線的部分進行比較，因為若是考慮加馬射線的射源，直接利用 Monte Carlo Method 無法求出可靠答案。原因在於加馬射線的平均自由徑（Mean Free Path）遠小於中子，從 TORT 計算的結果可以估計出從射源區到偵檢器加馬射線強度的衰減約為九個數量級，暗示十億個加馬射線射源才有一個會被偵檢器計數到，這種機率對於類以蒙地卡羅計算幾乎是不可能的，必須發展非常有效的變異數降低技巧不可。事實上，前面的計算我們除了比較 Deterministic Method 與 Monte Carlo Method 結果的差異之外，還有一個重要目的，就是如何利用 Deterministic Method 的結果來大幅加速 Monte Carlo Method 的計算速度，這將是下一節的主題。

6.2 變異數降低技巧

6.2.1 一般介紹

蒙地卡羅 MCNP 程式計算會將計算值歸一化至一個起始粒子所造成的結果，並且接著列出該計算值的相對統計誤差 R（定義為一個標準差比上該次計算的平均值），相對統計誤差值與粒子對於計算結果造成之貢獻有關。若進行模擬計算的案例沒有發生錯誤或是其他任何影響粒子真實行為的狀況發生時，相對統計誤差值 R 與被追蹤的粒子數 N 成開根號反比。因此，若要將相對統計誤差值減半，則總追蹤粒子數需增為原來的 4 倍。若案例設定有誤或是有影響粒子遷移行為的情況發生時，增加追蹤粒子數不一定會降低統計誤差值。

對一個蒙地卡羅計算結果而言，使用者必須依靠相對誤差值來評估該計算值的可信度，依照中央極限定理（Central Limit Theorem），當模擬的粒子數量 N 趨近無限大時，則真正的結果有 68%的機率會落在 $\tilde{x}(1 \pm R)$ 區間內，而有 95%的機率會落在 $\tilde{x}(1 \pm 2R)$ 內。值得注意的是這些信心區間所指的乃是該次蒙地卡羅計算結果本身的精確度，並非是與真實物理量相比較的準確度，若要考量準確度，則需詳細分析於案例中使用到的物理資料、模擬模型、取樣技巧以及所有近似等等。不同 R 值對於信心區間大小代表的意義如下表 6.2.1。除點偵檢器外的所有計數器，只有當其計數結果之相對統計誤差值 R 應小於 10%時，該結果才具有可靠性。點偵檢器之統計誤差變動較大，因此只有當其統計誤差值小於 5%時，該計算結果才具有可靠性。蒙地卡羅計算結果的不準確度必須與結果同時列出，才能估計該次計算的精確性。

表 6.2.1 相對誤差 R 值代表信心區間之意義。

R 值範圍	計算結果品質
0.5 ~ 1.0	無意義
0.2 ~ 0.5	參考價值低
0.1 ~ 0.2	稍具參考價值
< 0.10	可靠
< 0.05	對點偵檢器而言，是為可靠

除了計算結果的相對誤差值之外，對一個蒙地卡羅計算而言，計算效率也是非常重要的，MCNP 在輸出檔案最後的部分中會列出了每一個偵檢器的計算效率（FOM , Figure Of Merit），FOM 定義為

$$FOM = 1/(R^2 T)$$

其中 T 是計算所花費的時間。蒙地卡羅計算效率越高，可在越短的時間內得到一誤差較低的計算結果，因此 FOM 就越大。變異數（R^2）與 N 成反比，而計算時間 T 與 N 成正比，故當 N 值增加，FOM 值應趨近一個常數。使用者必須檢查 FOM 隨粒子數目增加的變化情形，並以 FOM 是否接近常數來確認計數行為是否良好。

一般而言，相對統計誤差 R 正比於 $1/\sqrt{N}$，MCNP 執行運算所耗費的時間 T 正比於進行追蹤的粒子總數 N，所以 $R = C/\sqrt{T}$，其中 C 是比例常數。由此來看，有兩個方式可以降低 R 值，一是增加計算時間 T，另一是降低比例常數 C。電腦的性能通常限制

了第一種方式，譬如計算兩小時得到結果之 R 值為 10%，那麼使用者將必需花費 200 小時才能得到誤差值為 1%的計算結果。因此，MCNP 採用一些特殊的變異數降低技巧來降低比例常數 C 值：

(1)選擇計數方式：

使用 MCNP 求取某一物理量時，可使用不同的計數方式來做計數。例如欲求取通量時，可使用碰撞估計或是粒子徑跡長度計數來取得。碰撞數計數是將材料體室內的每個碰撞記錄下來再乘上 $1/\Sigma t$ （Σt=巨觀總截面）來取得通量值，而粒子徑跡長度計數是記錄粒子行經材料體室內的路徑長度來取得通量值。如果該材料體室的 Σt 非常小時，粒子發生碰撞的數量很少。若使用碰撞計數來求取通量值，則容易導致誤差值變大的狀況發生。粒子徑跡長度計數方式是記錄每一個進入該材料體室的粒子，於該體室內所行經的路徑長度。因此，除了在估計有效增值因數 keff 以外，MCNP 使用的標準計數方式為粒子徑跡長度計數。

(2)非類比蒙地卡羅：

最簡單正確的蒙地卡羅遷移計算是使用類比的方式進行粒子遷移模擬，利用電腦對粒子生命週期中的每一個事件依其發生的自然機率來取樣，藉此取得系統中粒子的平均行為，由於這種模擬方式非常逼近真實情形，因此稱為類比蒙地卡羅模擬。只有當對計算目標貢獻高的粒子能夠被有效偵測到時，類比式蒙地卡羅計算法之效能才會很高。但一般而言在被模擬案例中，粒子對計算目標的貢獻度通常很低。在這情況下，使用類比式蒙地卡羅計算常常必需耗費大量的計算時間以求得一誤差值可接受的計算結果。儘管類比蒙地卡羅模擬在概念上非常簡單，但有其他可以獲得和類比模型相同平均結果的粒子遷移機率模型，且此模型所得答案之變異數遠小於類比模型之計算結果。因此將原本使用類比模型需耗費很長計算時間的案例，改使用非類比模型進行計算，可能僅需要一點時間即可完成。非類比模型採取的原則是花費較多的時間於追蹤"有利的"粒子，有利的粒子是指對計算結果貢獻度較大的粒子，有很多非類比的技巧可以用來增加粒子計數。為保證非類比模型之計算結果與類比模型一致，非類比模型之計算結果需修正，因此當一個粒子受人為因素影響，使其被取樣的數量變為原來的 q 倍時，該粒子造成的分數就被乘上 1/q。平均計數值是所有經亂數取樣後的機率與粒子造成結果之乘積的總和，經此調整後，非類比模型之計算結果才能保有正確性。

以下我們簡單列出 MCNP 中提供的變異降低技巧，至於詳細說明請參考附件三的使用手冊。MCNP 提供四種不同類別的變異降低技巧：

(1)截斷法：

最簡單的變異降低方法。截斷對計算目標貢獻度低之相空間內的運算，以加速整體計算的進行。此法中最簡單空間截斷方式是將不重要的幾何空間由模型中去除以加速計算的運行，在 MCNP 中可以使用的指定截斷法包含有能量及時間截斷。

(2)總數控制法：

藉由粒子分裂及俄羅斯輪盤來控制不同相空間內取樣的數量。在重要的區域中追蹤較多權重低的粒子，而在不重要的區域內則取樣追蹤少數權重高的粒子。調整權重才能確保計算結果正確。在 MCNP 中，可使用之特定的總數控制法包含有空間依存分裂/俄羅斯輪盤（space-dependent splitting/Russian roulette）、時間依存分裂/俄羅斯輪盤（time-dependent splitting/Russian roulette）、權重切斷（weight cutoff）、以及權重視窗

（weight window）。

(3)取樣修正法：

增加每個粒子的計數單位以改變案例中的統計取樣。對任何蒙地卡羅事件而言，只要粒子權重依照機率的變化來做調整，則不需依照真實的機率分佈來做取樣。利用取樣修正法從較有利的機率分佈函數中取樣，將粒子送入想要的方向或是其他需要的相空間內，如時間或是能區，或是改變碰撞的位置或型式。MCNP 中可以用到的取樣修正法包含有指數傳送（exponential transform）、隱含捕獲（implicit capture）、強制碰撞（forced collision）、射源加權偏重（source biasing），以及中子誘發光子加權偏移（neutron-induced photon production biasing）。

(4)半決定論混合法：

這是最複雜的變異降低法。此法使用類似決定論法的技巧，例如緊接事件估算，或是藉由控制亂數序列來取代正常的粒子取樣過程。在 MCNP 中，這方面的方法包括點偵檢器、DXTRAN，以及關連取樣（correlated sampling）。

正確的使用變異降低技巧可以有效的幫助使用者提高計算效率，但使用錯誤則可能會導致錯誤的計算結果。錯誤之計算結果其統計誤差可能很低，此外亦少有跡象顯示發生錯誤。有些變異降低法對一般運跑案例皆可使用，而有些則是在特定情況下才可使用。有些變異降低技巧則具有高度的專業性，任意使用會增加計算結果發生錯誤的機會。權重視窗（weight window）比重要性（imortance）更強大，但是在使用時須輸入更多資料且對問題需有深入的瞭解。對許多問題而言，變異降低技巧的使用不緊緊只是增加計算效率，而是為了得到計算結果，例如深穿透及穿管偵檢器問題，若不使用變異降低技巧則非常難以得到計算結果。

6.2.2 特殊 CADIS 理論

Consistent Adjoint Driven Importance Sampling（CADIS）是由 J. C. Wagner 與 A. Haghighat 等人所提出的一種非常有效的變異數降低技巧，包含 Source Biasing 與 Transport Biasing 兩部分。它利用 Deterministic Method 的解來達到加速 Monte Carlo Method 的目的，先由 TORT 程式進行伴隨（Adjoint）模式的計算求出整個相空間的 adjoint function，據此進而導出給 MCNP 程式使用的 biased source 與 weight windows，最後進行非類比的粒子追蹤運算，可以大幅降低統計誤差達到快速計算的目的。詳細理論推導如下：

粒子遷移計算最後所求的 response 值可由下式來表示：

$$R = \int_p \varphi(p)\,\sigma_d(p)\,dp \qquad p \in (r, E, \Omega) \tag{6.1}$$

其中 $\varphi(p)$ 是粒子於相空間(phase space) p 點的通率，$\sigma_d(p)$ 是指objective response function。根據數學上的adjoint identity

$$\left\langle \varphi^* H \varphi \right\rangle = \left\langle \varphi H^* \varphi^* \right\rangle \tag{6.2}$$

其中 H 是 adjoint operator，〈〉則表示對所有變數的積分。利用（6.2）式，可將式（6.1）改寫成

$$R = \int_p \varphi^*(p) S(p)\,dp \tag{6.3}$$

（6.3）式表示粒子遷移計算最後所求的 response 值，除了由（6.1）式來計算外，亦可經由 adjoint function $\varphi^*(p)$ 乘上射源 $S(p)$後積分來求得。由此可見 adjoint function $\varphi^*(p)$ 隱含的物理意義，就是相空間中該位置的粒子未來對最終結果 R 的預期貢獻度。MCNP 計算粒子通率時，射源粒子是對射源的真正機率分布函數進行亂數取樣。然而，可以找到另一個函數 $S^*(p)$ 來代替原本的射源函數 $S(p)$，而此替代的取樣函數 $S^*(p)$ 能提高 MCNP 的計算效率。為此，改寫（6.3）式為下列式子

$$R = \int_p \left[\frac{\varphi^*(p) S(p)}{S^*(p)} \right] S^*(p)\,dp$$

理論上能證明如果 $S^*(p)$ 取如下表示示可以得到最佳效果：

$$S^*(p) = \frac{\varphi^*(p) S(p)}{\int_p \varphi^*(p) S(p)\,dp} \tag{6.4}$$

（6.4）式顯示此新射源 $S^*(p)$ 乃是根據該位置之原來射源 $S(p)$對最終結果 R 的貢獻度來取樣，這與直覺的想法一致。依照各射源變數對於最終結果的貢獻度進行取樣，將使得最終結果的誤差值達到最低。在此同時，最終結果的期望值不能因為改變射源的機率函數而偏移，故個別射源粒子所帶有的權重（weight）需依照 $S^*(p)$ 而做調整，此調整的依據為下列式子：

$$W(p) S^*(p) = W_0(p) S(p)$$

依照上式，可以得到新射源粒子的權重為：

$$W(p) = W_0 \frac{S(p)}{S^*(p)} = \frac{\int_p \varphi^*(p) S(p)\,dp}{\varphi^*(p)} = \frac{R}{\varphi^*(p)} \tag{6.5}$$

至此，解決了新射源的取樣函數及其權重的問題。

接著考慮如何改變粒子的遷移過程以達到進一步加速的目的，粒子遷移方程式之積分型態如下：

$$\varphi(p)=\int K(p'\to p)\varphi(p')dp'+S(p)$$

未配合上述新射源形式，將上式乘上 $\dfrac{\varphi^*(p)}{\int_p \varphi^*(p)S(p)dp}$，並定義：$\bar{\varphi}(p)=\dfrac{\varphi(p)\varphi^*(p)}{\int_p \varphi^*(p)S(p)dp}$，

則上式經整理之後得

$$\bar{\varphi}(p)=\int K(p'\to p)\varphi(p')dp'\times\frac{\varphi^*(p)}{\int_p \varphi^*(p)S(p)dp}+S^*(p)$$

$$=\int K(p'\to p)\bar{\varphi}(p')\left[\frac{\varphi^*(p)}{\varphi^*(p')}\right]dp'+S^*(p) \qquad (6.6)$$

$$=\int \bar{K}(p'\to p)\bar{\varphi}(p')dp'+S^*(p)$$

其中，$\bar{K}(p)$ 是為新的 transport kernel，為原來 $K(p)$ 乘上遷移過程後與前兩個狀態間的 $\varphi^*(p)$ 值。實際模擬可以如下進行，粒子先依照原 $K(p)$ 由舊狀態遷移到新狀態，之後比對兩個狀態間的 $\varphi^*(p)$ 值，若新舊比值大於 1，則粒子會進行 Particle Splitting，若新舊比值小於 1 則進行 Russian Roulette。由於新的 transport kernel $\bar{K}(p)$ 已影響到真正的粒子遷移函數 $K(p)$，因此粒子的權重亦需配合進行調整以保持答案不變。調整的依據如下式所示：

$$W(p)K(p'\to p)\left[\frac{\varphi^*(p)}{\varphi^*(p')}\right]=W(p')K(p'\to p)$$

依照上式，則新的粒子權重為：

$$W(p)=W(p')\left[\frac{\varphi^*(p')}{\varphi^*(p)}\right] \qquad (6.7)$$

其中 $\varphi^*(p')/\varphi^*(p)$ 是為粒子於舊狀態與新狀態下，對於最後計算結果 R 的貢獻度比值。

以上的過程顯示當 MCNP 每一次進行亂數取樣時，若取樣的函數是依照該狀態對結果的貢獻大小而定，則最終計算結果 R 的誤差值將達到最小。由於在整個推導的過程中射源與遷移核心保持一致性，因此原作者將此理論稱為 Consistent Adjoint Driven Importance Sampling（CADIS）。

6.2.3 結合 TORT/MCNP 加速計算

CADIS Methodology 共包含 Source Biasing 與 Transport Biasing 兩部分，其中的 Source Biasing 可以直接利用 MCNP 所提供的 SI、SP、SB 卡片輸入來完成，至於 Transport Biasing 可以利用 MCNPP 4C 版本以後新增之 Superimposed Mesh Weight Window 來實現。

首先使用 TORT 進行 Adjoint 計算，可以得到$\varphi^*(p)$，此計算並不要求精確，我們的目的只是在於求得一個近似的解而已，依照（6.3）式可以得到最後結果 response R 的估計值。知道 R 值之後，可依照（6.4）式求得新射源的機率分布函數$S^*(p)$，而此新的$S^*(p)$即為 MCNP 的射源取樣修正的依據。另外，MCNP 允許使用者在相空間中設定能量與空間依存的所謂 weight window，如果粒子的權重落在 weight window 之內，則不對粒子作任何調整，如果粒子的權重不在 weight window 之內，則利用 Particle Splitting 或是 Russian Roulette 技巧將粒子的權重帶回 weight window 之內，此種權重控制技巧稱之 weight window technique，是一種非常有效的變異數降低技巧。利用$\varphi^*(p)$求得新射源的機率分布函數$S^*(p)$以後，接下來則需計算 weight window lower bound（W_L）的值來實現 weight window technique。為了使粒子於某一特定相空間中粒子的 weight 能夠落入該相空間對應的 weight window 中，我們使用下列式子來計算 W_L：

$$W_L(r,E)=\frac{W}{\left(\frac{C_u+1}{2}\right)}=\frac{R}{\varphi^*(r,E)}\frac{1}{\left(\frac{C_u+1}{2}\right)} \tag{6.8}$$

其中C_u是該 weight window 中 weight 上下限比值，此值在 MCNP 程式中可由使用者決定。一般而言，此值預設為 5，是指粒子進入該 weight window 後，該粒子的 weight 值須介於 W_L 至 $5W_L$ 之間，若該粒子的 weight 大於 $5W_L$，則 MCNP 會進行 Particle Splitting 讓粒子的 weight 落入該 weight window 中。相反地若粒子的 weight 小於 W_L，則 MCNP 會進行 Russian Roulette，提高粒子的 weight 至該 weight window 的範圍內。

TORT 結合 MCNP 計算流程是先使用 TORT 計算$\varphi^*(p)$後，接著求出 R 值，然後利用（6.4）式求得 biased source，以及（6.8）式求得 W_L 後，即可讓 MCNP 進行粒子追蹤計算，整體流程如圖 6.2.3 所示。利用 TORT 進行伴隨遷移計算時，必須注意下列事項：正常計算時的射源與偵檢器描述在伴隨遷移計算正好相反，粒子反應前後能量與角度關係也必須反過來解釋。因此我們也設計一個假想的偵檢器，它包含整個貯存桶在地面以上的表面區域，它的目的不在於劑量的計算，而是當作所謂的 Adjoint Source 擺設的位置，以吸引中子或加馬射線盡量往外遷移，增加實際上模擬遷移計算時粒子穿過屏蔽的機率，以達到加速 MCNP 的效果。

圖 6.2.3：TORT 結合 MCNP 之計算流程。

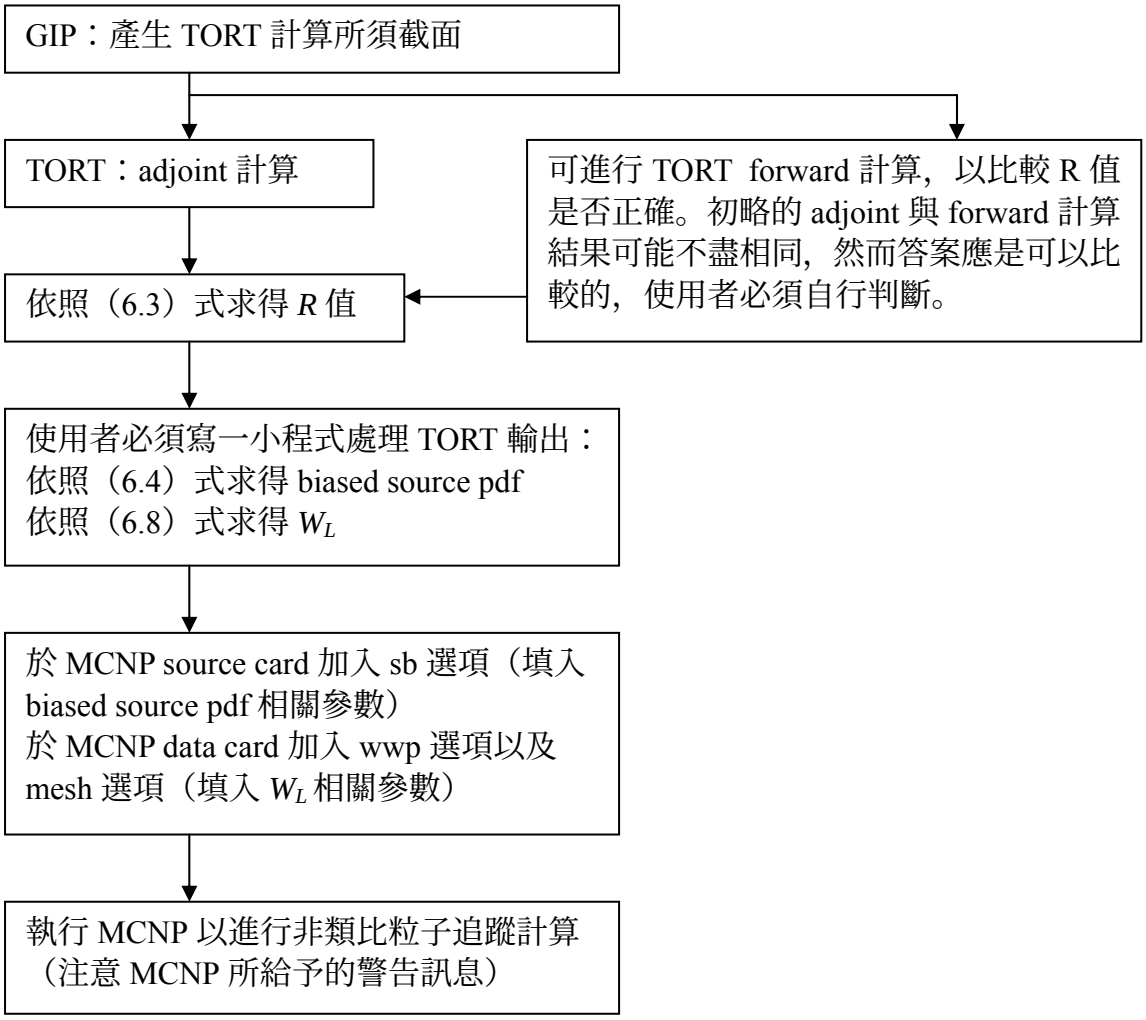

6.2.4 計算結果與比較討論

根據上一節方法的介紹，以用過核燃料乾式貯存桶假想案為參考，類比與加速之蒙地卡羅計算結果如下表所示。首先我們先列出 Deterministic Method TORT 計算的結果，從 TORT 結果的數量級來看，若是中子射源的問題，純類比之蒙地卡羅計算還不算太難，因此 TORT/MCNP 加速方法效果不是很可觀，大概只有幾十倍左右。加速效果（Speed-up）在此指的是蒙地卡羅計算結果 FOM 之比。但是若是考慮加馬射線射源，從 TORT 結果的數量級來看，純類比之蒙地卡羅計算幾乎是不可能的，再看看運用 CADIS methodology 後的蒙地卡羅運算結果，計算效率改善幅度高達十萬倍以上，這是非常驚人的改善，原本幾乎不能處理的問題一下子變成簡單的計算。這就是前面花那麼多功夫在研究 Deterministic Method 的好處，而且 Deterministic Method 的答案還可以當做一個參考，避免誤用 Variance Reduction Techniques 造成蒙地卡羅計算錯誤而不自知。

表 6.2.4 用過核燃料乾式貯存桶假想案蒙地卡羅計算結果（類比 vs. 加速）。

Detectors (μSv/h)	Side (neutron)	Side (photon)	Top (neutron)	Top (photon)	Outside (neutron)	Outside (photon)
	Uniform neutron source in fuel region (1 n/cm^3.s)					
TORT	2.32E-3	3.90E-3	6.43E-1	7.06E-3	1.95E-2	3.07E-3
MCNP (unbiased)	4.35E-3 (6.24%)	5.57E-3 (1.45%)	1.46E+0 (2.59%)	6.61E-3 (12.54%)	5.11E-2 (0.21%)	4.30E-3 (0.19%)
MCNP (CADIS)	3.89E-3 (1.63%)	5.73E-3 (2.03%)	1.49E+0 (0.60%)	7.09E-3 (9.59%)	5.00E-2 (0.11%)	4.26E-3 (0.29%)
Speed-up	50.0	1.7	62.3	5.5	12.7	1.4
	Uniform gamma-ray source in fuel region (1 r/cm^3.s)					
TORT		3.83E-9		4.62E-10		3.79E-9
MCNP (unbiased)		0.00E+0 (0.00%)		0.00E+0 (0.00%)		3.84E-9 (17.75%)
MCNP (CADIS)		5.60E-9 (0.24%)		8.85E-10 (5.83%)		4.64E-9 (0.06%)
Speed-up		N.A.		N.A.		104778

為了展示為什麼 CADIS methodology 有如此驚人的效果，我門先將它的兩大部分：Source Biasing 與 Transport Biasing 參數畫於下圖，這些參數事實上是告訴我們在整個問題相空間中那些區域是相對重要的，那些區域又是相對不重要的。其中 Source Biasing 的目的在於利用 TORT 計算的結果告訴 MCNP 如何改變射源取樣的機率分布，重要性或貢獻度高的粒子加強取樣，不重要或低貢獻度的部分省略一些以減少電腦時間。至於 Transport Biasing 則強迫粒子往重要區域遷移，相反方向則儘早結束該粒子追蹤，一樣可以大幅減少電腦時間的浪費。一致性地整合 Source Biasing 與 Transport Biasing 兩部分，如預期般可以達到非常好的效果，但是必須注意的是：使用者如何正確地判斷那些粒子或區域是重要，又那些是可省略的，沒有 Deterministic Method 計算的結果是很難做到的。我們的結論是，雖然 TORT/MCNP 整合計算方式有一點複雜，也有很多事情使用者必須自行處理，但是考慮到計算結果互相驗證與大幅加速蒙地卡羅運算的效果，絕對值得投入時間與經費來發展，因為有借重快速的計算方法，才能夠做好安全分析報告中必須的 Uncertainty and Sensitivity Analysis，因為它們是 QA/QC 的重要部份。附件三中我們列出 Unbiased 與 CADIS-biased 計算案例的 MCNP 輸入檔做為參考。

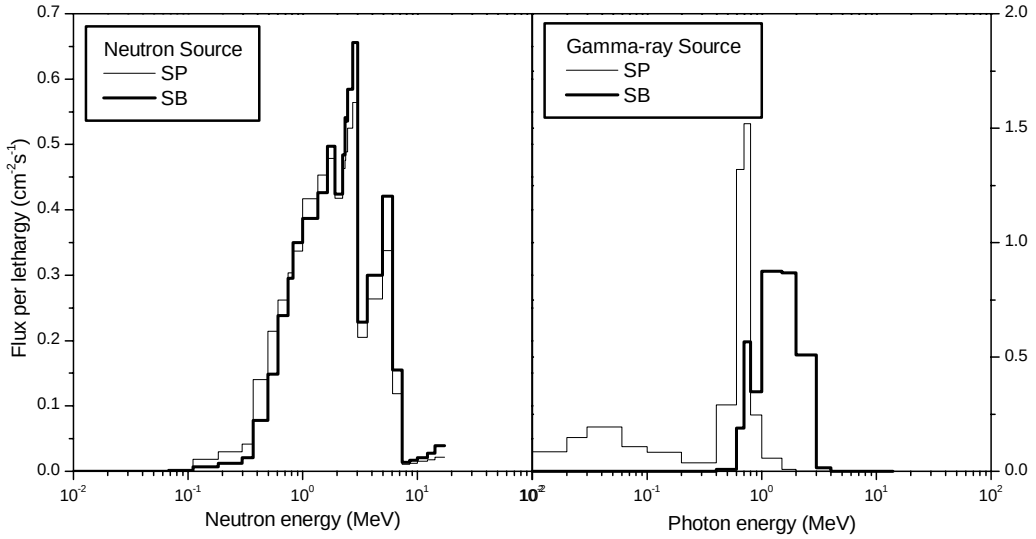

圖 6.2.4a 運用 CADIS methodology 於 MCNP 計算（Source Biasing）。

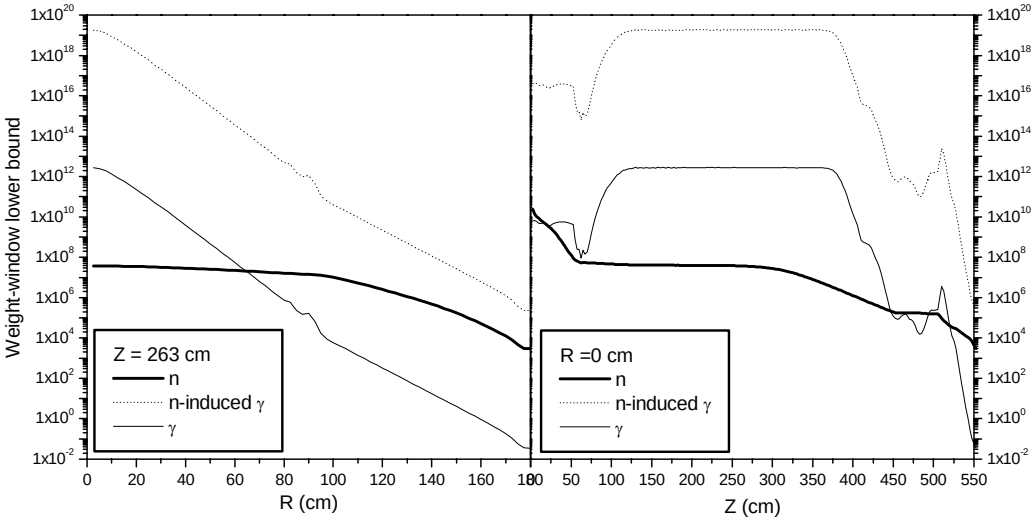

圖 6.2.4b 運用 CADIS methodology 於 MCNP 計算（Transport Biasing）。

6.3 審查注意要點

根據本研究進行過程與其結果所獲得的經驗，我們提出下列幾點作為未來審查用過核燃料乾式貯存設施安全分析報告中類似計算所應特別注意的事項：

1. 如果採用 Deterministic Method (Discrete Ordinates)，必須詳細交代反應截面庫的內容（例如：data source、group structure、collapsing weighting function、self-shielding effect、Legendre expansion order P_L），也必須測試各種數值選項可能造成的影響（spatial mesh size、directional quadrature order、multidimensional effect、flux-sweeping formulation）。
2. 如果採用 Monte Carlo Method，則必須著重在誤差與收斂分析，特別是所使用之變異數降低技巧（Variance Reduction Techniques）及其相關參數的靈敏度分析，最好使用最新的 continuous-energy cross sections。
3. 個別來源的射源及其可能引發之二次輻射也必須考慮進去。
4. 由於預期核研所將要採取的計算方法與 NAC-UMS SAR 會有明顯不同，而且核研所也會對 Transfer or Storage Cask 做一些修改或輻射屏蔽的加強，如果直接用不同的方法套用在不同幾何形狀問題上，最後的結果要驗證可能難度較高，建議先利用準備使用的方法應用在與 NAC-UMS 相同的問題上，這樣結果可以互相比較，也可以當做方法與能力驗證的一部分。
5. 大多數分析 ISFSI 所採用的計算程式都是利用 Deterministic method，例如 NAC-UMS SAR 中所採用的方式，另一種不同的輻射遷移計算方法是所謂的 Monte Carlo method，根據文獻以及本研究的結果顯示，使用這兩種方法在 ISFSI 的分析時，比起 Monte Carlo method 的結果來說，Deterministic method 通常傾向於低估最後的結果。如果使用完全相同的反應截面庫，兩種方法可能有只有 10%左右的誤差，若是使用不同的反應截面庫，則兩者之間的差距可能會超過 30%以上。通常 Monte Carlo method 搭配 continuous-energy cross sections 的結果應該是最準確可靠的，利用 Deterministic method 搭配 multigroup cross sections 可能會有一定程度的低估，這對輻射安全來說是不好的傾向，必須在設計之時納入考量（可以利用額外的安全因子或是事先自行驗證）。
6. 不管是採用那一種方法從事安全分析報告，Uncertainty & Sensitivity Studies 都是非常重要也是必須的，Uncertainty & Sensitivity Studies 包括的範圍是非常廣的，例如 source、geometry、detector、physics and numerical models 等等。特別若是利用 Monte Carlo method，如何分析變異數降低技巧對於計算結果的可能影響是一個很重要的問題。
7. 上述第 5 和第 6 點好像有點衝突，事實上是因為它們各有優缺點，在此特別說明一下：通常 Monte Carlo method 搭配 continuous-energy cross sections 的結果應該是最準確可靠的，這句話通常是正確的，前提是使用的變異數降低技巧要正確，在沒有使用變異數降低技巧的情況下，Monte Carlo method 是相當直接單純的，不像 Deterministic Method 有大多的數值參數需要有相當經驗才能掌握，因此學術上一般認為它是是最準確可靠的計算方法，非常適合用來做重要問題最後的 Benchmark。
8. Monte Carlo method 最大的缺點在於非常耗時，有很多實際的問題即使電腦再快也算不出來，本案例就是非常好的例子，非得引進有效的異數降低技巧不可，如何正確設定相關參數完全看使用者的經驗與能力了，使用的不恰當，可能只有影響計算

效率，更嚴重一點，連最後答案也會被導向錯誤的方向，這部分的問題不太像是使用者輸入方面的錯誤，事實上是非常難發現的，因此對於這部分結果的驗證或是 QA/QC 就相當重要了。

9. 在本研究中，我們同時採取 Deterministic method 與 Monte Carlo method，還使用幾種不同的程式配合一些重要參數變化的研究，它們之間除了互相驗證，還可輔助大幅改善計算效率，這樣一來出錯的機率微乎其微，應是一個值得建議的方法。

6.4 程式使用手冊

配合本研究需求，我們從原版英文 MCNP manual 中摘錄相關部分翻譯成中文簡易使用手冊，詳見附件三，使用手冊目錄如下所列。

7. 結論

本計畫之目的為提升用過核燃料乾式貯存設施安全分析報告中有關輻射屏蔽計算部分的審查與驗證能力。針對這個主要目標出發，我們詳細瀏覽與研究文獻上相關資料，探討可能運用於用過核燃料乾式貯存設施輻射屏蔽計算的技術與方法，利用一個假想的參考案例來測試可能的方法並發展最佳之解決方案。

本計畫完成之工作項目及具體成果簡單總結如下：

(1) 建立一個用過核燃料乾式貯存設施參考案例模型，它包含了所有計算上應該考慮的重要特徵（例如射源分布範圍大而且屏蔽尺寸厚），並且足夠簡化以測試大部分可能用到的計算工具。

(2) 輻射遷移計算方法上主要有兩大類：Deterministic Method 與 Monte Carlo Method。在 Deterministic Method 計算工具上我們測試了以下的程式：一維 ANISN、二維 DORT 與三維 TORT；在 Monte Carlo Method 計算工具上，我們選用目前最新的 MCNP5 程式。

(3) 不管使用那一種方法，事實上輻射遷移計算最重要的部分是反應截面庫，在 Deterministic Method 計算上我們採用 American Nuclear Society 目前建議的 multigroup BUGLE-96 截面庫；在 Monte Carlo Method 計算上，我們則選用目前公認最好的 continuous energy ENDF/B-VI 截面庫。

(4) 利用上述所介紹的計算工具與截面庫，我們分別完成參考案例模型之輻射屏蔽計算，並將所得結果作比較分析與檢討。

(5) 要詳細比較不同計算方法搭配不同反應截面庫所得的結果並不單純，本案例針對的是 Deterministic Method（Multigroup Cross Sections）與 Monte Carlo Method（Continuous Energy Cross Sections）結果的比較。可能造成差異的原因非常多，例如：Angular Mesh Distribution、Spatial Mesh Distribution、Multigroup Cross-Section Library、Multidimensionality Effect、Material Homogenization 等等，需要一一澄清分析，這部分的結果對未來從事相關計算可以提供很好的參考。

(6) 使用不同的工具與選項來處理同樣的問題，最大的好處就是互相驗證，分析它們之間的差異並找出可能原因，這是一個可靠的安全分析報告所必經的步驟。我們還可進一步互相利用不同方法彼此的優點，大幅改善蒙地卡羅模擬計算的效率，除了將原來非常困難的問題變為可行之外，對於最後答案的品質也將非常有信心。

(7) 整合 Deterministic Method 與 Monte Carlo Method，發展適用於用過核燃料乾式貯存設施輻射屏蔽計算的變異數降低技巧，可以達到非常有效（超過幾個數量級）加速蒙地卡羅模擬計算並確保結果的正確性。

(8) 建立蒙地卡羅程式（MCNP, version 5, parch 1.30）使用手冊，詳細說明參考案例中相關的程式輸入、輸出與執行步驟，強化研究人員乾式貯存設施輻射屏蔽平行驗證計算之能力，有效提升輻射屏蔽審查品質。

(9) 建立用過核燃料乾式貯存設施安全分析報告（SAR）輻射屏蔽相關審查注意要點，以利未來審查工作的進行。

(10) 本計畫的成果除了可協助審查核一廠用過核燃料乾式貯存設施輻射屏蔽安全分析報告之外，亦可為未來相關設施安全審查建立基礎，有效落實用過核燃料乾式貯存技術之本土化。

8. 參考文獻

中文資料：

1. 蔡春鴻、鄧希平、開執中、施存寬、江祥輝、歐陽敏盛，核一廠用過燃料中期貯存設施安全分析報告先期審查研究，行政院原子能委員會放射性物料管理局委託研究計畫研究報告 892001FCMA2003。
2. 蔡瑞燦、廖俐毅，核一廠用過燃料中期貯存設施之核臨界安全、熱傳與廠界輻射劑量驗算模式建立，行政院原子能委員會放射性物料管理局委託研究計畫研究報告 902001FCMA001。

英文資料：

1. A. Haghighat, J.C. Wagner, "Monte Carlo Variance Reduction with Deterministic Importance Functions," Progr. Nucl. Energy, 42, 25-53 (2003).
2. J.C. Wagner, A. Haghighat, "Automated Variance Reduction of Monte Carlo Shielding Calculations using the Discrete Ordinates Adjoint Function," Nucl. Sci. Eng. 128, 186-208 (1998).
3. J.C. Wagner, A. Haghighat, "A3MCNP: Automated Adjoint Accelerated MCNP. User's Manual, Version 1.0i," H&S Advanced Computing Technologies Corporation (2000).
4. J.F. Briesmeister, Ed., "MCNP - A General Purpose Monte Carlo N-particle Transport Code, version 4C," Los Alamos National Laboratory, LA-13709-M (2000).
5. "DOORS3.2: One-, Two- and Three-Dimensional Discrete Ordinate Neutron/Photon Transport Code System," RSICC Code Package CCC-650, Oak Ridge National Laboratory (1998).
6. International Commission on Radiological Protection, "Conversion coefficients for use in radiological protection against external radiation," ICRP Publication 74, Ann ICRP 26(3/4) (1996).
7. "BUGLE-96: Coupled 47 Neutron, 20 Gamma-ray Group Cross-section Library Derived from ENDF/B-VI for LWR Shielding and Pressure Vessel Dosimetry Applications," RSICC Data Library DLC-185, Oak Ridge National Laboratory (1996).
8. W.W. Engle, Jr., "ANISN, A One-Dimensional Discrete Ordinates Transport Code with Anisotropic Scattering," Oak Ridge National Laboratory, K-1693 (1967).
9. W.A. Rhoades, R.L. Childs, "An Updated Version of the DOT-4 One- and Two-Dimensional Neutron/Photon Transport Code," Oak Ridge National Laboratory, ORNL-5851 (1982).
10. W.A. Rhoades, D.B. Simpson, "The TORT Three-Dimensional Discrete Ordinates Neutron/Photon Transport Code," Oak Ridge National Laboratory, ORNL/TM-13221 (1997).
11. D. Shedlock, A. Haghighat, "Neutron Analysis of Spent Fuel Storage Installation using Parallel Computer and Advance Discrete Ordinates and Monte Carlo Techniques," presented at 10th Int. Conf. Radiation Shielding and 13th Topical Meeting on Radiation Protection and Shielding, Funchal, Madeira Island, Portugal (2004).
12. J.C. Wagner, A. Haghighat, "Monte Carlo Transport Calculations and Analysis for Reactor Pressure Vessel Neutron Fluence," Nucl. Technol., 114, 373-398 (1996).

13. B.G. Petrovic, A. Haghighat, “Effects of SN Method Numerics on Pressure Vessel Neutron Fluence Calculations,” Nucl. Sci. Eng. 122, 167-193 (1996).
14. R.J. Sheu, R.D. Sheu, S.H. Jiang, C.H. Kao, “Adjoint Acceleration of Monte Carlo Simulations using TORT/MCNP Coupling Approach : A Case Study on the Shielding Improvement for the Cyclotron Room of the Buddhist Tzu Chi General Hospital,” Radiat. Prot. Dosim., 113, 140-151 (2005).

9. 附件一：投稿論文

Manuscript entitled “Comparisons of Shielding Calculations for a Spent Fuel Storage Cask using Deterministic, Monte Carlo and Hybrid Methods”
Extended abstract submitted to The American Nuclear Society’s 14th Biennial Topical Meeting of the Radiation Protection and Shielding Division, Carlsbad New Mexico, USA. April 3-6, 2006

Draft (November 28, 2005)

Comparisons of Shielding Calculations for a Spent Fuel Storage Cask using Deterministic, Monte Carlo and Hybrid Methods

R. J. Sheu[1], A. Y. Chen[2], J. Liu[1], Y-W H. Liu[2]

[1]*National Synchrotron Radiation Research Center, Hsinchu Science Park, Hsinchu, Taiwan, ROC*
(srj@nsrrc.org.tw)
[2]*Department of Engineering and System Science, National Tsing Hua University, Hsinchu, Taiwan, ROC*

ABSTRACT

In this study, deterministic and Monte Carlo methods were applied to solve the radiation transport problem for a simplified spent fuel storage cask considering neutron and gamma-ray sources. The results were compared and the causes for their differences were investigated. In addition, the hybrid method based on the Consistent Adjoint Driven Importance Sampling (CADIS) methodology has been used to accelerate the Monte Carlo simulations. The CADIS utilizes a deterministic adjoint function for the variance reduction through the source biasing and consistent transport biasing. The problem encountered and its possible solution for applying the source biasing in such a large volume source was described. Compared with the unbiased case, the computational efficiency was improved by more than a factor of ten for neutron source problem; and the efficiency was increased significantly by about five orders of magnitude for gamma-ray source problem. It demonstrated that the biasing scheme applied here is very effective in the shielding calculations for spent fuel storage cask using Monte Carlo method.

INTRODUCTION

The purpose of this study is to enhance the abilities to review and verify the radiation shielding calculation in the design of the Independent Spent Fuel Storage Installation (ISFSI) at the Chin-Shan site where the first nuclear power plant in Taiwan is located. The shielding design of the ISFSI consists of two parts, namely, the shielding design of the spent fuel casks and the shielding design or dose analysis of the storage site. According to the preliminary proposal of Taiwan Power Company, Monte Carlo method was expected to be used mostly in the shielding calculation for the spent fuel storage cask. Monte Carlo method is considered to be the most accurate method presently available for solving radiation transport problems. The great advantage of using Monte Carlo method is no need of constructing space-energy-angle grids for problem modeling and hence no discretization errors are introduced. However, it is extremely time-consuming especially when huge attenuation process from source to detector is involved. To make a difficult Monte Carlo shielding calculation computationally practical or possible, variance reduction techniques are indispensable in most cases and must be used with great care because it may lead to an unreliable or wrong answer if not used properly.

Deterministic and Monte Carlo methods are two distinct approaches that have been developed to solve the radiation transport problem for several decades. Depending on the problem to solve, each method has its own strengths and weaknesses. They are fundamentally different in many aspects but could be used together in a complementary manner. Hybrid deterministic/Monte Carlo method usually makes use of the knowledge of deterministic adjoint function to bias the random walk sampling in Monte Carlo simulation. A review article by Haghighat and Wagner [1] pointed out that recent trends in advanced Monte Carlo code development have reflected a recognition of the benefits of using deterministic adjoint functions for Monte Carlo variance reduction. The adjoint function refers to a particle property, which is the expected contribution or "importance" of a particle with respect to a user-defined objective. This physical meaning makes the adjoint function well-suited to the variance reduction of Monte Carlo simulations. Based on deterministic adjoint functions, Wagner and Haghighat developed the CADIS methodology (Consistent Adjoint Driven Importance Sampling) [1,2] and the A^{3}MCNP code (Automated Adjoint Accelerated MCNP) [3] for complete automation of variance reduction for MCNP [4] shielding/fixed-source calculations. However, as described in the user's manual, the present version of A^{3}MCNP is only capable of calculating biased source distributions and weight-window bounds properly for point, surface, and volume sources defined by points. Replacing the actual source by an equivalent point-wise distribution is not always a good idea especially for a large volume source. In such a case, A^{3}MCNP may use thousands of equivalent point sources or even more to approximate to the biased distribution of the volume source. It could be a good approximation but the consumption of computer memory and the file length of MCNP input will increase significantly. In order to work around this restriction and to exploit the new features of the latest version of MCNP as well as to offer a great deal of flexibility, we therefore adopted a manual coupling approach of the discrete ordinates (S_N) and MCNP codes to implement the CADIS methodology for accelerating the Monte Carlo simulations.

In addition to use the deterministic adjoint solution for the purpose of variance reduction, we also compare results both from deterministic and Monte Carlo forward transport calculations for this simplified case. We know that it is not easy to make a reliable comparison between continuous energy Monte Carlo simulation and multigroup deterministic calculation. There are many possible uncertainties associated with phase-space discretization that is inherent in deterministic calculations. However, the Monte Carlo simulation is relatively straightforward both in physics and geometry modeling and the result is considered to be the reference from which the deterministic results will be evaluated. Here we do our best to make the comparison trustworthy by repeating a series of deterministic calculations using different discrete ordinates codes and with various numerical options.

PROBLEM DESCRIPTION

The calculational model for a spent fuel storage cask used in this study has been simplified to great extent to facilitate the calculations using various computer codes and the inter-comparison of the results afterward. Two types of neutral particle transport code system were used here, one is the deterministic code package DOORS [5] and the other is the Monte Carlo code MCNP. The storage cask made of iron liners and concrete shield is about 5.5 m high and 3.6 m in diameter. Effective source region inside is about 3.9 m high and 1.6 m in diameter. This thick shielding with large source volume presents difficulties for both S_N and Monte Carlo calculations. Fig. 1 shows the geometry and dimensions of this simplified spent fuel storage cask. The compositions of materials are listed in table 1. Neutron or gamma-ray sources were assumed to be uniformly distributed in the homogenized fuel region and the volumetric source strength was arbitrarily assigned to be one neutron or gamma-ray emitted per centimeter cube per second. The source spectrum of neutron or gamma-ray refers to a research report of FCMA [6]. Two volume detectors, placed on the top and around the side of the cask as shown in Fig. 1, were used to score the neutron and gamma-ray fluence rates and to estimate the resulting dose rates after multiplying fluence-to-dose conversion factors [7]. Another pseudo outside detector covering the entire surface above the ground was arranged to count the number of particles leaving the cask and put the adjoint source for developing biasing scheme, i.e. guiding particles to move as outward as possible to increase the number of particles having a chance to penetrate the thick shielding of the cask.

CALCULATION METHODS

Discrete Ordinates Calculation

The discrete ordinates code system DOORS version 3.2 with the BUGLE-96 [8] multigroup cross-section library was used to solve this fixed source shielding problem both in forward and adjoint modes. The DOORS software package includes the ANISN [9], DORT [10] and TORT [11] codes for one-, two- and three-dimensional S_N neutron/photon transport calculations, respectively. Because of θ-symmetry in this simplified cask model, the S_N calculations could be performed using the TORT model (R-θ-Z with only one interval for θ-dimension) and the DORT model (R-Z), respectively. For TORT calculations in this case, using R-θ-Z geometry (ingeom=1) actually gives the same answer as that using degenerated R-Z geometry (ingeom=11), but of course three-dimensional calculation takes more computer time. In one-dimensional ANISN calculations, infinite cylindrical geometry for R-dimension modeling should be a good approximation for the side detector of the cask; however infinite slab geometry for Z-dimension is obviously inappropriate for the top detector. For simplicity we further assumed that the spatial discretization employed a uniform mesh distribution with all R and Z intervals equal to Δs. Theta-weighted differencing scheme is the best method for flux-sweeping formulation in curved geometry, since the nodal and characteristic procedures are presently available only in XYZ geometry. In addition to the default value 0.9, other theta values were also used to test its sensitivity on results. The computational cost of S_N method is generally negligible compared to that of Monte Carlo method. However, using S_N method to solve radiation transport problem requires approximations on spatial, angular and energy variables. In this study, we evaluated the effects caused by three possible parameters: mesh size Δs for spatial discretization, directional quadrature order for angular discretization, and the Legendre expansion order for multigroup cross sections. The effects of multigroup cross sections for each material were also examined one by one through comparisons with the results predicted by Monte Carlo simulations using continuous energy cross sections.

Monte Carlo Simulation

The Monte Carlo code MCNP version 5 with the ENDF/B-VI continuous energy cross-section library was used to solve the same problem. The arrangement of geometry, materials and detectors were modeled identically as that in previous S_N calculation. Single cylindrical cell defines the effective fuel region. The source distribution in this volumetric cell was modeled by the form

$$S(r,z,E) = R(r)Z(z)\varepsilon(E) \quad (1)$$

which sampling three independent probability density functions with respect to the source positions in radial and axial directions as well as the source energies. In addition to the top, side, and pseudo outside detectors as described above, we also used superimposed mesh tally in MCNP to score dose distribution over the system for a detailed comparison with S_N results. All tallies are based on a track-length estimate of the cell-average flux over a particular volume. According to the results of S_N calculations, the maximal dose attenuation from source to detector is about five orders of magnitude for neutron transport and roughly eight orders of magnitude for gamma-ray transport. Although it will take a lot of computer time and the statistical uncertainty may be large, we still try to get a set of unbiased answers to provide the comparison basis for checking the convergence and measuring the speed-up of various biased runs afterward.

Hybrid Method

For accelerating the Monte Carlo simulations, we adopted a manual coupling approach of the TORT and MCNP codes to implement the CADIS methodology. The CADIS utilizes an S_N adjoint flux for the variance reduction through the source biasing and consistent transport biasing. The biased source probability density function is given by

$$S_B(r,z,E) = \phi^+(r,z,E)S(r,z,E)/R \tag{2}$$

where R in is an estimate of the final result, namely the total detector response. The biased transport process could be easily implemented by using the superimposed mesh weight window facility in MCNP after version 4C. The space- and energy-dependent weight-window lower bounds w_L are given by

$$w_L(r,z,E) = R/\phi^+(r,z,E)\times 3 \tag{3}$$

where the parameter 3 in denominator makes the weights of source particles right at the center of their corresponding weight-window intervals (default ratio of upper and lower weight-window values is 5). The implementation of transport biasing in this case is no problem, however, the source biasing is not straightforward. The major difficulty is how to sample the source variables correctly and effectively from the biased source distribution for such a large volumetric source according to Eq. 2. To keep the input file as simple and clear as possible, our approach was based on the assumption that the S_N adjoint flux distribution in source region could be separated into or roughly approximated by a product of three independent functions for each variable as given by

$$\phi^+(r,z,E) \approx \phi_R^+(r)\phi_Z^+(z)\phi_\varepsilon^+(E) \tag{4}$$

The biased source distribution in Eq. 2 can then be rewritten as given below

$$S_B(r,z,E) \approx R_B(r)Z_B(z)\varepsilon_B(E)/R \tag{5}$$

$$R_B(r) = \phi_R^+(r)R(r),\ Z_B(z) = \phi_Z^+(z)Z(z),\ \varepsilon_B(E) = \phi_\varepsilon^+(E)\varepsilon(E) \tag{6}$$

Since the biased source distribution now is also a product of three independent functions, it could be simply specified on three sets of SIn, SPn and SBn cards in MCNP input as a general volumetric source. The SIn card specifies the range of source variable, the SPn and SBn cards specify the original and biased source distribution, respectively. If the previous assumption is good enough, the resulting weights of source particles should be within the corresponding weight windows as desired. However, given Eq. 4 is true, how to construct the three functions in the right-hand side is another issue that requires more studies to resolve. As a preliminary test by intuitional thought, the radial dependence $\phi_R^+(r)$ in Eq. 4 was obtained by averaging total neutron or gamma-ray adjoint flux over the axial distribution in fuel region, and vice versa for $\phi_Z^+(z)$. The energy dependence $\phi_\varepsilon^+(E)$ was obtained by averaging adjoint flux over the entire fuel region. These three adjoint functions were then used to adjust their corresponding original source probability density functions, separately. The computational efficiency was finally compared using the concept of Figure-Of-Merit (FOM), defined as the reciprocal of the product of relative error squared and computer time.

RESULTS AND DISCUSSION

Comparison of Results Calculated by S_N and MCNP Codes

Table 2 shows the neutron and induced gamma-ray doses for the storage cask calculated using MCNP and DOORS code systems. The S_N calculations were carried out using different codes with various input options. The results of TORT calculations in adjoint mode are in consistence with those in forward mode as expected. The differences between the TORT and MCNP results seem unexpectedly large [12]. The MCNP results are considered to be more accurate since continuous energy cross-section library was used and no intentional biasing was applied. In a comparison of results between S_N and Monte Carlo methods, there are several possible sources of uncertainty in S_N calculations such as: the multigroup cross sections, the multidimensionality effect,

the discretization errors in spatial and angular meshes, and the choice of various numerical options [13,14]. Examining the S_N results with different input options reveals that neither the size of spatial meshes, Legendre expansion truncation or directional quadrature order are the essential causes for such a difference. Other numerical options such as differencing schemes, convergence criteria, acceleration methods and scattering source fixup are also tested, but the results seem rather insensitive. Some of these S_N results are also listed in Table 2 for comparison. If all the materials in the problem were removed from the calculational model, the S_N and Monte Carlo methods indeed gave identical results ($\leq$1%). This comparison has excluded many possible uncertainties associated with the modeling of source, geometry and detectors. Although the 1-D ANSIN calculations in Z-dimension are obviously not appropriate in this case, the results in R-dimension are reliable and could be considered as an upper limit of the S_N results since no buckling correction was applied. Except for that, all the S_N calculations with the same cross sections yield similar results as shown in Table 2 but they predict only half of the MCNP-calculated results for neutron dose rates outside the cask. Therefore, we expect large portion of this discrepancy to be associated with the multigroup cross sections because the BUGLE-96 library is not prepared for this particular application. More detailed comparison between the TORT and MCNP-calculated results are shown in Figs. 2 and 3. Fig. 2 compares radial and axial dose rate distributions for both neutron and induced gamma-ray; and Fig. 3 shows the distributions of the ratios (TORT/MCNP) to provide a better visualization of the magnitude and behavior of the differences. For neutron dose rate, the differences between them are negligible in the source region and gradually increasing as neutrons travel through the cask shielding. TORT predicts more induced gamma-ray dose rates about 20% in the source region than MCNP.

Our sensitivity analyses of materials indicated that the multigroup cross sections should be responsible for the majority of the discrepancies. Further comparison of the neutron spectra calculated by TORT and MCNP could obtain some insight into the differences between them. Fig. 4 shows the neutron energy spectra both at the side and top detectors. For the side detector where concrete is the major shielding material, lots of neutrons from source region are thermalized and the very sharp peak at 2.35 MeV in the spectra is obviously resulted from the cross-section window of ^{16}O at that energy (left-hand side of Fig. 5). The most significant difference between TORT and MCNP-calculated spectra at this position occurs in the thermal energy region. Thermal neurons are important and account for about 25%(TORT) or 35%(MCNP) of the total dose at the side detector. Our study indicated that the oxygen and hydrogen are the most critical isotopes that contribute to the difference. For the top detector where iron is the main shielding material, the spectrum is hard and there is nearly no thermal neutron due to the lack of materials for neutron moderation in this direction. The most pronounced peak in the spectra is the consequence of the very deep cross-section window of iron at 24.5 keV (right-hand side of Fig. 5). There exists evident discrepancy in the energy region between about 0.02 and 2 MeV, where corresponding to the dense resonance region of iron. This discrepancy suggested that the iron group cross sections in that region do not well represent the real interaction cross-section. Since both multigroup and continuous energy cross sections used here were all derived from the ENDF/B-VI library, the problem should be directly related to the process of how the broad-group cross sections were obtained, such as the choice of group structure and weighting function as well as the treatment of self-shielding effects. We are planning to perform a multigroup MCNP simulation with BUGLE-96 library and that would be helpful to clarify some issues. Nevertheless, the S_N calculations with BUGLE-96 cross-section library might lead to a considerable underestimation of the dose rates outside a cask. One should be aware of or cautious with the use of broad-group cross sections in the shielding calculation for a spent fuel storage cask. Numerous issues related to a precise comparison between S_N and Monte Carlo methods remain unresolved here, however, the accuracies of the S_N solutions at this stage are already good enough for us to develop the biasing parameters for subsequent Monte Carlo simulations.

Source and Transport Biasing Parameters

The CADIS performs both source biasing and transport biasing to reduce the variance of Monte Carlo calculations. The parameters for source biasing and transport biasing were derived from the information of TORT-calculated adjoint flux. In principle, the more accurate the adjoint flux, the more efficient the variance reduction, at the cost of both more execution time and memory space required for S_N calculation. As discussed in previous section, the adjoint flux in this case could be considered as a good approximation. Therefore, we can expect that the computational efficiency of the biased Monte Carlo simulation should be very effective. Fig. 6 shows the source energy distributions before and after biasing. The neutron source spectra do not change much, but the gamma-ray source spectra alter significantly. It means that the dependence of neutron source energy is not so important. On the contrary, the source particles in the high-energy tail of gamma-ray spectrum were forced to sample more frequently to increase the probability of penetrating thick shield to make contribution. Regarding to transport biasing, Fig. 7 shows one of the typical set of radial and axial distributions of weight-window lower bounds for neutron and gamma-ray with energies around 1 MeV. The lower the weight-window lower bound the more important the region contributes to the objective. The weight-window profile also shows us how hard for an individual particle history having a change to penetrate the thick shield. Clearly, the particle transport process from source region to outside detector involves several orders of

magnitude attenuation, in particular for gamma-ray transport. Without very effective biasing, it is almost impossible to keep gamma rays survive during its transport process till leaking out of the cask, nonetheless to say having a chance to hit the desired detectors to make contribution. However, with the help of these weight-window bounds covering over the whole phase space, the weight window technique in MCNP performs splitting or Russian roulette on particles both at collisions and surface crossings based on their expected contribution to detector. Thus, the Monte Carlo simulation could be run in a very efficient way compared with an analog game.

Performance of CADIS-biased Monte Carlo Simulations

Using Monte Carlo method to solve a deep-penetration problem with a large distributed source like this case, it means that extremely large number of particle histories and heavy computational cost are needed to achieve statistically reliable estimates. Without effective biasing scheme, it is almost impossible to get a trustworthy Monte Carlo result. As that shown in Table 3 for gamma-ray source problem, the unbiased MCNP run has taken more than several thousand minutes CPU time, but still no particle hits the relatively small top or side detectors and the statistical uncertainty of the pseudo outside detector is unsatisfactory. Using TORT/MCNP coupling approach based on the CADIS methodology, Table 3 shows that a factor of several tenths in speed-up for neutron source problem and about five orders of magnitude improvement in computational efficiency for gamma-ray source problem have been achieved. It demonstrated that the biasing scheme applied in our study is very effective for this kind of problems. However, we must admit that the assumption of Eq. 4 is unfounded and what we have got in the right-hand of Eq. 4 is not necessarily good enough especially when dealing with a large volumetric source like this case. We have to check the weights of source particles to see if they are really within the corresponding weight-window bounds. For neutron source problem, most of the weights of source particles indeed are lying between weight-window bounds. But for gamma-ray source problem, about one third of source particles are born carrying the weights above or below the weight-window bounds. This is because photon's mean free path is very short compared to that of neutron and therefore the resulting adjoint function varies significantly within the source region. If the weights of source particles are not within the weight windows, it will cause unnecessary splitting/rouletting and lose some computational efficiency. Even with such degradation, the overall gain of computational efficiency is still significant compared with the unbiased case.

Note that the preceding computational efficiencies could be better if we put the adjoint source just right in the positions of top and/or side detectors, but this will sacrifice the flexibility of biasing scheme for possible use in the future since one may be interested in the dose rates at other locations of the cask. The biasing scheme used here was developed based on the S_N adjoint flux calculated by using a very simplified geometry. If we modify the original MCNP model to include all the details of a real spent fuel storage cask, is it still directly applicable to the modified case? Based on the theory of CADIS methodology and our own experience [15], the answer is positive. The aim of the TORT calculation in the TORT/MCNP coupling approach is not intended to obtain a precise answer, but rather to generate an adjoint function with approximately the correct shape over the whole phase space. It does not put any restriction on the intrinsic accuracy of the subsequent MCNP simulations, e.g., very detailed 3-D geometry, continuous energy and angular treatments.

CONCLUDING REMARKS

A calculational model for a simplified spent fuel storage cask was built for comparisons of shielding calculations using different methods and codes. This shielding problem is simple in geometry but it is a typical deep-penetration problem with a large distributed source. In this study, various methods including S_N calculations in forward and adjoint modes, Monte Carlo simulations with and without biasing were applied to calculate the neutron and gamma-ray dose rates outside the cask. The biasing scheme used here is referred to as hybrid method because it uses the deterministic adjoint function in a biased forward Monte Carlo simulation. The result of adjoint S_N calculation is consistent with that in forward calculation. However, the difference between multigroup S_N and continuous energy Monte Carlo calculations seems significant in this case. While some calculational studies implied that the multigroup cross sections should be the major cause for such a discrepancy; however, we cannot identify the origin of the effect (i.e. group structure, weighting function, self-shielding effect, or their combinations). The TORT calculations with BUGLE-96 multigroup cross-section library underestimated the results by about 50%, compared with the MCNP results where continuous energy cross sections were used in default. This possible underestimation should be taken into account when using S_N method with broad-group cross sections in the shielding calculation for a spent fuel storage cask. On the other hand, Monte Carlo method without effective variance reduction techniques is impractical especially for gamma-ray source problem in this case. The TORT/MCNP manual coupling approach based on the CADIS methodology has been proved to be very effective and flexible. Compared with the unbiased case, the computational efficiency was improved by more than a factor of ten for neutron source problem; and the efficiency was increased significantly by about five orders of magnitude for gamma-ray source problem.

ACKNOWLEDGEMENTS
This work was funded by the Fuel Cycle and Material Administration of Atomic Energy Council, Taiwan, under the contract No. 942005FCMA007. The authors wish to thank Prof. Alireza Haghighat for fruitful discussion and comments on this subject during his visit to National Tsing Hua University.

REFERENCES

1. A. Haghighat, J.C. Wagner, "Monte Carlo Variance Reduction with Deterministic Importance Functions," *Progr. Nucl. Energy*, **42**, 25-53 (2003).
2. J.C. Wagner, A. Haghighat, "Automated Variance Reduction of Monte Carlo Shielding Calculations using the Discrete Ordinates Adjoint Function," *Nucl. Sci. Eng.* **128**, 186-208 (1998).
3. J.C. Wagner, A. Haghighat, "A^{3}MCNP: Automated Adjoint Accelerated MCNP. User's Manual, Version 1.0i," H&S Advanced Computing Technologies Corporation (2000).
4. J.F. Briesmeister, Ed., "MCNP - A General Purpose Monte Carlo N-particle Transport Code, version 4C," Los Alamos National Laboratory, LA-13709-M (2000).
5. "DOORS3.2: One-, Two- and Three-Dimensional Discrete Ordinate Neutron/Photon Transport Code System," RSICC Code Package CCC-650, Oak Ridge National Laboratory (1998).
6. Z.T. Tsai, L.Y. Liao, "Evaluation Model of Criticality, Cask Temperature and Site Boundary Dose for CSNPS Irradiated Nuclear Fuel On-Site Storage Cask System," Fuel Cycle and Materials Administration of Atomic Energy Council, Research Project Report No. 902001FCMA001 (2000).
7. International Commission on Radiological Protection, "Conversion coefficients for use in radiological protection against external radiation," ICRP Publication 74, Ann ICRP 26(3/4) (1996).
8. "BUGLE-96: Coupled 47 Neutron, 20 Gamma-ray Group Cross-section Library Derived from ENDF/B-VI for LWR Shielding and Pressure Vessel Dosimetry Applications," RSICC Data Library DLC-185, Oak Ridge National Laboratory (1996).
9. W.W. Engle, Jr., "ANISN, A One-Dimensional Discrete Ordinates Transport Code with Anisotropic Scattering," Oak Ridge National Laboratory, K-1693 (1967).
10. W.A. Rhoades, R.L. Childs, "An Updated Version of the DOT-4 One- and Two-Dimensional Neutron/Photon Transport Code," Oak Ridge National Laboratory, ORNL-5851 (1982).
11. W.A. Rhoades, D.B. Simpson, "The TORT Three-Dimensional Discrete Ordinates Neutron/Photon Transport Code," Oak Ridge National Laboratory, ORNL/TM-13221 (1997).
12. D. Shedlock, A. Haghighat, "Neutron Analysis of Spent Fuel Storage Installation using Parallel Computer and Advance Discrete Ordinates and Monte Carlo Techniques," presented at *10th Int. Conf. Radiation Shielding and 13th Topical Meeting on Radiation Protection and Shielding*, Funchal, Madeira Island, Portugal (2004).
13. J.C. Wagner, A. Haghighat, "Monte Carlo Transport Calculations and Analysis for Reactor Pressure Vessel Neutron Fluence," *Nucl. Technol.*, **114**, 373-398 (1996).
14. B.G. Petrovic, A. Haghighat, "Effects of S_N Method Numerics on Pressure Vessel Neutron Fluence Calculations," *Nucl. Sci. Eng.* **122**, 167-193 (1996).
15. R.J. Sheu, R.D. Sheu, S.H. Jiang, C.H. Kao, "Adjoint Acceleration of Monte Carlo Simulations using TORT/MCNP Coupling Approach : A Case Study on the Shielding Improvement for the Cyclotron Room of the Buddhist Tzu Chi General Hospital," *Radiat. Prot. Dosim.*, **113**, 140-151 (2005).

TABLE 1. Compositions of materials in different regions of the simplified spent fuel storage cask.

Region	Isotope	Atomic density
Fuel	^{10}B	1.204E-4[a]
	^{11}B	3.832E-4
	^{nat}C	1.004E-4
	^{16}O	8.092E-3
	^{27}Al	5.576E-4
	^{56}Fe	7.463E-3
	^{nat}Zr	2.155E-3
	^{238}U	4.038E-3
Iron	^{56}Fe	8.487E-2
Concrete	^{1}H	7.860E-3
	^{16}O	4.380E-2
	^{23}Na	1.050E-3
	^{nat}Mg	1.400E-4
	^{27}Al	2.390E-3
	^{nat}Si	1.580E-2
	^{nat}K	6.900E-4
	^{nat}Ca	2.920E-3
	^{56}Fe	3.100E-4
Air	^{14}N	4.020E-5
	^{16}O	1.070E-5

[a]Read as 1.204×10^{-4}. (Unit: $\times10^{24}$ cm^{-3})

TABLE 2. Neutron and induced gamma-ray doses for the storage cask considering neutron source calculated using MCNP and DOORS code systems. The S_N calculations include various numerical options (mesh size Δs in centimeter, Legendre expansion order P_L and directional quadrature order S_N). Without explicitly stated, the S_N calculations were carried out in forward mode with theta-weighted differencing scheme (default θ=0.9).

Detectors(μSv/h)	Side (neutron)	Side (photon)	Top (neutron)	Top (photon)
MCNP (relative error)	4.35E-3 (6.24%)	5.57E-3 (1.45%)	1.46E+0 (2.59%)	6.61E-3 (12.54%)
TORT (Δs=2.5, P3S8)	2.32E-3	3.90E-3	6.43E-1	7.06E-3
TORT/MCNP	0.53	0.70	0.44	1.07
TORT (adjoint) (Δs=2.5, P3S8)	2.46E-3	3.98E-3	7.00E-1	7.48E-3
TORT (θ=0.3) (Δs=2.5, P3S8)	2.35E-3	3.91E-3	6.94E-1	7.21E-3
TORT (Δs=2.5, P5S8)	2.32E-3	3.91E-3	6.44E-1	7.07E-3
DORT (Δs=2.5, P3S16)	2.35E-3	3.96E-3	6.47E-1	6.89E-3
DORT (Δs=1.25, P3S16)	2.43E-3	3.99E-3	6.45E-1	7.05E-3
ANISN (Δs=2.5, P3S16)	2.25E-3	3.84E-3	1.38E+0	2.07E-2
ANISN (Δs=0.625,P3S16)	2.39E-3	3.94E-3	1.39E+0	2.13E-2

TABLE 3. Neutron and gamma-ray doses for the storage cask calculated using unbiased and CADIS-biased MCNP simulations. The speed-up is measured as the FOM ratio between biased and unbiased runs.

Detectors (μ Sv/h)	Side (neutron)	Side (photon)	Top (neutron)	Top (photon)	Outside (neutron)	Outside (photon)
	Uniform neutron source in fuel region (1 n/cm^3.s)					
TORT	2.32E-3	3.90E-3	6.43E-1	7.06E-3	1.95E-2	3.07E-3
MCNP (unbiased)	4.35E-3 (6.24%)	5.57E-3 (1.45%)	1.46E+0 (2.59%)	6.61E-3 (12.54%)	5.11E-2 (0.21%)	4.30E-3 (0.19%)
MCNP (CADIS)	3.89E-3 (1.63%)	5.73E-3 (2.03%)	1.49E+0 (0.60%)	7.09E-3 (9.59%)	5.00E-2 (0.11%)	4.26E-3 (0.29%)
Speed-up	50.0	1.7	62.3	5.5	12.7	1.4
	Uniform gamma-ray source in fuel region (1 r/cm^3.s)					
TORT		3.83E-9		4.62E-10		3.79E-9
MCNP (unbiased)		0.00E+0 (0.00%)		0.00E+0 (0.00%)		3.84E-9 (17.75%)
MCNP (CADIS)		5.60E-9 (0.24%)		8.85E-10 (5.83%)		4.64E-9 (0.06%)
Speed-up		N.A.		N.A.		104778

Fig. 1. Geometry and dimensions of a simplified spent fuel storage cask.

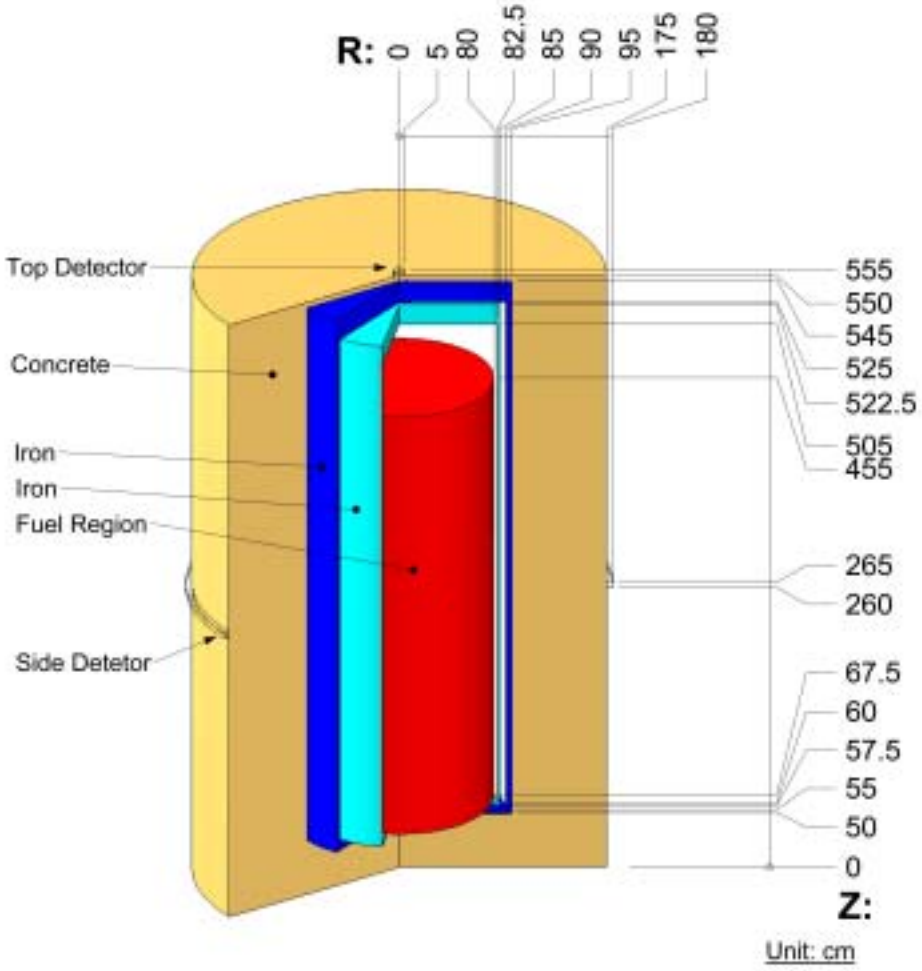

Fig. 2. Radial and axial distributions of the neutron and induced gamma-ray dose rates calculated by TORT and MCNP.

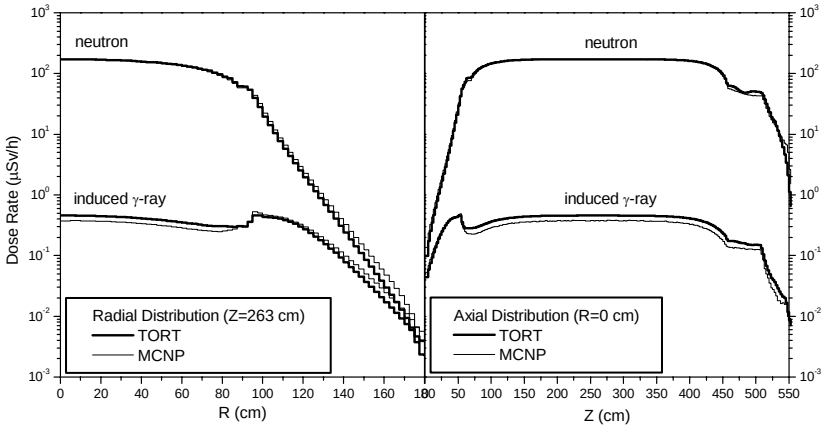

Fig. 3. Radial and axial distributions of the ratios between doses calculated by TORT and MCNP, respectively.

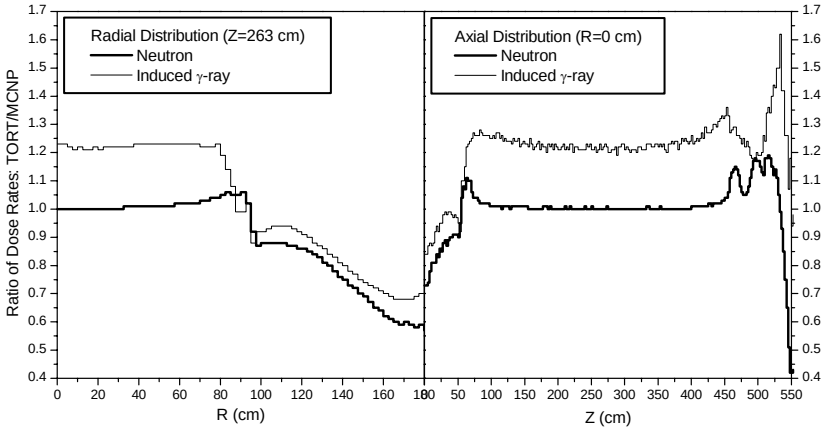

Fig. 4. Neutron energy spectra at the side and top detectors of the storage cask.

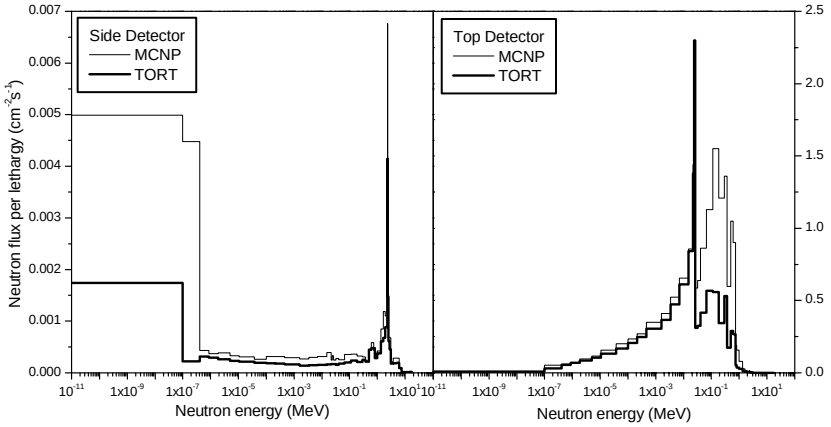

Fig. 5. Microscopic total neutron cross sections for ^{16}O and ^{56}Fe extracted from the continuous energy ENDF/B-VI and multigroup BUGLE-96 libraries.

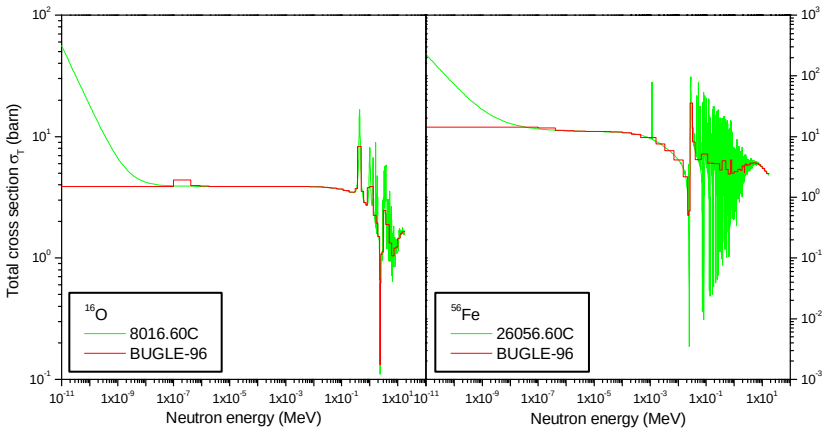

Fig. 6. Normalized energy distributions of original (SP) and biased (SB) sources.

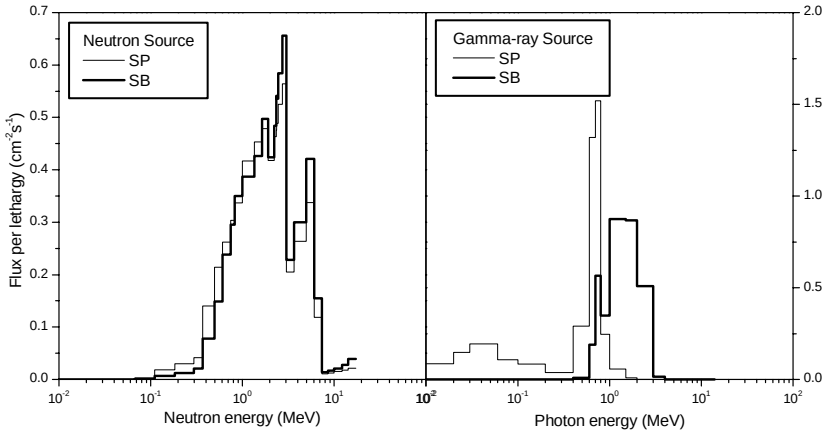

Fig. 7. Radial and axial distributions of the weight-window lower bounds for both neutron and gamma-ray in the energy range (0.8~1.0 MeV).

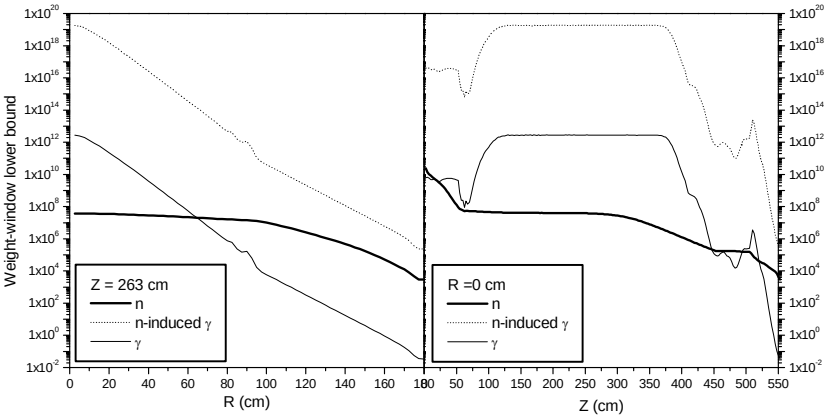

10. 附件二：中子反應總截面比較

Comparison of Microscopic Neutron Total Cross Section σ_T from MCNP(ENDF-B/VI), BUGLE-96 and CASK-81 libraries

Hydrogen:

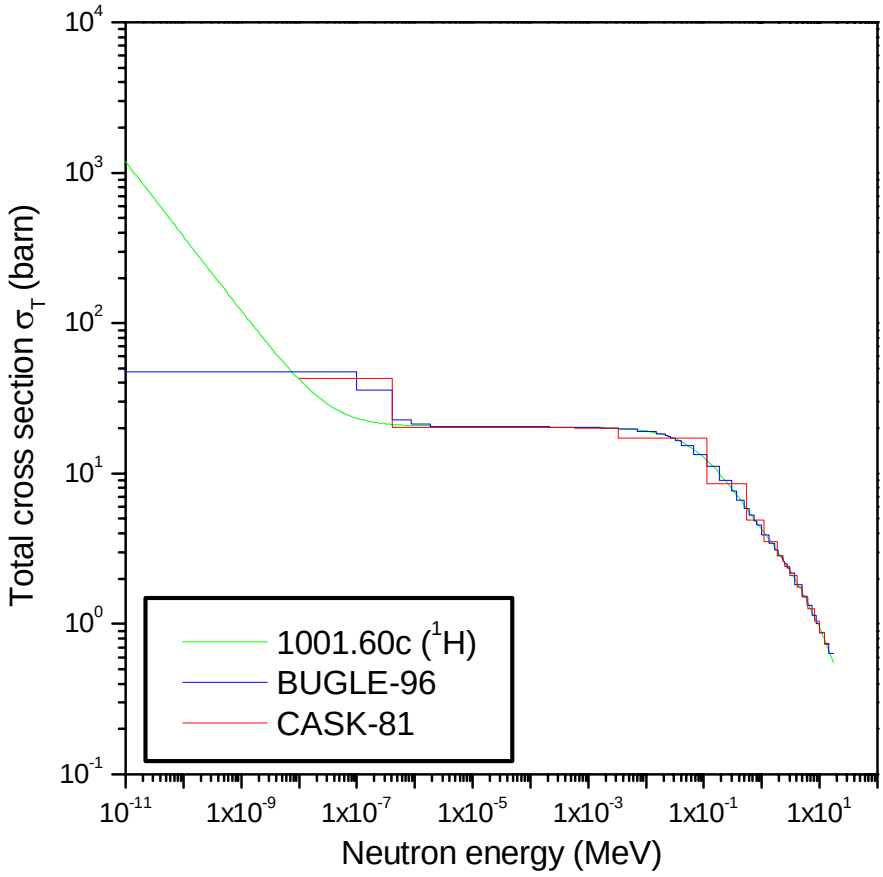

Boron-10:

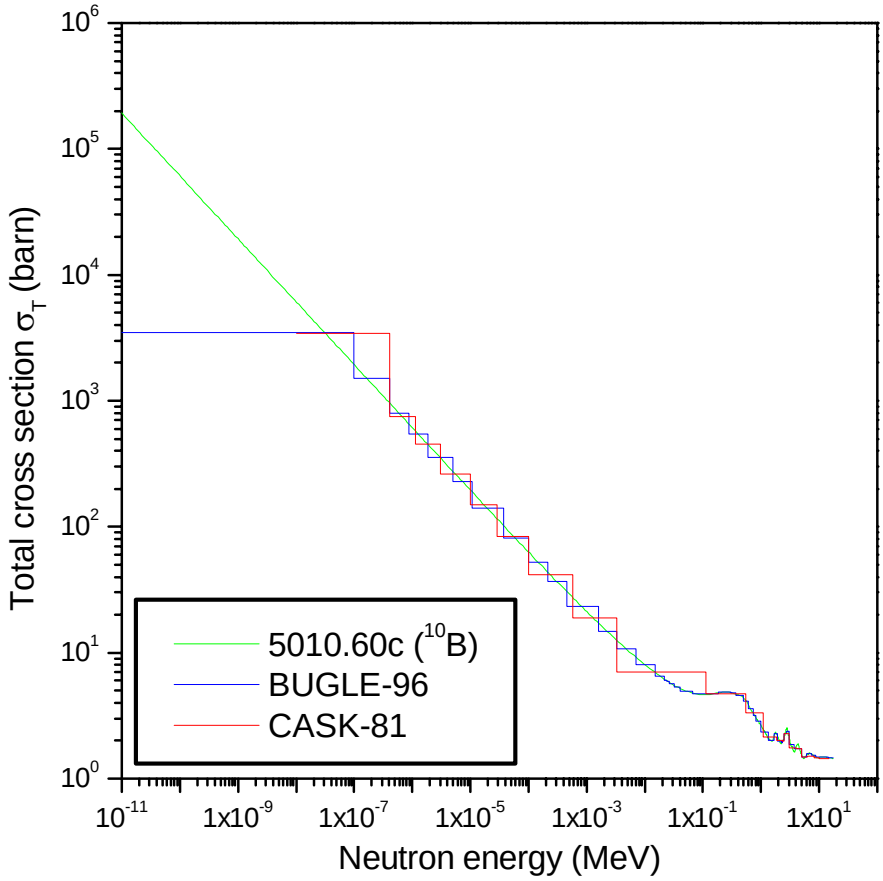
Total cross section σ_T (barn)
10^6
10^5
10^4
10^3
10^2
10^1
10^0
10^{-11}
1x10^{-9}
1x10^{-7}
1x10^{-5}
1x10^{-3}
1x10^{-1}
1x10^{1}
Neutron energy (MeV)
5010.60c (^{10}B)
BUGLE-96
CASK-81

Boron-11:

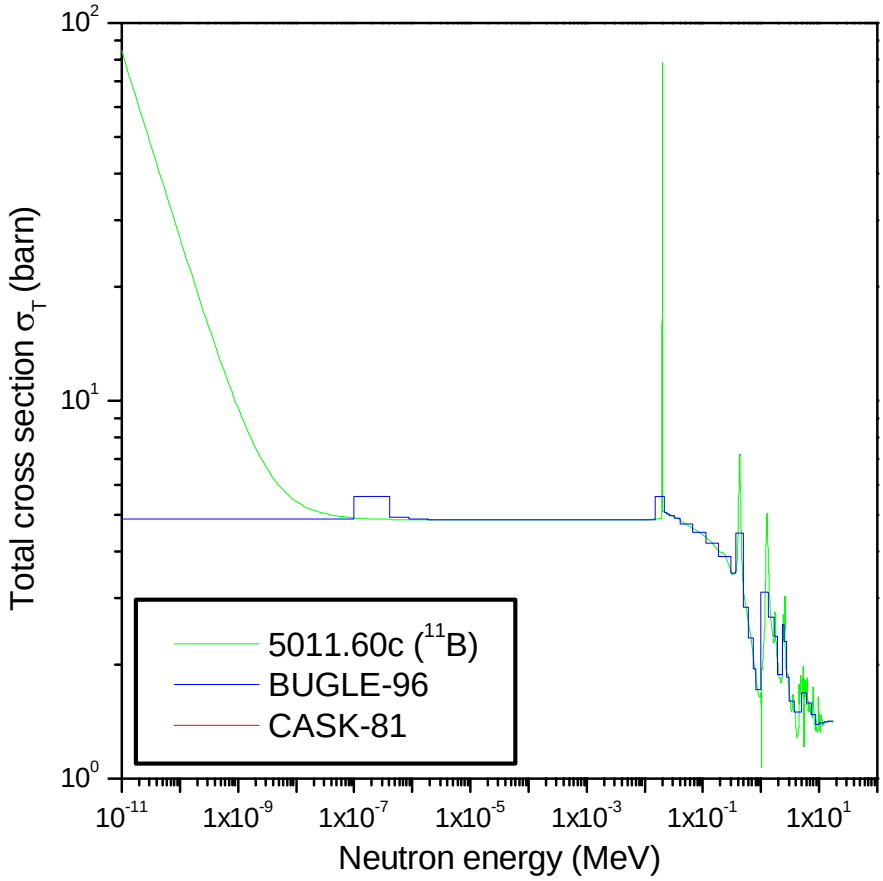
Total cross section σ_T (barn)
10^2
10^1
10^0
10^{-11}
1x10^{-9}
1x10^{-7}
1x10^{-5}
1x10^{-3}
1x10^{-1}
1x10^1
Neutron energy (MeV)
5011.60c (^{11}B)
BUGLE-96
CASK-81

Carbon:

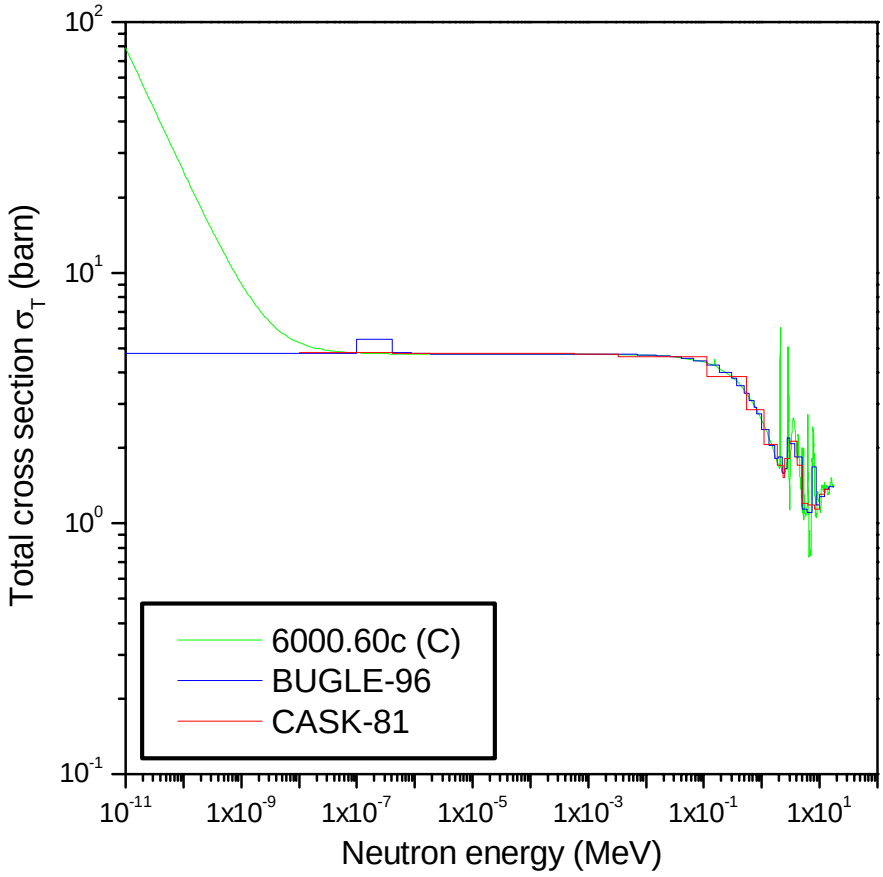
Total cross section σ_T (barn)
10^2
10^1
10^0
10^{-1}
10^{-11}
$1x10^{-9}$
$1x10^{-7}$
$1x10^{-5}$
$1x10^{-3}$
$1x10^{-1}$
$1x10^{1}$
Neutron energy (MeV)
6000.60c (C)
BUGLE-96
CASK-81

Nitrogen:

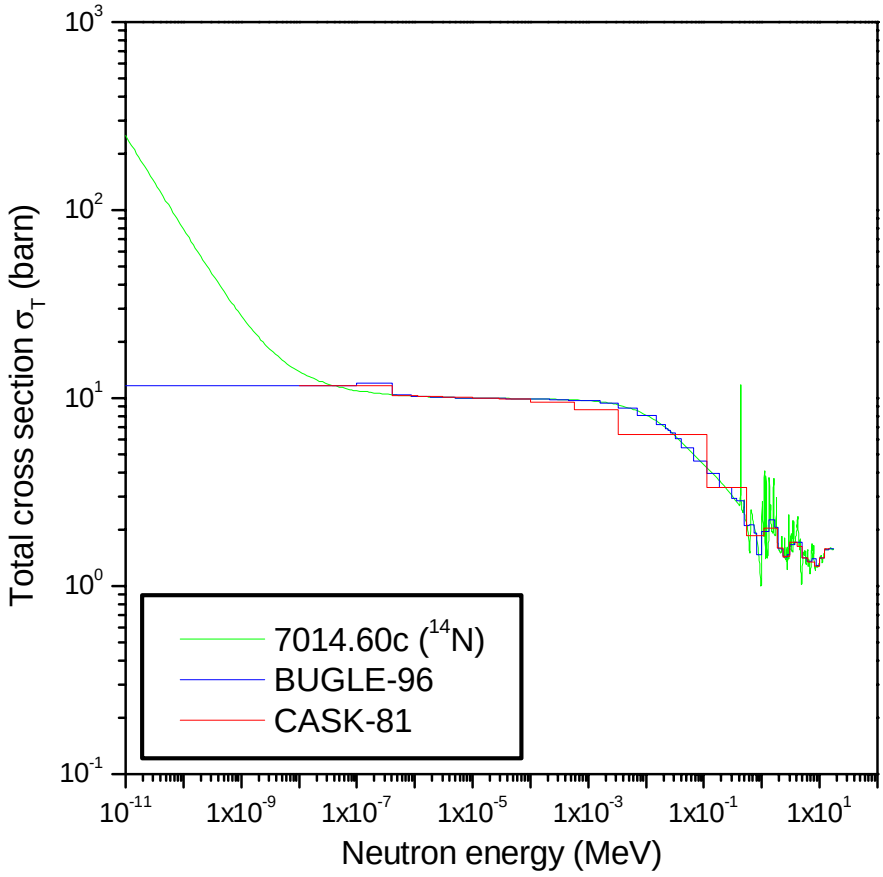
Total cross section σ_T (barn)
10^3
10^2
10^1
10^0
10^{-1}
10^{-11}
$1x10^{-9}$
$1x10^{-7}$
$1x10^{-5}$
$1x10^{-3}$
$1x10^{-1}$
$1x10^{1}$
Neutron energy (MeV)
7014.60c (^{14}N)
BUGLE-96
CASK-81

Oxygen:

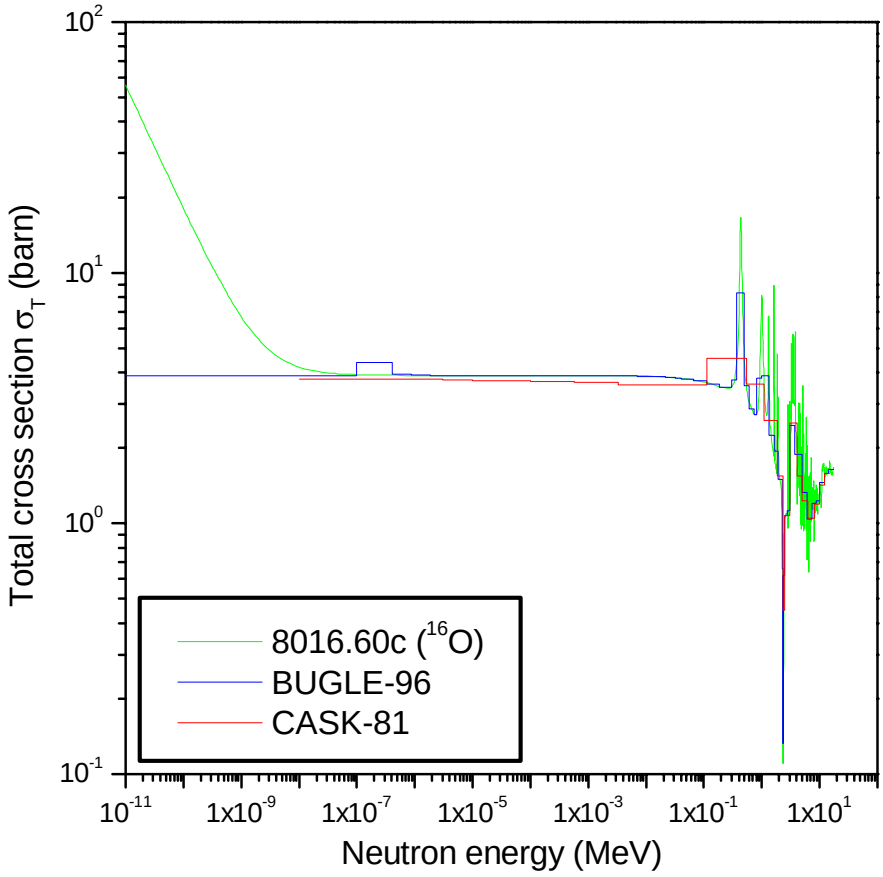
Total cross section σ_T (barn)
10^2
10^1
10^0
10^{-1}
10^{-11}
$1x10^{-9}$
$1x10^{-7}$
$1x10^{-5}$
$1x10^{-3}$
$1x10^{-1}$
$1x10^{1}$
Neutron energy (MeV)
8016.60c (^{16}O)
BUGLE-96
CASK-81

Sodium:

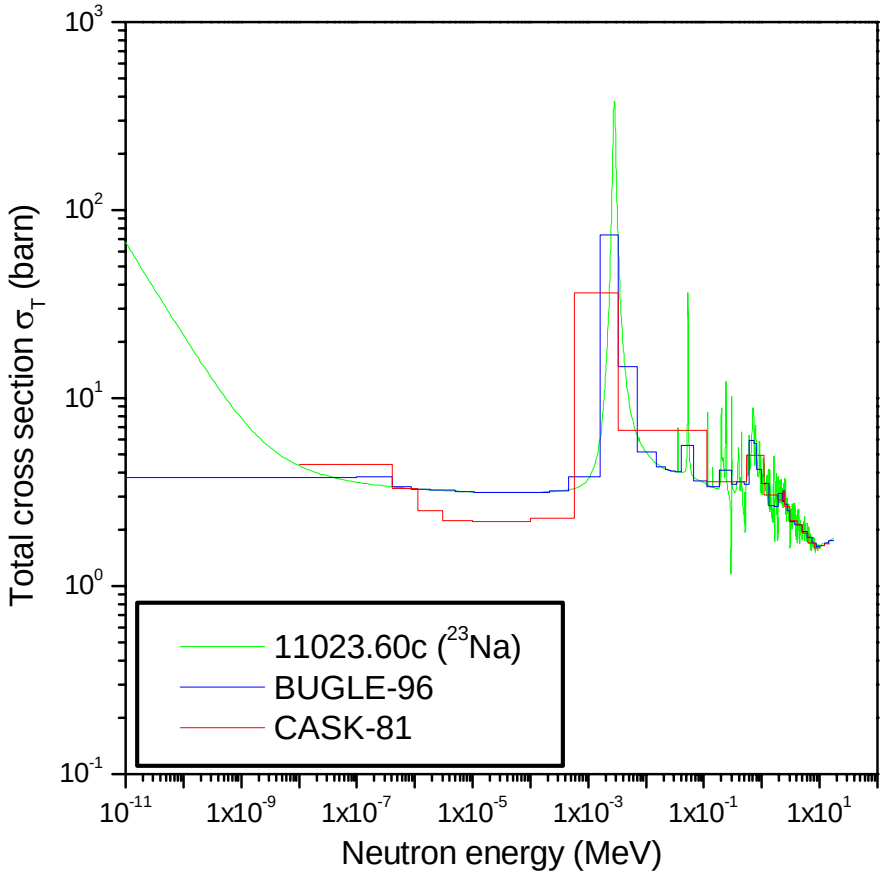
Total cross section σT (barn)
Neutron energy (MeV)
11023.60c (23Na)
BUGLE-96
CASK-81

Magnesium:

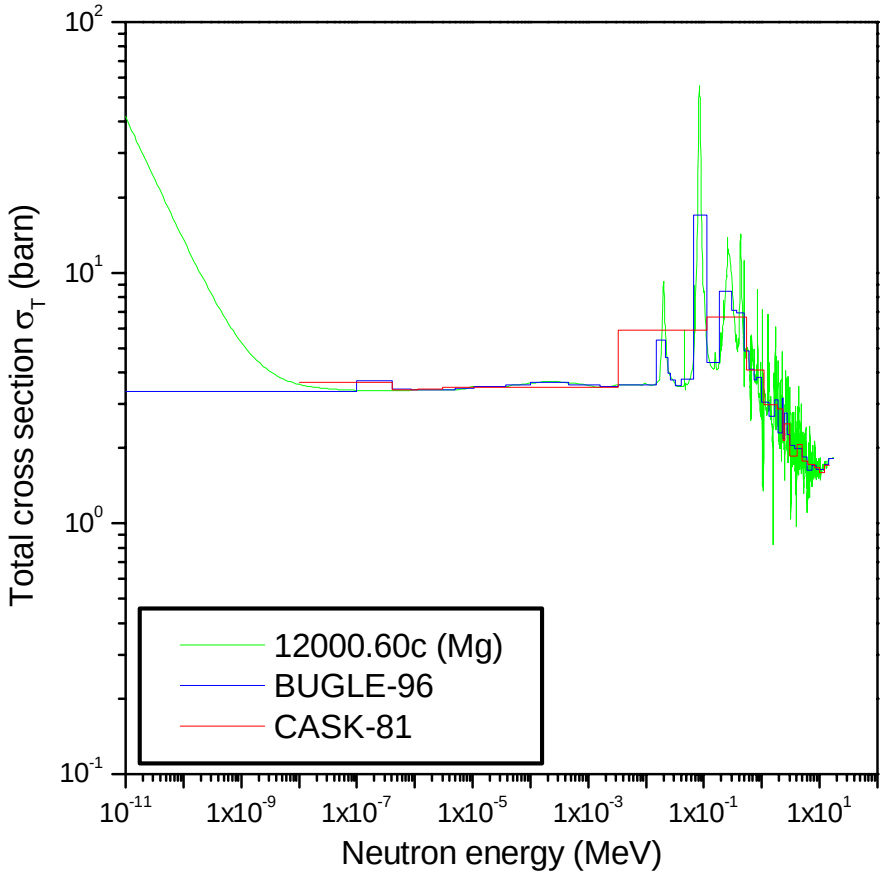
Total cross section σ_T (barn)
10^2
10^1
10^0
10^{-1}
12000.60c (Mg)
BUGLE-96
CASK-81
10^{-11}
$1x10^{-9}$
$1x10^{-7}$
$1x10^{-5}$
$1x10^{-3}$
$1x10^{-1}$
$1x10^{1}$
Neutron energy (MeV)

Aluminum:

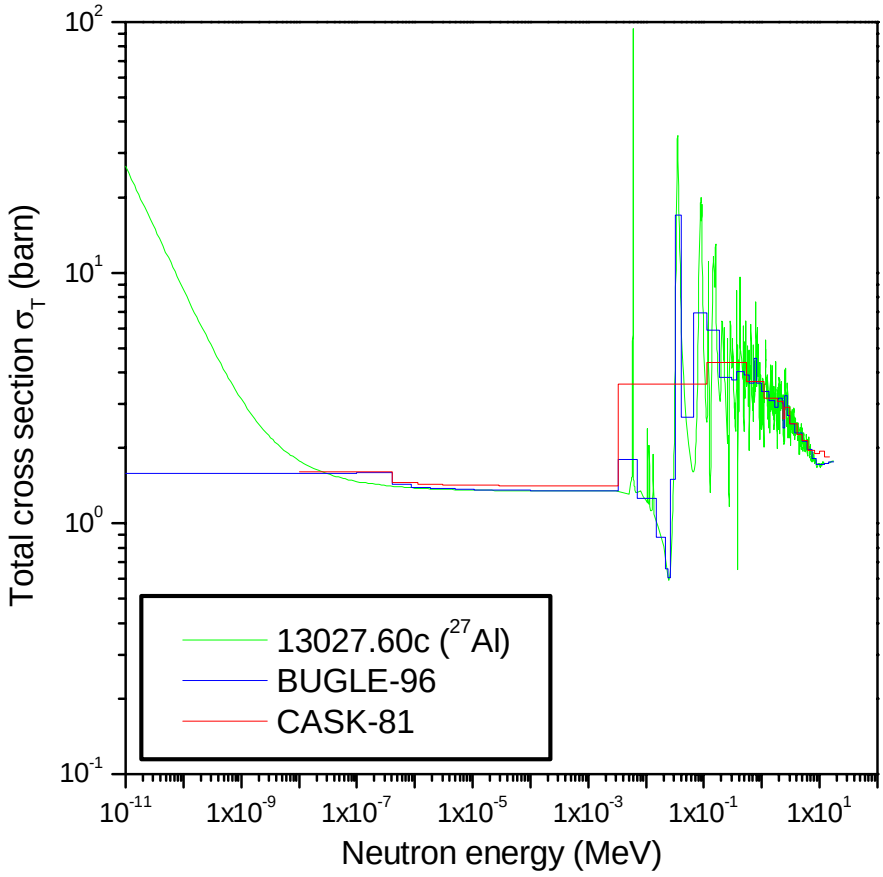
Total cross section σ_T (barn)
10^2
10^1
10^0
10^{-1}
10^{-11}
1x10^{-9}
1x10^{-7}
1x10^{-5}
1x10^{-3}
1x10^{-1}
1x10^{1}
Neutron energy (MeV)
13027.60c (^{27}Al)
BUGLE-96
CASK-81

Silicon:

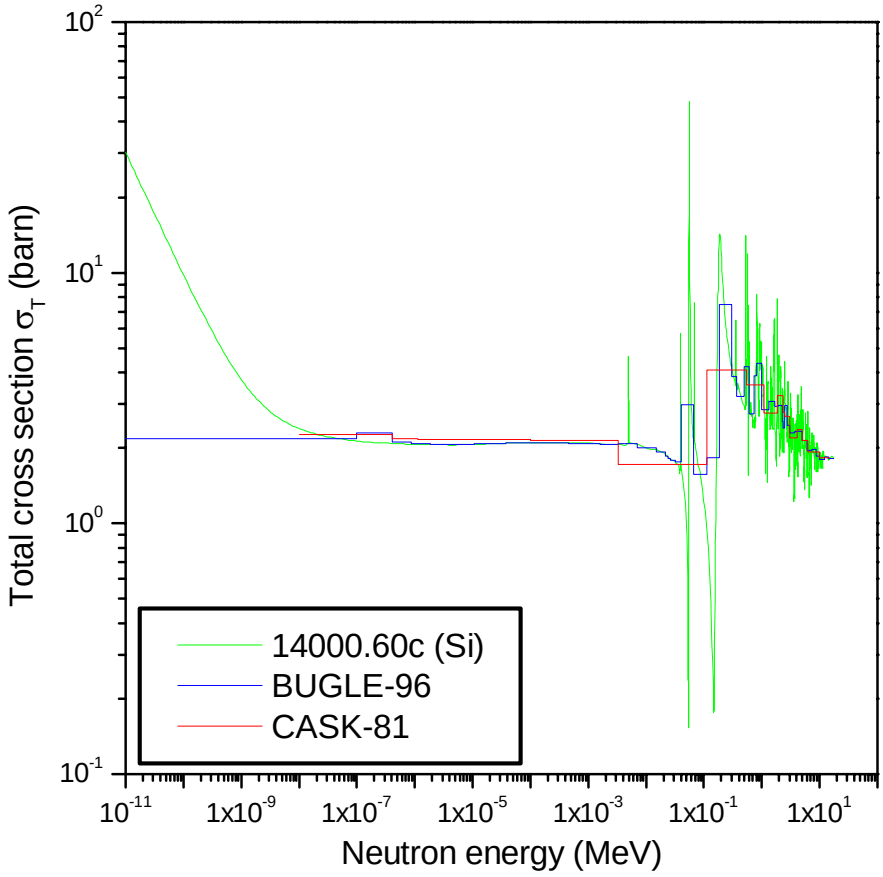
Total cross section σ_T (barn)
10^2
10^1
10^0
10^{-1}
10^{-11}
$1x10^{-9}$
$1x10^{-7}$
$1x10^{-5}$
$1x10^{-3}$
$1x10^{-1}$
$1x10^{1}$
Neutron energy (MeV)
14000.60c (Si)
BUGLE-96
CASK-81

Potassium:

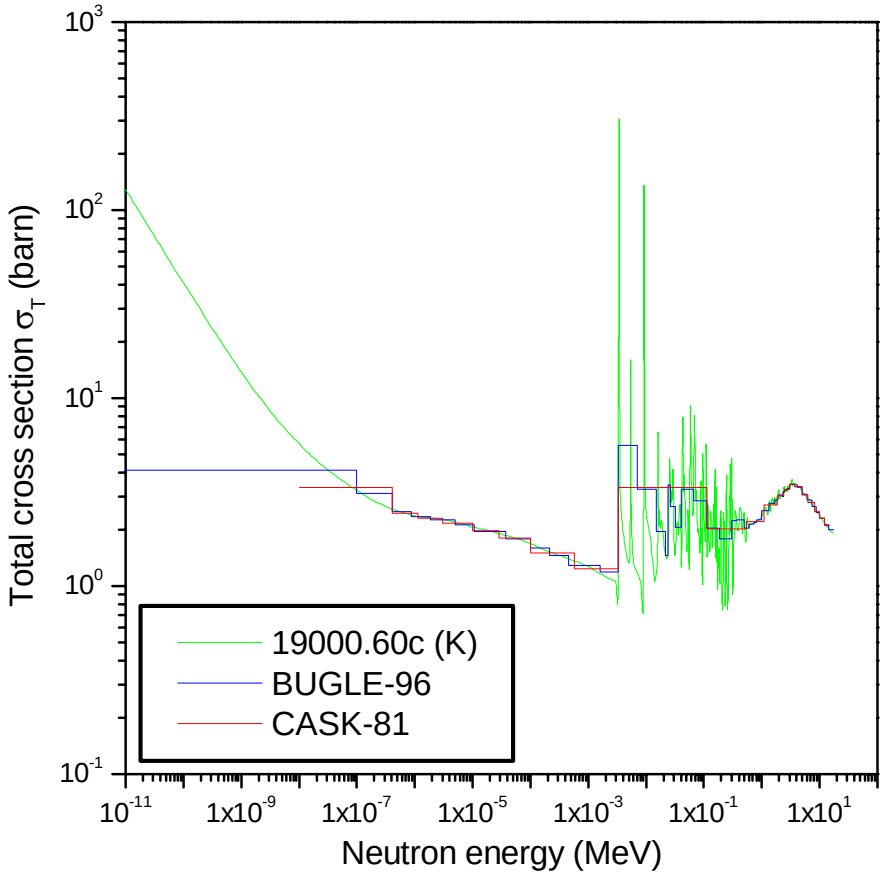
Total cross section σ_T (barn)
10^3
10^2
10^1
10^0
10^{-1}
10^{-11}
$1x10^{-9}$
$1x10^{-7}$
$1x10^{-5}$
$1x10^{-3}$
$1x10^{-1}$
$1x10^{1}$
Neutron energy (MeV)
19000.60c (K)
BUGLE-96
CASK-81

Calcium:

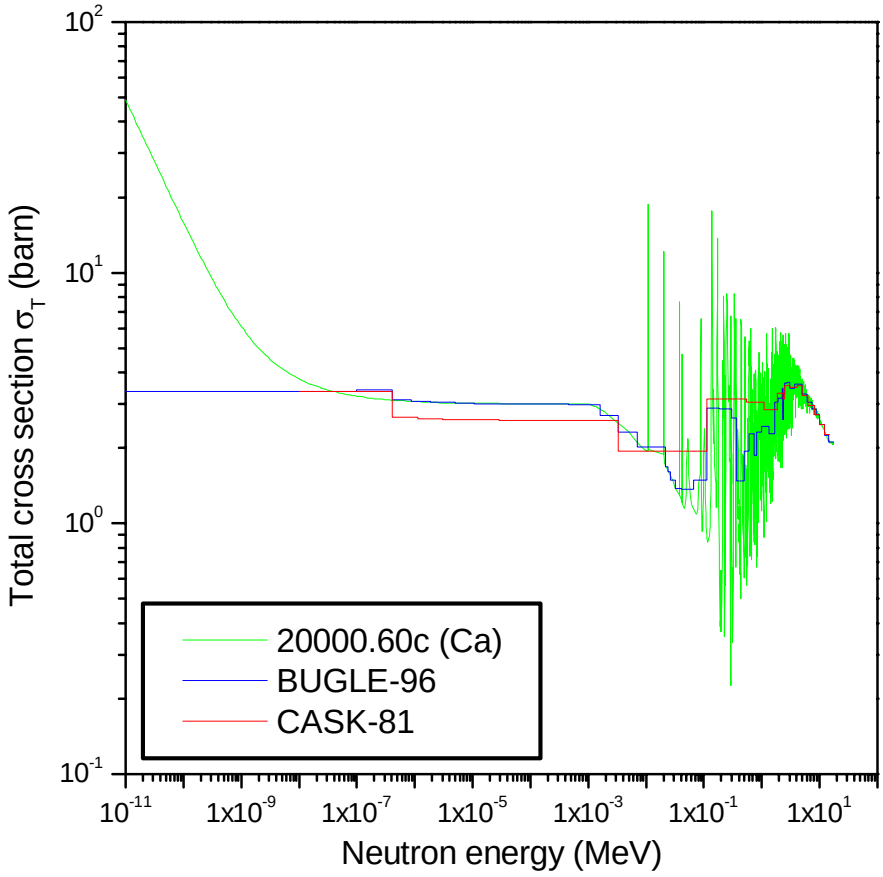
Total cross section σ_T (barn)
10^2
10^1
10^0
10^{-1}
10^{-11}
$1x10^{-9}$
$1x10^{-7}$
$1x10^{-5}$
$1x10^{-3}$
$1x10^{-1}$
$1x10^{1}$
Neutron energy (MeV)
20000.60c (Ca)
BUGLE-96
CASK-81

Iron:

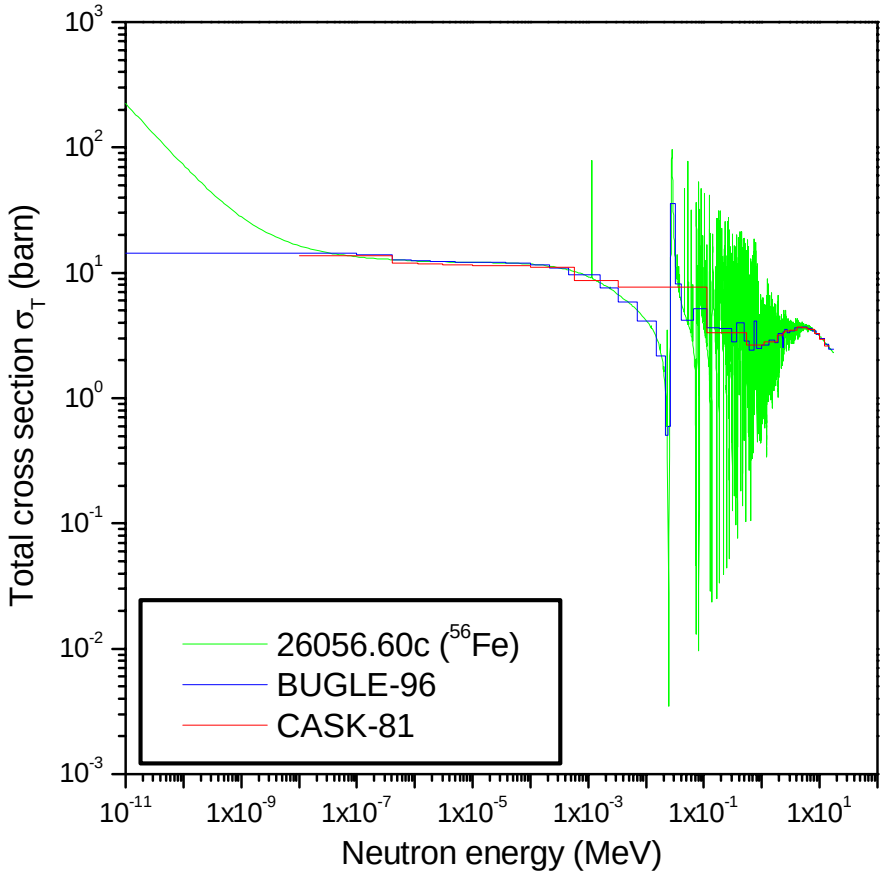
Total cross section σ_T (barn)
Neutron energy (MeV)
26056.60c (^{56}Fe)
BUGLE-96
CASK-81

Zirconium:

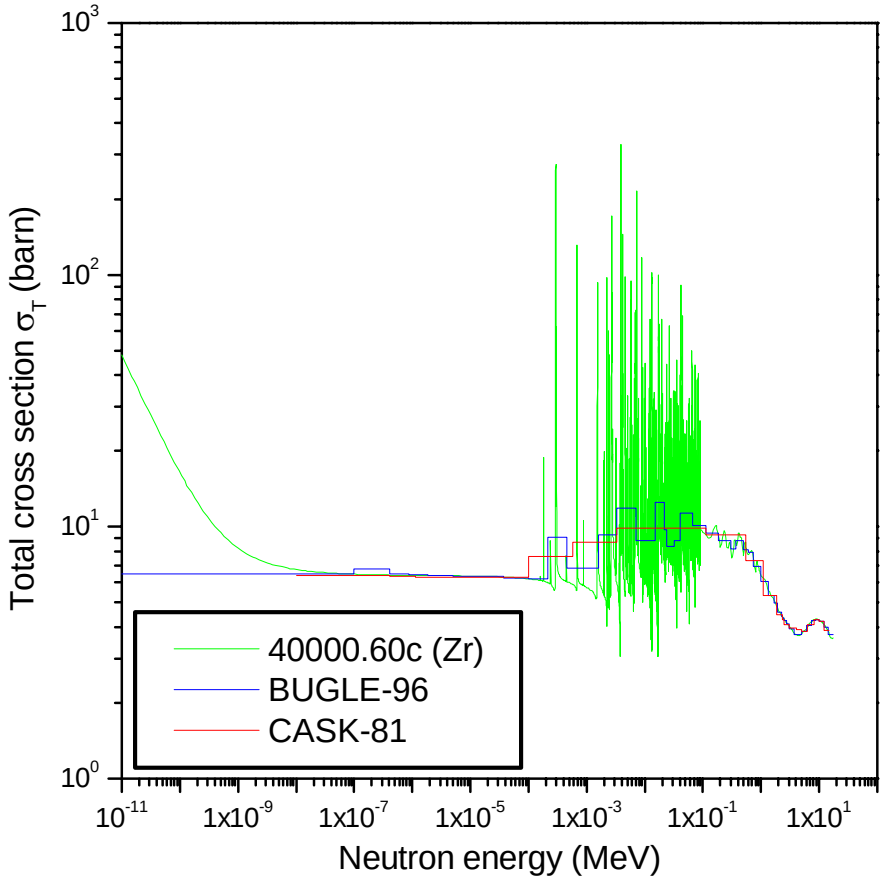
Total cross section σ_T (barn)
10^3
10^2
10^1
10^0
40000.60c (Zr)
BUGLE-96
CASK-81
10^{-11}
$1x10^{-9}$
$1x10^{-7}$
$1x10^{-5}$
$1x10^{-3}$
$1x10^{-1}$
$1x10^{1}$
Neutron energy (MeV)

Uranium:

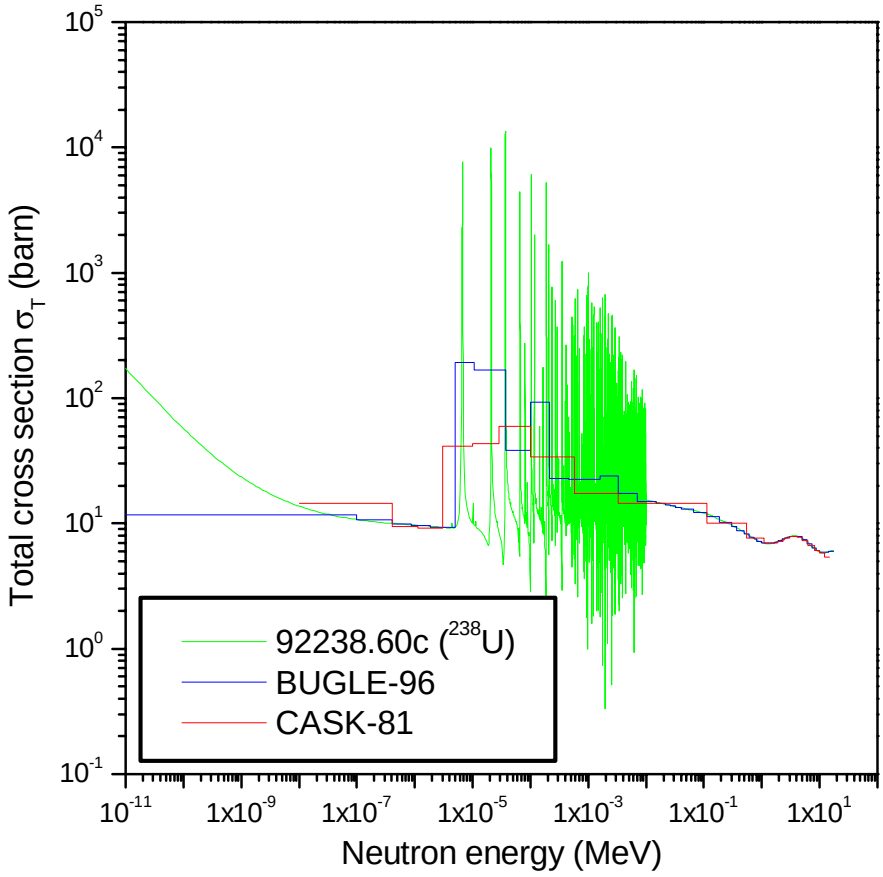
Total cross section σ_T (barn)
Neutron energy (MeV)
92238.60c (^{238}U)
BUGLE-96
CASK-81

11. 附件三：示範案例輸入檔

==========

(1) MCNP input file: Cnd_n.i (Unbiased case)

```
A simple CASK model for study of radiation shielding of SFISF
c     Note: Unbiased case (add a surrounding detector)
c     >>> Cell cards <<<
1     1  2.291e-2  -1                          $ effective fuel
2     4  5.090e-5  -2 1                        $ air region
3     2  8.487e-2  -3 2                        $ inner basket
4     4  5.090e-5  -4 3                        $ air region
5     2  8.487e-2  -5 4                        $ outer basket
6     3  7.496e-2  -6 5                        $ concrete cask
7     4  5.090e-5  -7 14                       $ outside air
8     0             7                          $ outside the world
11    4  5.090e-5  -12 11                      $ detector 1
12    4  5.090e-5  -13                         $ detector 2
13    4  5.090e-5  -14 6 #11 #12               $ surrounding detector

c     >>> Surface/Macrobody cards <<<
1     rcc    0.0    0.0   67.5    0.0    0.0  387.5   80.0
2     rcc    0.0    0.0   60.0    0.0    0.0  445.0   82.5
3     rcc    0.0    0.0   57.5    0.0    0.0  465.0   85.0
4     rcc    0.0    0.0   55.0    0.0    0.0  470.0   90.0
5     rcc    0.0    0.0   50.0    0.0    0.0  495.0   95.0
6     rcc    0.0    0.0    0.0    0.0    0.0  550.0  175.0
7     so  1000.0
11    rcc    0.0    0.0  260.0    0.0    0.0    5.0  175.0
12    rcc    0.0    0.0  260.0    0.0    0.0    5.0  180.0
13    rcc    0.0    0.0  550.0    0.0    0.0    5.0    5.0
14    rcc    0.0    0.0    0.0    0.0    0.0  555.0  180.0

c     >>> Data cards <<<
mode  n p
imp:n 1 1 1 1 1 1 1 0 1 1 1
imp:p 1 1 1 1 1 1 1 0 1 1 1
c     turn off fission in the fuel region
nonu  2 1 1 1 1 1 1 1 1 1 1
c     m1 : effective fuel
c     m2 : iron
```

```
c     m3 : concrete (ANS-6.6.1)
c     m4 : air (ANS-6.6.1)
m1     5010.60c  1.204e-4   5011.60c  3.832e-4   6000.60c  1.004e-4
       8016.60c  8.092e-3  13027.60c  5.576e-4  26056.60c  7.463e-3
      40000.60c  2.155e-3  92238.60c  4.038e-3
m2    26056.60c  8.487e-2
m3     1001.60c  7.860e-3   8016.60c  4.380e-2  11023.60c  1.050e-3
      12000.60c  1.400e-4  13027.60c  2.390e-3  14000.60c  1.580e-2
      19000.60c  6.900e-4  20000.60c  2.920e-3  26056.60c  3.100e-4
m4     7014.60c  4.020e-5   8016.60c  1.070e-5
c     source definition
c     particle : neutron
c     geometry : uniform cylinder volume source
c     energy   : UMS FSAR Table 5.2-19
c     strength : 1 n/cm^3.s (wgt=pi*r^2*z)
sdef  par=1  cel=1  pos=0 0 67.5  rad=d1  axs=0 0 1  ext=d2
      erg=d3  wgt=7.8e+6
si1   0.0 80.0
sp1   -21 1
si2   0.0 387.5
sp2   -21 0
si3   1.000e-11 1.000e-07 4.140e-07 8.764e-07 1.855e-06
      5.044e-06 1.068e-05 3.727e-05 1.013e-04 2.145e-04
      4.540e-04 1.585e-03 3.355e-03 7.102e-03 1.503e-02
      2.188e-02 2.418e-02 2.606e-02 3.183e-02 4.087e-02
      6.738e-02 1.111e-01 1.832e-01 2.972e-01 3.688e-01
      4.979e-01 6.081e-01 7.427e-01 8.209e-01 1.003e+00
      1.353e+00 1.653e+00 1.921e+00 2.231e+00 2.346e+00
      2.365e+00 2.466e+00 2.725e+00 3.012e+00 3.678e+00
      4.966e+00 6.065e+00 7.408e+00 8.607e+00 1.000e+01
      1.221e+01 1.419e+01 1.733e+01
sp3   0.000e+00 0.000e+00 0.000e+00 0.000e+00 0.000e+00
      0.000e+00 0.000e+00 0.000e+00 0.000e+00 0.000e+00
      0.000e+00 0.000e+00 0.000e+00 0.000e+00 0.000e+00
      0.000e+00 0.000e+00 0.000e+00 0.000e+00 0.000e+00
      0.000e+00 1.402e-03 9.106e-03 1.440e-02 9.043e-03
      4.185e-02 4.267e-02 5.212e-02 3.028e-02 6.715e-02
      1.241e-01 9.026e-02 7.162e-02 6.251e-02 2.319e-02
      3.831e-03 2.037e-02 5.223e-02 5.619e-02 4.076e-02
      7.882e-02 6.725e-02 2.367e-02 1.635e-03 1.899e-03
      3.013e-03 2.699e-03 4.281e-03
c     tally definition
c     F4 track length estimate gives cell flux #/cm^2, per source particle
c     => ICRP-74 neutron and gamm-ray AP fluence-to-dose unit : Sv.cm^2
```

```
c     => AP effective dose
c     => MCNP give the answer : Sv per source particle
c     => considering source strength gives the answer : Sv/s
c     => * 3600 * 1.0e+6 gives the answer : uSv/h
c     => Tally multiplier card = 3.6e+9
f14:n 11
fm14  3.6e+9
de14  1.0e-9     1.0e-8     2.5e-8     1.0e-7     2.0e-7
      5.0e-7     1.0e-6     2.0e-6     5.0e-6     1.0e-5
      2.0e-5     5.0e-5     1.0e-4     2.0e-4     5.0e-4
      1.0e-3     2.0e-3     5.0e-3     1.0e-2     2.0e-2
      3.0e-2     5.0e-2     7.0e-2     1.0e-1     1.5e-1
      2.0e-1     3.0e-1     5.0e-1     7.0e-1     9.0e-1
      1.0        1.2        2.0        3.0        4.0
      5.0        6.0        7.0        8.0        9.0
      1.0e+1     1.2e+1     1.4e+1     1.5e+1     1.6e+1
      1.8e+1     2.0e+1
df14  5.24e-12   6.55e-12   7.60e-12   9.95e-12   11.2e-12
      12.8e-12   13.8e-12   14.5e-12   15.0e-12   15.1e-12
      15.1e-12   14.8e-12   14.6e-12   14.4e-12   14.2e-12
      14.2e-12   14.4e-12   15.7e-12   18.3e-12   23.8e-12
      29.0e-12   38.5e-12   47.2e-12   59.8e-12   80.2e-12
      99.0e-12   133e-12    188e-12    231e-12    267e-12
      282e-12    310e-12    383e-12    432e-12    458e-12
      474e-12    483e-12    490e-12    494e-12    497e-12
      499e-12    499e-12    496e-12    494e-12    491e-12
      486e-12    480e-12
f24:p 11
fm24  3.6e+9
de24  1.00e-2    1.5e-2     2.0e-2     3.0e-2     4.0e-2
      5.0e-2     6.0e-2     8.0e-2     1.0e-1     1.5e-1
      2.0e-1     3.0e-1     4.0e-1     5.0e-1     6.0e-1
      8.0e-1     1.0        1.5        2.0        3.0
      4.0        5.0        6.0        8.0        1.0e+1
      2.0e+1
df24  0.049e-12  0.125e-12  0.205e-12  0.300e-12  0.338e-12
      0.357e-12  0.378e-12  0.440e-12  0.517e-12  0.752e-12
      1.004e-12  1.508e-12  1.996e-12  2.466e-12  2.908e-12
      3.727e-12  4.483e-12  6.125e-12  7.490e-12  9.885e-12
      12.015e-12 14.001e-12 15.987e-12 19.919e-12 23.760e-12
      34.4e-12
f34:n 12
fm34  3.6e+9
de34  1.0e-9     1.0e-8     2.5e-8     1.0e-7     2.0e-7
```

```
      5.0e-7     1.0e-6     2.0e-6     5.0e-6     1.0e-5
      2.0e-5     5.0e-5     1.0e-4     2.0e-4     5.0e-4
      1.0e-3     2.0e-3     5.0e-3     1.0e-2     2.0e-2
      3.0e-2     5.0e-2     7.0e-2     1.0e-1     1.5e-1
      2.0e-1     3.0e-1     5.0e-1     7.0e-1     9.0e-1
      1.0        1.2        2.0        3.0        4.0
      5.0        6.0        7.0        8.0        9.0
      1.0e+1     1.2e+1     1.4e+1     1.5e+1     1.6e+1
      1.8e+1     2.0e+1
df34  5.24e-12   6.55e-12   7.60e-12   9.95e-12   11.2e-12
      12.8e-12   13.8e-12   14.5e-12   15.0e-12   15.1e-12
      15.1e-12   14.8e-12   14.6e-12   14.4e-12   14.2e-12
      14.2e-12   14.4e-12   15.7e-12   18.3e-12   23.8e-12
      29.0e-12   38.5e-12   47.2e-12   59.8e-12   80.2e-12
      99.0e-12   133e-12    188e-12    231e-12    267e-12
      282e-12    310e-12    383e-12    432e-12    458e-12
      474e-12    483e-12    490e-12    494e-12    497e-12
      499e-12    499e-12    496e-12    494e-12    491e-12
      486e-12    480e-12
f44:p 12
fm44  3.6e+9
de44  1.00e-2    1.5e-2     2.0e-2     3.0e-2     4.0e-2
      5.0e-2     6.0e-2     8.0e-2     1.0e-1     1.5e-1
      2.0e-1     3.0e-1     4.0e-1     5.0e-1     6.0e-1
      8.0e-1     1.0        1.5        2.0        3.0
      4.0        5.0        6.0        8.0        1.0e+1
      2.0e+1
df44  0.049e-12  0.125e-12  0.205e-12  0.300e-12  0.338e-12
      0.357e-12  0.378e-12  0.440e-12  0.517e-12  0.752e-12
      1.004e-12  1.508e-12  1.996e-12  2.466e-12  2.908e-12
      3.727e-12  4.483e-12  6.125e-12  7.490e-12  9.885e-12
      12.015e-12 14.001e-12 15.987e-12 19.919e-12 23.760e-12
      34.4e-12
c     Special case for developing future biasing scheme
C     => average over the huge surrounding detector
f114:n 13
fm114 3.6e+9
de114 1.0e-9     1.0e-8     2.5e-8     1.0e-7     2.0e-7
      5.0e-7     1.0e-6     2.0e-6     5.0e-6     1.0e-5
      2.0e-5     5.0e-5     1.0e-4     2.0e-4     5.0e-4
      1.0e-3     2.0e-3     5.0e-3     1.0e-2     2.0e-2
      3.0e-2     5.0e-2     7.0e-2     1.0e-1     1.5e-1
      2.0e-1     3.0e-1     5.0e-1     7.0e-1     9.0e-1
      1.0        1.2        2.0        3.0        4.0
```

```
      5.0         6.0         7.0         8.0         9.0
      1.0e+1      1.2e+1      1.4e+1      1.5e+1      1.6e+1
      1.8e+1      2.0e+1
df114 5.24e-12    6.55e-12    7.60e-12    9.95e-12    11.2e-12
      12.8e-12    13.8e-12    14.5e-12    15.0e-12    15.1e-12
      15.1e-12    14.8e-12    14.6e-12    14.4e-12    14.2e-12
      14.2e-12    14.4e-12    15.7e-12    18.3e-12    23.8e-12
      29.0e-12    38.5e-12    47.2e-12    59.8e-12    80.2e-12
      99.0e-12    133e-12     188e-12     231e-12     267e-12
      282e-12     310e-12     383e-12     432e-12     458e-12
      474e-12     483e-12     490e-12     494e-12     497e-12
      499e-12     499e-12     496e-12     494e-12     491e-12
      486e-12     480e-12
f124:p 13
fm124 3.6e+9
de124 1.00e-2     1.5e-2      2.0e-2      3.0e-2      4.0e-2
      5.0e-2      6.0e-2      8.0e-2      1.0e-1      1.5e-1
      2.0e-1      3.0e-1      4.0e-1      5.0e-1      6.0e-1
      8.0e-1      1.0         1.5         2.0         3.0
      4.0         5.0         6.0         8.0         1.0e+1
      2.0e+1
df124 0.049e-12   0.125e-12   0.205e-12   0.300e-12   0.338e-12
      0.357e-12   0.378e-12   0.440e-12   0.517e-12   0.752e-12
      1.004e-12   1.508e-12   1.996e-12   2.466e-12   2.908e-12
      3.727e-12   4.483e-12   6.125e-12   7.490e-12   9.885e-12
      12.015e-12  14.001e-12  15.987e-12  19.919e-12  23.760e-12
      34.4e-12
c     F4 track length estimate gives cell flux #/cm^2, per source particle
c     => BUGLE energy binning
f54:n 11
e54   1.000e-11 1.000e-07 4.140e-07 8.764e-07 1.855e-06
      5.044e-06 1.068e-05 3.727e-05 1.013e-04 2.145e-04
      4.540e-04 1.585e-03 3.355e-03 7.102e-03 1.503e-02
      2.188e-02 2.418e-02 2.606e-02 3.183e-02 4.087e-02
      6.738e-02 1.111e-01 1.832e-01 2.972e-01 3.688e-01
      4.979e-01 6.081e-01 7.427e-01 8.209e-01 1.003e+00
      1.353e+00 1.653e+00 1.921e+00 2.231e+00 2.346e+00
      2.365e+00 2.466e+00 2.725e+00 3.012e+00 3.678e+00
      4.966e+00 6.065e+00 7.408e+00 8.607e+00 1.000e+01
      1.221e+01 1.419e+01 1.733e+01
f64:p 11
e64   1.000e-02 2.000e-02 3.000e-02 6.000e-02 1.000e-01
      2.000e-01 4.000e-01 6.000e-01 7.000e-01 8.000e-01
      1.000e+00 1.500e+00 2.000e+00 3.000e+00 4.000e+00
```

```
      5.000e+00 6.000e+00 7.000e+00 8.000e+00 1.000e+01
      1.400e+01
f74:n 12
e74   1.000e-11 1.000e-07 4.140e-07 8.764e-07 1.855e-06
      5.044e-06 1.068e-05 3.727e-05 1.013e-04 2.145e-04
      4.540e-04 1.585e-03 3.355e-03 7.102e-03 1.503e-02
      2.188e-02 2.418e-02 2.606e-02 3.183e-02 4.087e-02
      6.738e-02 1.111e-01 1.832e-01 2.972e-01 3.688e-01
      4.979e-01 6.081e-01 7.427e-01 8.209e-01 1.003e+00
      1.353e+00 1.653e+00 1.921e+00 2.231e+00 2.346e+00
      2.365e+00 2.466e+00 2.725e+00 3.012e+00 3.678e+00
      4.966e+00 6.065e+00 7.408e+00 8.607e+00 1.000e+01
      1.221e+01 1.419e+01 1.733e+01
f84:p 12
e84   1.000e-02 2.000e-02 3.000e-02 6.000e-02 1.000e-01
      2.000e-01 4.000e-01 6.000e-01 7.000e-01 8.000e-01
      1.000e+00 1.500e+00 2.000e+00 3.000e+00 4.000e+00
      5.000e+00 6.000e+00 7.000e+00 8.000e+00 1.000e+01
      1.400e+01
phys:n 17.332       $ neutron highest energy of BUGLE
cut:n  j 1.0e-11    $ neutron lowest energy of BUGLE
phys:p j j j 0      $ detailed photon physics and no photonuclear
cut:p  j 0.01       $ photon lowest energy of BUGLE
nps    50000000
print
```

---

(2) MCNP input file: Cn_a.i (CADIS-biased case)

```
A simple CASK model for study of radiation shielding of SFISF
c     Note: CADIS-biased case (add a surrounding detector)
c     >>> Cell cards <<<
1     1  2.291e-2  -1                          $ effective fuel
2     4  5.090e-5  -2 1                        $ air region
3     2  8.487e-2  -3 2                        $ inner basket
4     4  5.090e-5  -4 3                        $ air region
5     2  8.487e-2  -5 4                        $ outer basket
6     3  7.496e-2  -6 5                        $ concrete cask
7     4  5.090e-5  -7 14                       $ outside air
8     0             7                          $ outside the world
11    4  5.090e-5  -12 11                      $ detector 1
12    4  5.090e-5  -13                         $ detector 2
13    4  5.090e-5  -14 6 #11 #12               $ surrounding detector
```

```
c     >>> Surface/Macrobody cards <<<
1     rcc    0.0    0.0   67.5    0.0    0.0  387.5   80.0
2     rcc    0.0    0.0   60.0    0.0    0.0  445.0   82.5
3     rcc    0.0    0.0   57.5    0.0    0.0  465.0   85.0
4     rcc    0.0    0.0   55.0    0.0    0.0  470.0   90.0
5     rcc    0.0    0.0   50.0    0.0    0.0  495.0   95.0
6     rcc    0.0    0.0    0.0    0.0    0.0  550.0  175.0
7     so  1000.0
11    rcc    0.0    0.0  260.0    0.0    0.0    5.0  175.0
12    rcc    0.0    0.0  260.0    0.0    0.0    5.0  180.0
13    rcc    0.0    0.0  550.0    0.0    0.0    5.0    5.0
14    rcc    0.0    0.0    0.0    0.0    0.0  555.0  180.0

c     >>> Data cards <<<
mode  n p
imp:n 1 1 1 1 1 1 0 0 1 1 1
imp:p 1 1 1 1 1 1 0 0 1 1 1
c     turn off fission in the fuel region
nonu  2 1 1 1 1 1 1 1 1 1 1
c     m1 : effective fuel
c     m2 : iron
c     m3 : concrete (ANS-6.6.1)
c     m4 : air (ANS-6.6.1)
m1     5010.60c  1.204e-4   5011.60c  3.832e-4   6000.60c  1.004e-4
       8016.60c  8.092e-3  13027.60c  5.576e-4  26056.60c  7.463e-3
      40000.60c  2.155e-3  92238.60c  4.038e-3
m2    26056.60c  8.487e-2
m3     1001.60c  7.860e-3   8016.60c  4.380e-2  11023.60c  1.050e-3
      12000.60c  1.400e-4  13027.60c  2.390e-3  14000.60c  1.580e-2
      19000.60c  6.900e-4  20000.60c  2.920e-3  26056.60c  3.100e-4
m4     7014.60c  4.020e-5   8016.60c  1.070e-5
c     source definition
c     particle : neutron
c     geometry : uniform cylinder volume source
c     energy   : UMS FSAR Table 5.2-19
c     strength : 1 n/cm^3.s (wgt=pi*r^2*z)
sdef  par=1  cel=1  pos=0 0 0  rad=d1  axs=0 0 1  ext=d2
      erg=d3  wgt=7.8e+6
si1    0.0  2.5  5.0  7.5 10.0 12.5 15.0 17.5 20.0 22.5
      25.0 27.5 30.0 32.5 35.0 37.5 40.0 42.5 45.0 47.5
      50.0 52.5 55.0 57.5 60.0 62.5 65.0 67.5 70.0 72.5
      75.0 77.5 80.0
sp1         0.0 9.766E-04 2.930E-03 4.883E-03 6.836E-03
      8.789E-03 1.074E-02 1.270E-02 1.465E-02 1.660E-02
```

```
       1.855E-02 2.051E-02 2.246E-02 2.441E-02 2.637E-02
       2.832E-02 3.027E-02 3.223E-02 3.418E-02 3.613E-02
       3.809E-02 4.004E-02 4.199E-02 4.395E-02 4.590E-02
       4.785E-02 4.980E-02 5.176E-02 5.371E-02 5.566E-02
       5.762E-02 5.957E-02 6.152E-02
sb1          0.0 1.053E-03 3.158E-03 5.259E-03 7.352E-03
       9.435E-03 1.150E-02 1.356E-02 1.559E-02 1.760E-02
       1.960E-02 2.159E-02 2.355E-02 2.551E-02 2.744E-02
       2.936E-02 3.127E-02 3.313E-02 3.492E-02 3.669E-02
       3.843E-02 4.014E-02 4.187E-02 4.360E-02 4.529E-02
       4.703E-02 4.883E-02 5.055E-02 5.210E-02 5.358E-02
       5.514E-02 5.691E-02 5.896E-02
si2     67.5  70.0  72.5  75.0  77.5  80.0  82.5  85.0  87.5  90.0
        92.5  95.0  97.5 100.0 102.5 105.0 107.5 110.0 112.5 115.0
       117.5 120.0 122.5 125.0 127.5 130.0 132.5 135.0 137.5 140.0
       142.5 145.0 147.5 150.0 152.5 155.0 157.5 160.0 162.5 165.0
       167.5 170.0 172.5 175.0 177.5 180.0 182.5 185.0 187.5 190.0
       192.5 195.0 197.5 200.0 202.5 205.0 207.5 210.0 212.5 215.0
       217.5 220.0 222.5 225.0 227.5 230.0 232.5 235.0 237.5 240.0
       242.5 245.0 247.5 250.0 252.5 255.0 257.5 260.0 262.5 265.0
       267.5 270.0 272.5 275.0 277.5 280.0 282.5 285.0 287.5 290.0
       292.5 295.0 297.5 300.0 302.5 305.0 307.5 310.0 312.5 315.0
       317.5 320.0 322.5 325.0 327.5 330.0 332.5 335.0 337.5 340.0
       342.5 345.0 347.5 350.0 352.5 355.0 357.5 360.0 362.5 365.0
       367.5 370.0 372.5 375.0 377.5 380.0 382.5 385.0 387.5 390.0
       392.5 395.0 397.5 400.0 402.5 405.0 407.5 410.0 412.5 415.0
       417.5 420.0 422.5 425.0 427.5 430.0 432.5 435.0 437.5 440.0
       442.5 445.0 447.5 450.0 452.5 455.0
sp2          0.0 6.452E-03 6.452E-03 6.452E-03 6.452E-03
       6.452E-03 6.452E-03 6.452E-03 6.452E-03 6.452E-03
       6.452E-03 6.452E-03 6.452E-03 6.452E-03 6.452E-03
       6.452E-03 6.452E-03 6.452E-03 6.452E-03 6.452E-03
       6.452E-03 6.452E-03 6.452E-03 6.452E-03 6.452E-03
       6.452E-03 6.452E-03 6.452E-03 6.452E-03 6.452E-03
       6.452E-03 6.452E-03 6.452E-03 6.452E-03 6.452E-03
       6.452E-03 6.452E-03 6.452E-03 6.452E-03 6.452E-03
       6.452E-03 6.452E-03 6.452E-03 6.452E-03 6.452E-03
       6.452E-03 6.452E-03 6.452E-03 6.452E-03 6.452E-03
       6.452E-03 6.452E-03 6.452E-03 6.452E-03 6.452E-03
       6.452E-03 6.452E-03 6.452E-03 6.452E-03 6.452E-03
       6.452E-03 6.452E-03 6.452E-03 6.452E-03 6.452E-03
       6.452E-03 6.452E-03 6.452E-03 6.452E-03 6.452E-03
       6.452E-03 6.452E-03 6.452E-03 6.452E-03 6.452E-03
       6.452E-03 6.452E-03 6.452E-03 6.452E-03 6.452E-03
```

```
        6.452E-03 6.452E-03 6.452E-03 6.452E-03 6.452E-03
        6.452E-03 6.452E-03 6.452E-03 6.452E-03 6.452E-03
        6.452E-03 6.452E-03 6.452E-03 6.452E-03 6.452E-03
        6.452E-03 6.452E-03 6.452E-03 6.452E-03 6.452E-03
        6.452E-03 6.452E-03 6.452E-03 6.452E-03 6.452E-03
        6.452E-03 6.452E-03 6.452E-03 6.452E-03 6.452E-03
        6.452E-03 6.452E-03 6.452E-03 6.452E-03 6.452E-03
        6.452E-03 6.452E-03 6.452E-03 6.452E-03 6.452E-03
        6.452E-03 6.452E-03 6.452E-03 6.452E-03 6.452E-03
        6.452E-03 6.452E-03 6.452E-03 6.452E-03 6.452E-03
        6.452E-03 6.452E-03 6.452E-03 6.452E-03 6.452E-03
        6.452E-03 6.452E-03 6.452E-03 6.452E-03 6.452E-03
        6.452E-03 6.452E-03 6.452E-03 6.452E-03 6.452E-03
        6.452E-03 6.452E-03 6.452E-03 6.452E-03 6.452E-03
        6.452E-03 6.452E-03 6.452E-03 6.452E-03 6.452E-03
        6.452E-03
sb2           0.0 9.322E-04 9.125E-04 9.044E-04 9.043E-04
        9.067E-04 9.122E-04 9.176E-04 9.233E-04 9.305E-04
        9.364E-04 9.434E-04 9.494E-04 9.547E-04 9.599E-04
        9.638E-04 9.686E-04 9.718E-04 9.759E-04 9.791E-04
        9.819E-04 9.854E-04 9.866E-04 9.894E-04 9.915E-04
        9.937E-04 9.954E-04 9.969E-04 9.988E-04 9.997E-04
        1.001E-03 1.002E-03 1.003E-03 1.004E-03 1.005E-03
        1.006E-03 1.006E-03 1.007E-03 1.008E-03 1.008E-03
        1.009E-03 1.009E-03 1.010E-03 1.010E-03 1.011E-03
        1.011E-03 1.011E-03 1.012E-03 1.012E-03 1.012E-03
        1.013E-03 1.013E-03 1.014E-03 1.014E-03 1.014E-03
        1.014E-03 1.015E-03 1.015E-03 1.016E-03 1.016E-03
        1.017E-03 1.018E-03 1.018E-03 1.019E-03 1.019E-03
        1.020E-03 1.021E-03 1.022E-03 1.024E-03 1.025E-03
        1.026E-03 1.028E-03 1.030E-03 1.032E-03 1.034E-03
        1.037E-03 1.039E-03 1.042E-03 1.046E-03 1.050E-03
        1.054E-03 1.059E-03 1.064E-03 1.070E-03 1.077E-03
        1.084E-03 1.092E-03 1.101E-03 1.111E-03 1.122E-03
        1.135E-03 1.149E-03 1.164E-03 1.181E-03 1.200E-03
        1.221E-03 1.244E-03 1.270E-03 1.298E-03 1.330E-03
        1.365E-03 1.404E-03 1.447E-03 1.494E-03 1.547E-03
        1.605E-03 1.670E-03 1.741E-03 1.821E-03 1.908E-03
        2.004E-03 2.111E-03 2.229E-03 2.359E-03 2.503E-03
        2.661E-03 2.836E-03 3.029E-03 3.241E-03 3.476E-03
        3.734E-03 4.019E-03 4.333E-03 4.677E-03 5.058E-03
        5.476E-03 5.935E-03 6.442E-03 6.998E-03 7.611E-03
        8.284E-03 9.024E-03 9.837E-03 1.073E-02 1.171E-02
        1.279E-02 1.396E-02 1.526E-02 1.667E-02 1.823E-02
```

```
      1.994E-02 2.180E-02 2.385E-02 2.610E-02 2.855E-02
      3.126E-02 3.421E-02 3.744E-02 4.100E-02 4.491E-02
      4.917E-02 5.377E-02 5.867E-02 6.371E-02 6.853E-02
      7.220E-02
si3   1.000e-11 1.000e-07 4.140e-07 8.764e-07 1.855e-06
      5.044e-06 1.068e-05 3.727e-05 1.013e-04 2.145e-04
      4.540e-04 1.585e-03 3.355e-03 7.102e-03 1.503e-02
      2.188e-02 2.418e-02 2.606e-02 3.183e-02 4.087e-02
      6.738e-02 1.111e-01 1.832e-01 2.972e-01 3.688e-01
      4.979e-01 6.081e-01 7.427e-01 8.209e-01 1.003e+00
      1.353e+00 1.653e+00 1.921e+00 2.231e+00 2.346e+00
      2.365e+00 2.466e+00 2.725e+00 3.012e+00 3.678e+00
      4.966e+00 6.065e+00 7.408e+00 8.607e+00 1.000e+01
      1.221e+01 1.419e+01 1.733e+01
sp3         0.0 0.000e+00 0.000e+00 0.000e+00 0.000e+00
      0.000e+00 0.000e+00 0.000e+00 0.000e+00 0.000e+00
      0.000e+00 0.000e+00 0.000e+00 0.000e+00 0.000e+00
      0.000e+00 0.000e+00 0.000e+00 0.000e+00 0.000e+00
      0.000e+00 1.402e-03 9.106e-03 1.440e-02 9.043e-03
      4.185e-02 4.267e-02 5.212e-02 3.028e-02 6.715e-02
      1.241e-01 9.026e-02 7.162e-02 6.251e-02 2.319e-02
      3.831e-03 2.037e-02 5.223e-02 5.619e-02 4.076e-02
      7.882e-02 6.725e-02 2.367e-02 1.635e-03 1.899e-03
      3.013e-03 2.699e-03 4.281e-03
sb3         0.0 0.000E+00 0.000E+00 0.000E+00 0.000E+00
      0.000E+00 0.000E+00 0.000E+00 0.000E+00 0.000E+00
      0.000E+00 0.000E+00 0.000E+00 0.000E+00 0.000E+00
      0.000E+00 0.000E+00 0.000E+00 0.000E+00 0.000E+00
      0.000E+00 4.220E-04 3.282E-03 6.149E-03 4.534E-03
      2.340E-02 2.981E-02 4.753E-02 2.947E-02 7.007E-02
      1.156E-01 8.510E-02 7.450E-02 6.355E-02 2.435E-02
      4.365E-03 2.242E-02 5.838E-02 6.560E-02 4.562E-02
      8.996E-02 8.410E-02 3.104E-02 2.136E-03 2.532E-03
      4.120E-03 4.112E-03 7.824E-03
c     tally definition
c     F4 track length estimate gives cell flux #/cm^2, per source particle
c     => ICRP-74 neutron and gamm-ray AP fluence-to-dose unit : Sv.cm^2
c     => AP effective dose
c     => MCNP give the answer : Sv per source particle
c     => considering source strength gives the answer : Sv/s
c     => * 3600 * 1.0e+6 gives the answer : uSv/h
c     => Tally multiplier card = 3.6e+9
f14:n 11
fm14  3.6e+9
```

```
de14  1.0e-9     1.0e-8     2.5e-8     1.0e-7     2.0e-7
      5.0e-7     1.0e-6     2.0e-6     5.0e-6     1.0e-5
      2.0e-5     5.0e-5     1.0e-4     2.0e-4     5.0e-4
      1.0e-3     2.0e-3     5.0e-3     1.0e-2     2.0e-2
      3.0e-2     5.0e-2     7.0e-2     1.0e-1     1.5e-1
      2.0e-1     3.0e-1     5.0e-1     7.0e-1     9.0e-1
      1.0        1.2        2.0        3.0        4.0
      5.0        6.0        7.0        8.0        9.0
      1.0e+1     1.2e+1     1.4e+1     1.5e+1     1.6e+1
      1.8e+1     2.0e+1
df14  5.24e-12   6.55e-12   7.60e-12   9.95e-12   11.2e-12
      12.8e-12   13.8e-12   14.5e-12   15.0e-12   15.1e-12
      15.1e-12   14.8e-12   14.6e-12   14.4e-12   14.2e-12
      14.2e-12   14.4e-12   15.7e-12   18.3e-12   23.8e-12
      29.0e-12   38.5e-12   47.2e-12   59.8e-12   80.2e-12
      99.0e-12   133e-12    188e-12    231e-12    267e-12
      282e-12    310e-12    383e-12    432e-12    458e-12
      474e-12    483e-12    490e-12    494e-12    497e-12
      499e-12    499e-12    496e-12    494e-12    491e-12
      486e-12    480e-12
f24:p 11
fm24  3.6e+9
de24  1.00e-2    1.5e-2     2.0e-2     3.0e-2     4.0e-2
      5.0e-2     6.0e-2     8.0e-2     1.0e-1     1.5e-1
      2.0e-1     3.0e-1     4.0e-1     5.0e-1     6.0e-1
      8.0e-1     1.0        1.5        2.0        3.0
      4.0        5.0        6.0        8.0        1.0e+1
      2.0e+1
df24  0.049e-12  0.125e-12  0.205e-12  0.300e-12  0.338e-12
      0.357e-12  0.378e-12  0.440e-12  0.517e-12  0.752e-12
      1.004e-12  1.508e-12  1.996e-12  2.466e-12  2.908e-12
      3.727e-12  4.483e-12  6.125e-12  7.490e-12  9.885e-12
      12.015e-12 14.001e-12 15.987e-12 19.919e-12 23.760e-12
      34.4e-12
f34:n 12
fm34  3.6e+9
de34  1.0e-9     1.0e-8     2.5e-8     1.0e-7     2.0e-7
      5.0e-7     1.0e-6     2.0e-6     5.0e-6     1.0e-5
      2.0e-5     5.0e-5     1.0e-4     2.0e-4     5.0e-4
      1.0e-3     2.0e-3     5.0e-3     1.0e-2     2.0e-2
      3.0e-2     5.0e-2     7.0e-2     1.0e-1     1.5e-1
      2.0e-1     3.0e-1     5.0e-1     7.0e-1     9.0e-1
      1.0        1.2        2.0        3.0        4.0
      5.0        6.0        7.0        8.0        9.0
```

```
      1.0e+1     1.2e+1     1.4e+1     1.5e+1     1.6e+1
      1.8e+1     2.0e+1
df34  5.24e-12   6.55e-12   7.60e-12   9.95e-12   11.2e-12
      12.8e-12   13.8e-12   14.5e-12   15.0e-12   15.1e-12
      15.1e-12   14.8e-12   14.6e-12   14.4e-12   14.2e-12
      14.2e-12   14.4e-12   15.7e-12   18.3e-12   23.8e-12
      29.0e-12   38.5e-12   47.2e-12   59.8e-12   80.2e-12
      99.0e-12   133e-12    188e-12    231e-12    267e-12
      282e-12    310e-12    383e-12    432e-12    458e-12
      474e-12    483e-12    490e-12    494e-12    497e-12
      499e-12    499e-12    496e-12    494e-12    491e-12
      486e-12    480e-12
f44:p 12
fm44  3.6e+9
de44  1.00e-2    1.5e-2     2.0e-2     3.0e-2     4.0e-2
      5.0e-2     6.0e-2     8.0e-2     1.0e-1     1.5e-1
      2.0e-1     3.0e-1     4.0e-1     5.0e-1     6.0e-1
      8.0e-1     1.0        1.5        2.0        3.0
      4.0        5.0        6.0        8.0        1.0e+1
      2.0e+1
df44  0.049e-12  0.125e-12  0.205e-12  0.300e-12  0.338e-12
      0.357e-12  0.378e-12  0.440e-12  0.517e-12  0.752e-12
      1.004e-12  1.508e-12  1.996e-12  2.466e-12  2.908e-12
      3.727e-12  4.483e-12  6.125e-12  7.490e-12  9.885e-12
      12.015e-12 14.001e-12 15.987e-12 19.919e-12 23.760e-12
      34.4e-12
c     Special case for developing future biasing scheme
C     => average over the huge surrounding detector
f114:n 13
fm114 3.6e+9
de114 1.0e-9     1.0e-8     2.5e-8     1.0e-7     2.0e-7
      5.0e-7     1.0e-6     2.0e-6     5.0e-6     1.0e-5
      2.0e-5     5.0e-5     1.0e-4     2.0e-4     5.0e-4
      1.0e-3     2.0e-3     5.0e-3     1.0e-2     2.0e-2
      3.0e-2     5.0e-2     7.0e-2     1.0e-1     1.5e-1
      2.0e-1     3.0e-1     5.0e-1     7.0e-1     9.0e-1
      1.0        1.2        2.0        3.0        4.0
      5.0        6.0        7.0        8.0        9.0
      1.0e+1     1.2e+1     1.4e+1     1.5e+1     1.6e+1
      1.8e+1     2.0e+1
df114 5.24e-12   6.55e-12   7.60e-12   9.95e-12   11.2e-12
      12.8e-12   13.8e-12   14.5e-12   15.0e-12   15.1e-12
      15.1e-12   14.8e-12   14.6e-12   14.4e-12   14.2e-12
      14.2e-12   14.4e-12   15.7e-12   18.3e-12   23.8e-12
```

```
      29.0e-12   38.5e-12   47.2e-12   59.8e-12   80.2e-12
      99.0e-12   133e-12    188e-12    231e-12    267e-12
      282e-12    310e-12    383e-12    432e-12    458e-12
      474e-12    483e-12    490e-12    494e-12    497e-12
      499e-12    499e-12    496e-12    494e-12    491e-12
      486e-12    480e-12
f124:p 13
fm124 3.6e+9
de124 1.00e-2    1.5e-2     2.0e-2     3.0e-2     4.0e-2
      5.0e-2     6.0e-2     8.0e-2     1.0e-1     1.5e-1
      2.0e-1     3.0e-1     4.0e-1     5.0e-1     6.0e-1
      8.0e-1     1.0        1.5        2.0        3.0
      4.0        5.0        6.0        8.0        1.0e+1
      2.0e+1
df124 0.049e-12  0.125e-12  0.205e-12  0.300e-12  0.338e-12
      0.357e-12  0.378e-12  0.440e-12  0.517e-12  0.752e-12
      1.004e-12  1.508e-12  1.996e-12  2.466e-12  2.908e-12
      3.727e-12  4.483e-12  6.125e-12  7.490e-12  9.885e-12
      12.015e-12 14.001e-12 15.987e-12 19.919e-12 23.760e-12
      34.4e-12
c     F4 track length estimate gives cell flux #/cm^2, per source particle
c     => BUGLE energy binning
f54:n 11
e54   1.000e-11 1.000e-07 4.140e-07 8.764e-07 1.855e-06
      5.044e-06 1.068e-05 3.727e-05 1.013e-04 2.145e-04
      4.540e-04 1.585e-03 3.355e-03 7.102e-03 1.503e-02
      2.188e-02 2.418e-02 2.606e-02 3.183e-02 4.087e-02
      6.738e-02 1.111e-01 1.832e-01 2.972e-01 3.688e-01
      4.979e-01 6.081e-01 7.427e-01 8.209e-01 1.003e+00
      1.353e+00 1.653e+00 1.921e+00 2.231e+00 2.346e+00
      2.365e+00 2.466e+00 2.725e+00 3.012e+00 3.678e+00
      4.966e+00 6.065e+00 7.408e+00 8.607e+00 1.000e+01
      1.221e+01 1.419e+01 1.733e+01
f64:p 11
e64   1.000e-02 2.000e-02 3.000e-02 6.000e-02 1.000e-01
      2.000e-01 4.000e-01 6.000e-01 7.000e-01 8.000e-01
      1.000e+00 1.500e+00 2.000e+00 3.000e+00 4.000e+00
      5.000e+00 6.000e+00 7.000e+00 8.000e+00 1.000e+01
      1.400e+01
f74:n 12
e74   1.000e-11 1.000e-07 4.140e-07 8.764e-07 1.855e-06
      5.044e-06 1.068e-05 3.727e-05 1.013e-04 2.145e-04
      4.540e-04 1.585e-03 3.355e-03 7.102e-03 1.503e-02
      2.188e-02 2.418e-02 2.606e-02 3.183e-02 4.087e-02
```

```
      6.738e-02 1.111e-01 1.832e-01 2.972e-01 3.688e-01
      4.979e-01 6.081e-01 7.427e-01 8.209e-01 1.003e+00
      1.353e+00 1.653e+00 1.921e+00 2.231e+00 2.346e+00
      2.365e+00 2.466e+00 2.725e+00 3.012e+00 3.678e+00
      4.966e+00 6.065e+00 7.408e+00 8.607e+00 1.000e+01
      1.221e+01 1.419e+01 1.733e+01
f84:p 12
e84   1.000e-02 2.000e-02 3.000e-02 6.000e-02 1.000e-01
      2.000e-01 4.000e-01 6.000e-01 7.000e-01 8.000e-01
      1.000e+00 1.500e+00 2.000e+00 3.000e+00 4.000e+00
      5.000e+00 6.000e+00 7.000e+00 8.000e+00 1.000e+01
      1.400e+01
phys:n 17.332       $ neutron highest energy of BUGLE
cut:n  j 1.0e-11    $ neutron lowest energy of BUGLE
phys:p j j j 0      $ detailed photon physics and no photonuclear
cut:p  j 0.01       $ photon lowest energy of BUGLE
c read lower weight window bounds from an external wwinp file
c copy and paste from ww4n.tpe & ww4p.tpe (A2CADISn) (wwinp=ww4Cn.e)
wwp:n 5 3 5 0 -1 0
wwp:p 5 3 5 0 -1 0
mesh  geom=rzt ref=1e-6 1e-6 1e-6 origin=0.0 -0.1 0.0
      imesh 180.1
      iints 72
      jmesh 555.1
      jints 222
      kmesh 1.0
      kints 1
nps   10000000
print

=======================================================================
```

12. 附件四：MCNP5 使用手冊

MCNP5 簡易中文使用手冊共 96 頁，為方便閱讀起見，另外裝訂成一冊。